



• Article •

SPECIAL TOPIC:

Multiplexed Survey Telescope: Perspectives for Large-Scale Structure Cosmology in the Era of Stage-V Spectroscopic Survey

Cheng Zhao^{*1}, Song Huang^{†1}, Mengfan He^{1,2}, Paulo Montero-Camacho³, Yu Liu¹, Pablo Renard¹, Yunyi Tang¹, Aurélien Verdier⁴, Wenshuo Xu¹, Xiaorui Yang¹, Jiayi Yu⁴, Yao Zhang¹, Siyi Zhao¹, Xingchen Zhou^{5,6}, Sheng-Yu He⁴, Jean-Paul Kneib⁴, Jiayi Li⁷, Zhuoyang Li¹, Wen-Ting Wang^{8,9}, Zhong-Zhi Xianyu¹⁰, Yidian Zhang⁷, Rafaela Gsponer⁴, Xiao-Dong Li¹¹, Antoine Rocher⁴, Siwei Zou¹², Ting Tan¹³, Zhiqi Huang¹¹, Zhuoxiao Wang¹, Pei Li¹, Maxime Rombach⁴, Chenxing Dong³, Daniel Forero-Sánchez⁴, Yuanhang Ning^{14,1}, Huanyuan Shan², Tao Wang^{15,16}, Yin Li³, Zhongxu Zhai^{8,9}, Yuting Wang^{5,17}, Gong-Bo Zhao^{5,18,17,12}, Yong Shi^{14,15}, Shude Mao¹, Lei Huang¹, Liquan Guo¹, and Zheng Cai¹

¹Department of Astronomy, Tsinghua University, Beijing 100084, China;²Shanghai Astronomical Observatory, Chinese Academy of Sciences, 80 Nandan Road, Shanghai 200030, China;³Pengcheng Laboratory, Nanshan District, Shenzhen, Guangdong 518000, China;⁴Institute of Physics, Laboratory of Astrophysics, École Polytechnique Fédérale de Lausanne (EPFL), Observatoire de Sauverny, CH-1290 Versoix, Switzerland;⁵National Astronomical Observatories, CAS, Beijing 100101, China;⁶Science Center for China Space Station Telescope, National Astronomical Observatories, Chinese Academy of Science, 20A Datun Road, Beijing 100101, China;⁷Zhili College, Tsinghua University, Beijing 100084, China;⁸Department of Astronomy, Shanghai Jiao Tong University, Shanghai 200240, China;⁹Shanghai Key Laboratory for Particle Physics and Cosmology, Shanghai 200240, China;¹⁰Department of Physics, Tsinghua University, Beijing 100084, China;¹¹School of Physics and Astronomy, Sun Yat-sen University, Zhuhai 519082, China;¹²Chinese Academy of Sciences South America Center for Astronomy (CASSACA), National Astronomical Observatories of China, Beijing 100101, China;¹³IRFU, CEA, Université Paris-Saclay, F-91191 Gif-sur-Yvette, France;¹⁴Department of Scientific Research, Beijing Planetarium, Beijing 100044, China;¹⁵School of Astronomy and Space Science, Nanjing University, 163 Xianlin Avenue, Nanjing 210023, China;¹⁶Key Laboratory of Modern Astronomy and Astrophysics, Nanjing University, Ministry of Education, 163 Xianlin Avenue, Nanjing 210023, China;¹⁷Institute for Frontiers in Astronomy and Astrophysics, Beijing Normal University, Beijing 102206, China;¹⁸School of Astronomy and Space Science, University of Chinese Academy of Sciences, Beijing 100049, China

Received January 11, 2023; accepted April 6, 2023

The Multiplexed Survey Telescope (MUST) is a 6.5-meter telescope under development. Dedicated to highly-multiplexed, wide-field spectroscopic surveys, MUST observes over 20,000 targets simultaneously using 6.2-mm pitch positioning robots within a $\sim 5 \text{ deg}^2$ field of view. MUST aims to conduct the first Stage-V spectroscopic survey in the 2030s, mapping the 3D Universe with over 100 million galaxies and quasars, spanning from the nearby Universe to a redshift of $z \sim 5.5$, corresponding to approximately 1 billion years after the Big Bang. To cover this extensive redshift range, we present an initial conceptual target selection algorithm for different types of galaxies, ranging from local bright galaxies and luminous red galaxies to emission-line galaxies, and high-redshift ($2 < z < 5.5$) Lyman-break galaxies. Using Fisher forecasts, we demonstrate that MUST can address fundamental questions in cosmology, including the nature of dark energy, tests of gravity theories, and investigations into primordial physics. This is the first paper in the series of science white papers for MUST, with subsequent developments focusing on additional scientific cases such as galaxy and quasar evolution, Milky Way physics, and dynamic phenomena in the time-domain Universe.

Optical instruments, Sky surveys, Cosmology

PACS number(s): 07.60.-j, 95.80.+p, 98.80.-k

Citation: Zhao, et al.,
, Sci. China-Phys. Mech. Astron. **66**, 000000 (2023), <https://doi.org/??>

Contents

| | | |
|----------|---|-----------------|
| 1 | Introduction | 000000-3 |
| 2 | MULTiplexed Survey Telescope | 000000-5 |
| 2.1 | A 6.5-m Telescope for Spectroscopic Surveys | 000000-5 |
| 2.2 | Multiplexed Focal Plane & Instruments | 000000-5 |
| 2.3 | Site and Observing Conditions | 000000-7 |
| 2.4 | Survey Capability and Overall Scientific Potential | 000000-8 |
| 3 | Scientific Motivations of the Stage-V Cosmological Surveys | 000000-8 |
| 3.1 | Nature & Evolution of Dark Energy | 000000-8 |
| 3.2 | Growth of Structure & Nature of Gravity | 000000-10 |
| 3.3 | Inflation & Primordial Physics | 000000-11 |
| 3.4 | Neutrinos & Light Relics | 000000-11 |
| 3.5 | Dark Matter | 000000-12 |
| 3.6 | Synergy with Other Probes | 000000-13 |
| 3.6.1 | Imaging surveys | 000000-13 |
| 3.6.2 | CMB S4 | 000000-13 |
| 3.6.3 | Radio surveys | 000000-13 |
| 3.6.4 | Gravitational waves and Fast Radio Bursts | 000000-14 |

*Email: czhao@tsinghua.edu.cn

†Email: shuang@tsinghua.edu.cn

| | |
|--|------------------|
| 4 Target Selection | 000000-14 |
| 4.1 Challenges of Target Selection for Stage-V Spectroscopic Surveys | 000000-14 |
| 4.2 Low-Redshift Tracers | 000000-16 |
| 4.2.1 Bright Galaxy Sample (BGS) | 000000-16 |
| 4.2.2 Luminous Red Galaxies (LRG) | 000000-17 |
| 4.2.3 Emission Line Galaxies (ELG) | 000000-18 |
| 4.3 High-Redshift Tracers | 000000-19 |
| 4.3.1 Lyman-Break Galaxies (LBG) | 000000-19 |
| 4.3.2 Lyman- α Emitters (LAE) | 000000-21 |
| 4.3.3 Quasi-Stellar Objects (QSO) | 000000-21 |
| 4.4 Summary of the Target Selection | 000000-21 |
| 4.5 Conceptual Survey Design | 000000-22 |
| 4.5.1 Dark Time Survey | 000000-22 |
| 4.5.2 Gray Time Survey | 000000-22 |
| 5 Cosmological Forecasts | 000000-23 |
| 5.1 Methodology | 000000-24 |
| 5.1.1 Fisher forecast | 000000-24 |
| 5.1.2 Cosmological inference | 000000-24 |
| 5.2 Cosmic Expansion History & Dark Energy | 000000-24 |
| 5.3 Structure Growth & Modified Gravity | 000000-26 |
| 5.4 Primordial Non-Gaussianity | 000000-28 |
| 5.5 Neutrinos | 000000-28 |
| 5.6 Warm Dark Matter | 000000-29 |
| 6 Conclusions | 000000-30 |

1 Introduction

Over the past four decades, beginning with the “Stick Man” from the CfA Redshift Survey in 1982 [1, 2], spectroscopic mapping of large-scale structures (LSS) has accumulated more than 30 million redshifts of nearby and distant galaxies. This monumental achievement has contributed significantly to the establishment of the current cosmological model Λ CDM, along with other cosmological probes, i.e., cosmic microwave background (CMB; [3, 4]), Type-Ia supernovae (SN; [5–7]), or measurements of weak lensing (e.g., [8, 9]). For two decades (2000–2020), major experiments such as the Sloan Digital Sky Survey (SDSS; [10]), followed by the ongoing (2021–2026) survey from the Dark Energy Spectroscopic Instrument¹⁾ (DESI; [11]), have mapped the 3D universe at low and intermediate redshift ($z \lesssim 3$). Clustering measurements from spectroscopic surveys of galaxies and quasars have become a key probe of cosmology. They pro-

vide precise measurements on the baryon acoustic oscillations (BAO) scale [12] and the linear growth rate of structure $f\sigma_8$ through redshift space distortions (RSD) [13]. Recent results from the DESI collaboration [14] suggest a potential deviation from the cosmological constant to time-varying dark energy. By the end of this decade, we expect to have sub-percent-level constraints on dark energy and gravity from galaxy clustering up to redshift $z \sim 2$. When the DESI project concludes, we will have completed the spectroscopic survey component of the four stages outlined in the Dark Energy Task Force (DETF) report [15]. Yet, many fundamental questions remain unanswered, calling for a new era of cosmological experiments in the 2030s.

Going one step further, 3D maps of the universe at high redshift ($z > 2$) will enable the observation of linear modes in the primordial universe, significantly enhancing our ability to constrain dark energy and inflation [16]. In the next decade, a series of ground- and space-based photometric surveys CSST

1) <https://www.desi.lbl.gov/the-desi-survey/>

[17], Euclid [18], Nancy Grace Roman Space Telescope [19], LSST [20] will provide deep and high-quality images for future galaxy spectroscopic surveys allowing to target galaxies such as Lyman Break Galaxy (LBG) or Lyman- α emitter (LAE) [21, 22] as tracer of matter at high redshift $2 < z < 5$. Large-volume high-redshift surveys using these new tracers have the unprecedented potential to help us test primordial non-Gaussianity, probe dynamic dark energy, and reveal possible new features in the primordial power spectrum, uncovering tantalizing hints for new physics.

At the same time, a high-density spectroscopic survey of low-redshift ($z < 1.5$) can provide a high-fidelity 3D map of the cosmic web and trace the matter distributions into the non-linear regimes, opening doors to unexplored scientific opportunities. Such a multi-purpose dataset can also enhance the scientific performance of other cosmological probes, such as calibrating the photometric redshift and intrinsic alignment models for weak gravitational lensing surveys (e.g., [23; 24, 25]), providing spectroscopic follow-up and host galaxy properties for supernova surveys (e.g., [26, 27]), or exploring new approaches to map the low-redshift large-scale structures (LSS) such as a peculiar velocities survey (e.g., [28, 29]). More importantly, it will help maximize the potential for synergies between spectroscopic surveys and other cosmological probes, such as CMB (e.g., [30]), weak lensing (e.g., [31–34]), and intensity mapping (IM, e.g., [35]) experiments.

Motivated by these two promising directions, the cosmological & high-energy physics community has recently coined the concept for a Stage-V spectroscopic experiment (e.g., [36, 37]) to fulfill these high expectations. By definition, a Stage-V spectroscopic facility should utilize a telescope with a high etendue value ($A\Omega$; A and Ω represent the collecting area and field of view of the telescope, respectively) to ensure a high survey speed. More importantly, the facility should have significantly improved multiplexed capability (i.e., the number of targets that can be observed simultaneously) compared to the Stage-IV survey (e.g., 5,000 fibers for DESI). Conceptually, a Stage-V facility demands a minimum of 10,000 fibers that could be easily reconfigured to target different objects. This is the primary technical challenge now for such an ambitious vision. At the same time, a Stage-V facility should also have excellent optical performance, high-performance multi-object spectrographs that cover at least the entire optical wavelength range, and a site with favorable observing conditions. Building on these requirements, multiple ground-based concepts have been proposed, including the

6.5 m MegaMapper telescope [38, 39], the dual-6 m & dual-hemisphere Spec-S5 project²⁾ [40], the 11 m Maunakea Spectroscopic Explorer³⁾ (MSE; [41]), the 12 m Wide-field Spectroscopic Telescope⁴⁾ (WST; [42]), and the ~ 12 m Extremely Large Spectroscopic Survey Telescope (ESST; [43]).

The Multiplexed Survey Telescope⁵⁾ (MUST) is a 6.5-meter telescope [44] under active development. MUST will be located at the 4358 m Peak A of Saishiteng Mountain in Qinghai, China. Equipped with over 20,000 fibers over a ~ 5 deg² field of view (FoV), it features three-channel spectrographs covering wavelengths from 370–960 nm, with spectral resolution between $R = 2,000$ and 4,500. MUST is designed to conduct an ambitious Stage-V cosmological spectroscopic survey, aiming to precisely measure key cosmological parameters and improve our understanding of dark energy and cosmic evolution. With the first light scheduled for 2031, MUST expects to conduct the first Stage-V spectroscopic survey, targeting Lyman Break Galaxy (LBG) and Lyman- α emitter (LAE) at high redshift across $\sim 13,000$ deg² of the northern sky. Clustering analysis of these tracers will provide sub-percent precision measurements on BAO parameters – $D_A(z)/r_d$ and $H(z)r_d$ – and the linear growth rate of structure, $f\sigma_8$, at redshift $2 < z < 5$, a region not yet covered by current spectroscopic galaxy surveys. Additionally, MUST will provide stringent constraints on primordial non-Gaussianities (PNG, local type) through the parameter f_{NL}^{local} with a precision of $\sigma(f_{NL}^{local}) \sim 1$. This will enable stringent testing of a wide range of inflationary models. MUST is expected to provide sufficient precision (~ 0.03 eV when combined with CMB data) on the sum of neutrino masses to constrain a nonzero neutrino mass with $\sim 2\sigma$ significance, assuming normal hierarchy. The inverted mass hierarchy can be tested with a significance $\sim 1.3\sigma$. Finally, from power spectrum measurements of the Lyman- α forest, MUST will yield the most precise constraint on warm dark matter mass to date $m_X > 10.5$ keV at 95% confidence level (assuming 14,000 deg² and $k_{max} = 0.67 h \text{ Mpc}^{-1}$).

Besides the unique potential of the MUST project, synergies with other cosmological surveys, i.e., future imaging surveys (e.g., CSST, Euclid, LSST), CMB experiments (e.g., Simon Observatory [45], CMB-S4 [46], LiteBird [47]) or radio surveys (e.g., SKAO [48]) will enhance the constraining power of MUST and will result in a better understanding of our Universe. As a dedicated spectroscopic survey facility, MUST can also conduct spectroscopic surveys that support a wide range of scientific topics beyond LSS cosmology, including the study of galaxy evolution, super-massive black

2) <https://www.spec-s5.org/>

3) <https://mse.cfht.hawaii.edu/>

4) <https://www.wstlescope.com/>

5) <https://must.astro.tsinghua.edu.cn/en>

holes (SMBHs), the structure of the Milky Way, and time-domain astrophysics.

This paper describes the MUST instrument and the scientific objectives of the cosmological survey that will be conducted over a 5-year period of observation. Section 2 provides an overview of the MUST project, including the current status of the whole project, the design of the telescope (Section 2.1), the focal plane system & the spectrograph (Section 2.2), the site & observing condition (Section 2.3), and the overall scientific capabilities (Section 2.4). Section 3 describes the key scientific motivations of MUST for the Stage-V cosmological surveys. The primary scientific goals are covered in detail while briefly summarizing the potential for new probes and the potential synergies with other cosmological surveys. Section 4 presents the current target selection strategy and provides the redshift distribution and target density estimations for the cosmological forecast. We will also introduce the conceptual survey design for MUST. Finally, Section 5 describes the method for theoretically forecasting the cosmological potential of MUST and summarizes the forecast for dark energy, structure growth, primordial non-Gaussianity, neutrino mass, and warm dark matter constraints. Discussions and main conclusions of this project and future directions are described in Section 6.

Throughout this work, we adopt as fiducial baseline Λ CDM cosmology with parameters $H_0 = 67.6 \text{ km s}^{-1} \text{ Mpc}^{-1}$, $\Omega_b = 0.046$ and $\Omega_m = 0.31$. All magnitudes in this work are defined in the AB magnitude system [49].

2 Multiplexed Survey Telescope

The Multiplexed Survey Telescope (MUST) is a dedicated spectroscopic survey facility proposed and led by the Department of Astronomy at Tsinghua University and co-founded with École Polytechnique Fédérale de Lausanne (EPFL).

The MUST project aims to build a 6.5-meter wide-field telescope with multiplexed spectroscopic observation capability by 2030. While designed as a flexible platform for various spectroscopic surveys, the primary scientific drive of MUST is to become the first Stage-V spectroscopic survey [50] that answers fundamental questions in cosmology and physics. The concept and early design of MUST drew inspiration from the MegaMapper project [38, 39]. The MUST collaboration has independently completed the preliminary design of the optical system [44], structure, and dome [51] of the telescope, and is working with collaborators and vendors to design the modular focal plane, fiber, and spectrograph systems [52]. Here, we provide a brief introduction to the design and technical capabilities of MUST. A summary of the key specifications is available in Table 1. An upcoming

paper will summarize a more detailed description and analysis of the MUST project's technical aspects.

2.1 A 6.5-m Telescope for Spectroscopic Surveys

Driven by the demanding scientific requirements of next-generation surveys for cosmology, a Stage-V spectroscopic telescope requires excellent optical quality over a large Field-of-View (FoV) on a telescope with a diameter greater than 6 m. The optical design of MUST is driven by solving these technical challenges. Currently, MUST adopts a compact Ritchey-Chretien (R-C) design with a multi-element Wide Field Corrector (WFC). The hyperboloid primary and secondary mirrors of MUST are 6.5 m and 2.4 m in diameter. The primary mirror has a 2 m diameter central hole to facilitate the installation of a five-lens WFC that ensures excellent imaging quality of MUST. The largest lens for the WFC of MUST is 1.6 m in diameter, even slightly larger than the largest lens of the camera of LSST [20]. MUST published the conceptual optical design in 2023 [44]. Since then, the collaboration has made a series of modifications, primarily to the configuration of the WFC, to improve the engineering feasibility of the telescope and reduce the risk during the manufacture and assembly of critical sub-systems (Zhang et al. in prep.). Under the updated design, MUST imaging quality over the entire 2.8° diameter FoV is excellent: up to a 50° zenith angle and within the wavelength range of 0.365 to $1.0 \mu\text{m}$, the 80% Encircled Energy (EE80) size of the image spot is < 0.6 arcsec. At the Cassegrain focus, which hosts the modular focal plane system of MUST, the optical system has a focal ratio of F/3.7.

2.2 Multiplexed Focal Plane & Instruments

Enabled by the optimized optical design, MUST can achieve a significantly improved multiplexed capability compared to current Stage-IV spectroscopic facilities, using a novel modular focal plane design (See Figure 1). Starting from the LAMOST survey, modern spectroscopic surveys have adopted different types of robotic fiber positioners ([53-57]) to guide the light from distant targets to the scientific instruments and enable efficient & flexible survey design. The largest multiplexed survey facility, DESI, currently hosts 5,000 fiber positioners, each with an outer diameter of 10 mm [58]. Each positioner was installed and operated individually and independently on the focal plate of DESI. However, as a Stage-V facility, MUST has a much more demanding requirement for multiplexed capability; individually managing more than 10,000 fiber positioners significantly increases the complexity and risk of operating the instruments.

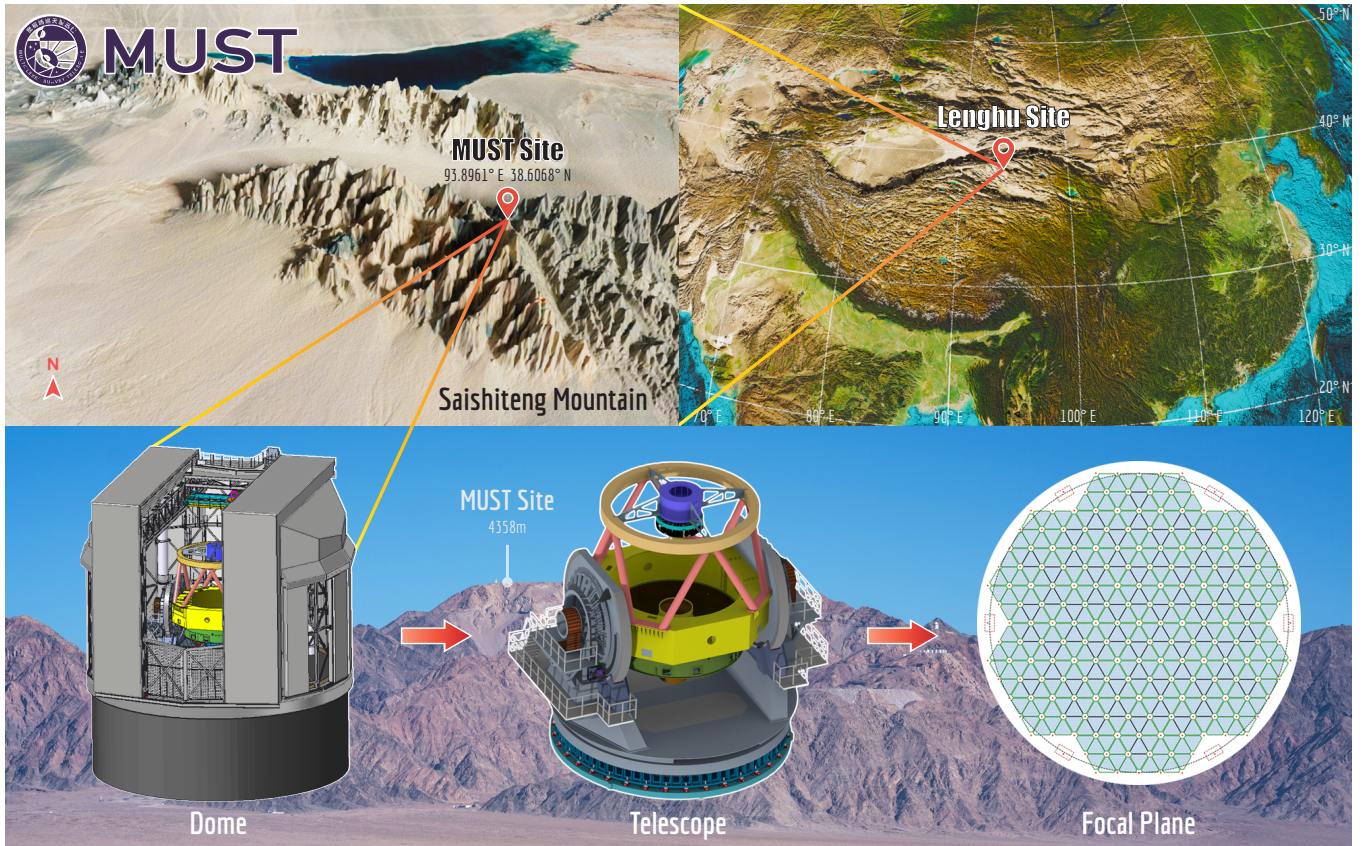


Figure 1 Overview of the MUST project. The top right panel displays the location of the currently selected MUST site in Qinghai Province, China. The top left panel and background image of the bottom panel feature pictures of Saishiteng Mountain near Lenghu. The highest peak with an altitude of 4358 m, was selected as the site for MUST. From left to right, the bottom panels illustrate the preliminary design of the dome of MUST and the telescope, as well as a sketch of the conceptual design of the focal plane of MUST. By current design, MUST will host 21,168 robotic fiber positioners using 336 triangular modules.

| Optical System | | | |
|--|-----------------------|--|--------------------|
| Optical Design | R-C with WFC | | |
| Primary Mirror Diameter | 6.5 m Hyperboloid | With 2 m central hole | |
| Secondary Mirror Diameter | 2.4 m Hyperboloid | Convex | |
| Wide Field Corrector | Five-Lens Design | Largest lens diameter: 1.6 m | |
| Throughput Requirement | > 50% from 370-960 nm | Considering the reflectance of the primary & secondary mirror, WFC throughput, and the vignetting of the secondary & corrector | |
| Focal Ratio | F/3.7 | Cassegrain Focus | |
| Field of View | 2.8° in Diameter | | |
| Focal Plane & Fiber System (Preliminary) | | | |
| Focal Plane Diameter | 1.2 m | | |
| Total # of Modules | 336 | Semi-frameless design | |
| # of Positioners per Module | 63 | 21 × 3 groups | |
| Total # of Fiber Positioners | 21,168 | | |
| Effective Positioner Coverage | 74.0% | | |
| Pitch Distance between Positioners | 6.2 mm | Using a θ - ϕ design | |
| Fiber Core Diameter | 140 μ m | 1.2 arcsec on the sky | |
| Fiber Route Length | 45-50 m | From the fiber tip to the slithead | |
| Spectrograph (Preliminary) | | | |
| Channel | Wavelength Coverage | Spectral Resolution | Average Throughput |
| Blue | 370-590 nm | R~ 1900-3300 | ≥ 55% |
| Red | 565-775 nm | R~ 3300-4500 | ≥ 60% |
| NIR | 750-960 nm | R~ 4300-5500 | ≥ 60% |

Table 1 Summary of the key specifications of the optical, focal plane & fiber, and spectrograph systems of MUST. Please note that the design specifications for the focal plane and spectrograph systems are still preliminary.

MUST is collaborating with EPFL and industrial partners to develop a novel modular focal plane system [59]. This

modular design was originally proposed for the MegaMapper project by [60] and is also being developed for the SpecS5 project [61]. The MUST design vastly benefits from the open-source design and the model file⁶⁾ released by [60]. The Trillium design is one of the candidates that is being tested for MUST.

For MUST, as shown in the bottom-right panel of Figure 1, a 1.2-m diameter focal plate will host 336 triangular fiber positioner modules at the Cassegrain focus under the current preliminary design. Each module will integrate 60 or 63 fiber positioning robots in three groups, depending on whether three positioning references are required for each module. MUST plans to adopt a miniaturized fiber positioning robot with a 6.2 mm outer diameter and optical fiber with a $\sim 140\ \mu\text{m}$ core diameter corresponding to 1.2 arcsecs on the sky to ensure the fiber density satisfies the requirement of future cosmology surveys. To optimize the effective coverage of the fibers, the focal plate assembles four modules into a group. The gaps between modules are 1 and 3 mm within the group and between adjacent groups. Altogether, this allows MUST to equip 20,160 or 21,168 fiber positioners over the focal plane with a 74% coverage, which results in a $\sim 5\ \text{deg}^2$ FoV covered by fibers with a $\sim 4,000\ \text{deg}^{-2}$ fiber density. It is worth noting that, given the aspheric shape of the focal plane and the requirements of the fiber throughput & focal ratio degradation (FRD) budgets of MUST, the fiber tips of all the positioners should be located within $\pm 100\ \mu\text{m}$ from the theoretical focal plane. The design of MUST achieves this goal by approximating the focal plane with a best-fit spherical surface that meets the requirement. In this way, all the modules can have an identical configuration, and within each module, the tips of the 60 or 63 positioners will match the shape of the spherical surface. This challenging and ambitious design is essential to the overall scientific capability of MUST, especially for the LSS survey discussed here.

The first-generation instruments of MUST consist of ~ 42 multi-object spectrographs; each will host ~ 500 optical fibers on a $4\text{k}\times 4\text{k}$ -pixels CCD detector. The preliminary design of the spectrograph of MUST is still underway. Regardless, given the very similar scientific goals to the DESI project, the current concept adopts a similar three-channel design as the spectrograph of DESI, covering the wavelength range between ~ 3700 to $\sim 9600\ \text{\AA}$ with a $R \sim 1,900$ to 5,500 spectroscopic resolution. We currently aim to achieve a $> 60\%$ average throughput in all three channels while exploring different approaches to further improve it to an average $\sim 70\%$ efficiency.

In addition to the fiber positioning system and the spectro-

graphs, the scientific instrument system of MUST includes other crucial sub-systems, such as the fiber view camera (FVC), fiducial fibers, focal plate adjustment & derotation mechanism, and a complex fiber route (see Figure 1). Altogether, they will enable the Stage-V LSS survey potential of MUST. In the upcoming publications, we will describe the technical design of the whole focal plane system and the spectrographs.

2.3 Site and Observing Conditions

MUST has selected Peak A of Saishiteng Mountain, located near Lenghu Town in Haixi Mongol and Tibetan Autonomous Prefecture, Qinghai Province, China, as its candidate site (referred to as the “Lenghu” site). The Lenghu site was first reported in [62] and has been selected by a series of domestic astronomical projects in China, including the Mozi Survey Telescope⁷⁾ (a 2.5 m wide field imaging survey telescope in operation) and the Jiao-tong University Spectroscopic Telescope (JUST; a planned 4 m segmented mirror telescope; [63]), and more. Along with several other peaks (see Figure 1), Peak A, at 4,358 m, has been flattened for construction. Starting from Oct. 2023, the MUST collaboration has begun to monitor the weather and seeing condition on Peak A. While we are still accumulating data for a more precise site condition assessment, combining our data with the public data collected by the NAOC team at the nearby Peak C⁸⁾, we estimate that the Lenghu site has an annual clear night fraction between 60% to 70%, with worse observing conditions during the summer, and a median DIMM seeing FWHM between 0.8 to 1.0 arcsec. These specifications meet the site requirements for conducting a fiber-spectroscopic survey. While the light pollution from the development of nearby towns and mining businesses is a concern, the local government has passed legislation to protect the dark night conditions within a 50 km area around the Lenghu site.

At 4,358 m, Peak A enjoys significantly less atmospheric attenuation in the shorter wavelength range. Preliminary photometric observations from the Mozi telescope indicate a promising result: the atmospheric attenuation level at $\lambda < 450\ \text{nm}$ for Lenghu is comparable to that of Mauna Kea and significantly better than lower-altitude sites, such as Kitt Peak. This presents MUST an opportunity to improve the overall throughput in the blue wavelength end, which is crucial for identifying the Lyman- α ($\text{Ly}\alpha$) emission line at $z > 2$. Meanwhile, the high altitude also results in a median nighttime air temperature of -8.1°C (minimum & maximum temperatures are -25°C and 15.2°C), which increases the chal-

6) The model files can be found at <https://zenodo.org/records/6354859>.

7) <https://wfst.ustc.edu.cn/>

8) <http://lenghu.china-vo.org/>

lenges for the construction and maintenance of MUST. At the same time, the median nighttime humidity is $\sim 30\%$ at Peak A.

2.4 Survey Capability and Overall Scientific Potential

Given the current monthly statistics of clear night fraction, the Lenghu site could provide $\sim 2,400$ and $2,800$ observing hours per year. Assuming a configuration with $20,000$ working fibers and a $> 90\%$ uptime, MUST will have $210\text{--}270$ million fiber hours in a five-year survey, allowing MUST to conduct Stage-V LSS surveys (see Figure 2). As a dedicated survey facility, MUST's long-term commitment to spectroscopic surveys is another unique strength in fulfilling the Stage-V cosmological goals. Compared to DESI, MUST has a $3.4\times$ higher light collecting capability and $4\times$ more fibers. Even considering the throughput costs of the secondary mirror, the more complex WFC design, the longer fiber route, and challenges in the spectrograph design, MUST can still improve the spectroscopic survey efficiency—the number of redshifts measured for the same set of targets during the same time—by an order of magnitude.

While the Stage-V cosmological survey will be the highest priority of MUST during the first phase of its operation, the significant fiber-hour budget will allow us to design versatile programs with a wide range of scientific goals. In addition to mapping the large-scale structures for cosmology, the same dataset will enable robust statistical studies of galaxies and Active Galactic Nuclei (AGN) near and far. These data can help us understand the rise and fall of star formation in galaxies over the last 10 Billion Years and the assembly of different populations of galaxies. It will also enable us to measure the accretion rate and mass of supermassive black holes (SMBHs) in a galaxy sample that is one order of magnitude larger than the existing one, significantly improving our understanding of the growth of SMBHs and their impact on galaxy evolution. At the small, non-linear scale, a detailed picture of galaxy clustering will enable better modeling of galaxy-halo connections, which in turn will benefit cosmology. During bright nights, MUST can measure the radial velocities and chemical abundances of many halo stars in the Milky Way, shedding light on its assembly history and constraining the nature of dark matter. Located at a longitude less populated with large ground-based telescopes, MUST is also poised to play an exciting role in the age of time-domain spectroscopic surveys. The list can go on.

In addition, the modular focal plane of MUST secures future opportunities for instrument upgrades, as a high-resolution fiber spectrograph and an integrated field spectrograph (IFS) can be straightforwardly added to the focal plane, provided their front-end optics fit into the current fiber posi-

tioner module. In the following publications from this series, we will discuss the scientific potential and strategy of these topics in detail.

For the remainder of this work, we will focus on the primary scientific goal of MUST: the Stage-V LSS spectroscopic survey, aimed at deepening our understanding of several fundamental questions in cosmology and physics.

3 Scientific Motivations of the Stage-V Cosmological Surveys

Ever since the discovery of the accelerated expansion of the Universe using Type Ia supernova data [66, 67], Λ CDM has been widely accepted as the standard cosmological model (cf., however, [68] for earlier observational evidence of a nonzero Λ). However, several key components of the Λ CDM model remain unknown, including the physical origin of Λ (or, more generally, dark energy), the nature of dark matter, and the establishment of initial conditions for cosmic structures. Meanwhile, several observational challenges to Λ CDM have emerged as the precision of cosmological measurements improves (e.g., [69]). Massive spectroscopic surveys are expected to help address these issues. By analyzing the clustering of large-scale structures (LSS) from spectroscopic data, we can investigate the properties of dark energy and dark matter through the dynamic evolution of the Universe governed by these competing components and extract signatures of fundamental physical processes at an extremely high energy scale in the primordial Universe.

In this section, we review the scientific motivations for the next-generation (Stage V) spectroscopic survey to be carried out by MUST. Figure 3 shows some of the key scientific cases that can be tested by MUST with a high significance level.

3.1 Nature & Evolution of Dark Energy

Dark energy is one of the key scientific problems of our time, posing a significant challenge to the Standard Model of particle physics. While CMB observations suggest that dark energy constitutes about 70% of the energy density of the Universe in the Λ CDM model [4], its physical properties are largely unexplored. One exception is the equation of state (EoS) parameter w , which influences the dynamics of the Universe and can be probed through geometrical measurements. The most straightforward interpretation of dark energy is the cosmological constant (Λ), corresponding to a constant $w = -1$, which is well consistent with most observations to date (e.g., [4, 10]). A natural extension beyond Λ involves introducing dynamic dark energy, which potentially originates from various physical mechanisms [70] and

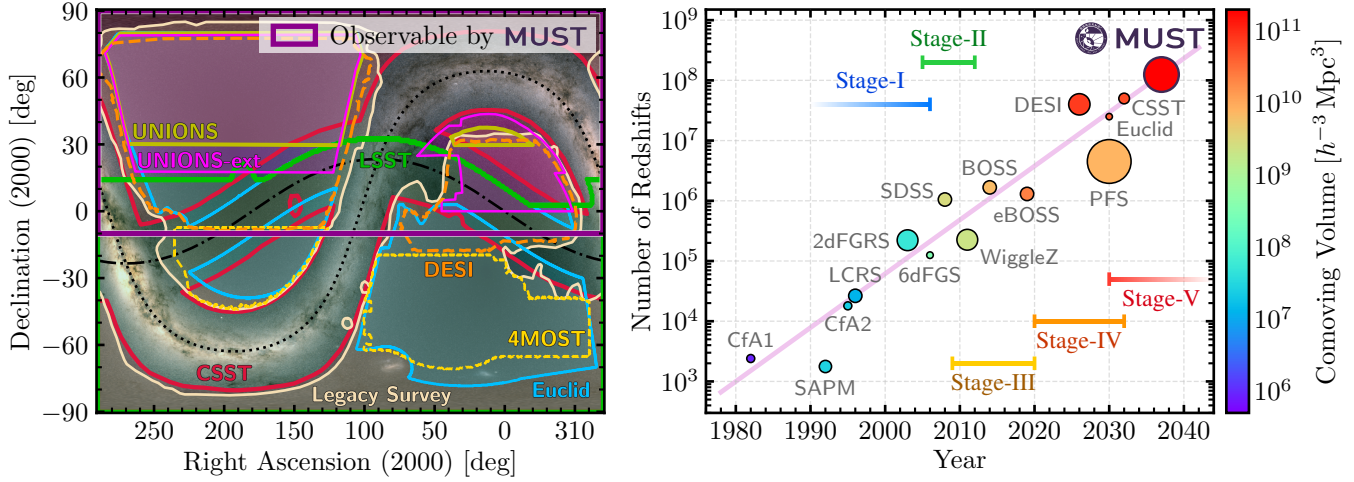


Figure 2 *Left panel:* full-sky map showing the region observable by MUST (declination above -10°), overlaid with the footprints of relevant imaging surveys (Legacy Survey, CSST, UNIONS, LSST, and Euclid) and spectroscopic surveys (DESI and 4MOST) on top of the stellar density map from *Gaia* EDR3 [64]. The black dotted and dash-dotted lines show the Galactic and ecliptic planes, respectively. *Right panel:* accumulation of galaxy and quasar redshifts from spectroscopic surveys since the early 1980s. The aperture of the telescopes scales the sizes of circles used, and filled colors represent the comoving volumes probed by direct LSS tracers (excluding Ly α forest tracers). Also shown are the rough divisions between stages of the spectroscopic surveys. MUST aims to become the first Stage-V survey in operation by the early 2030s.

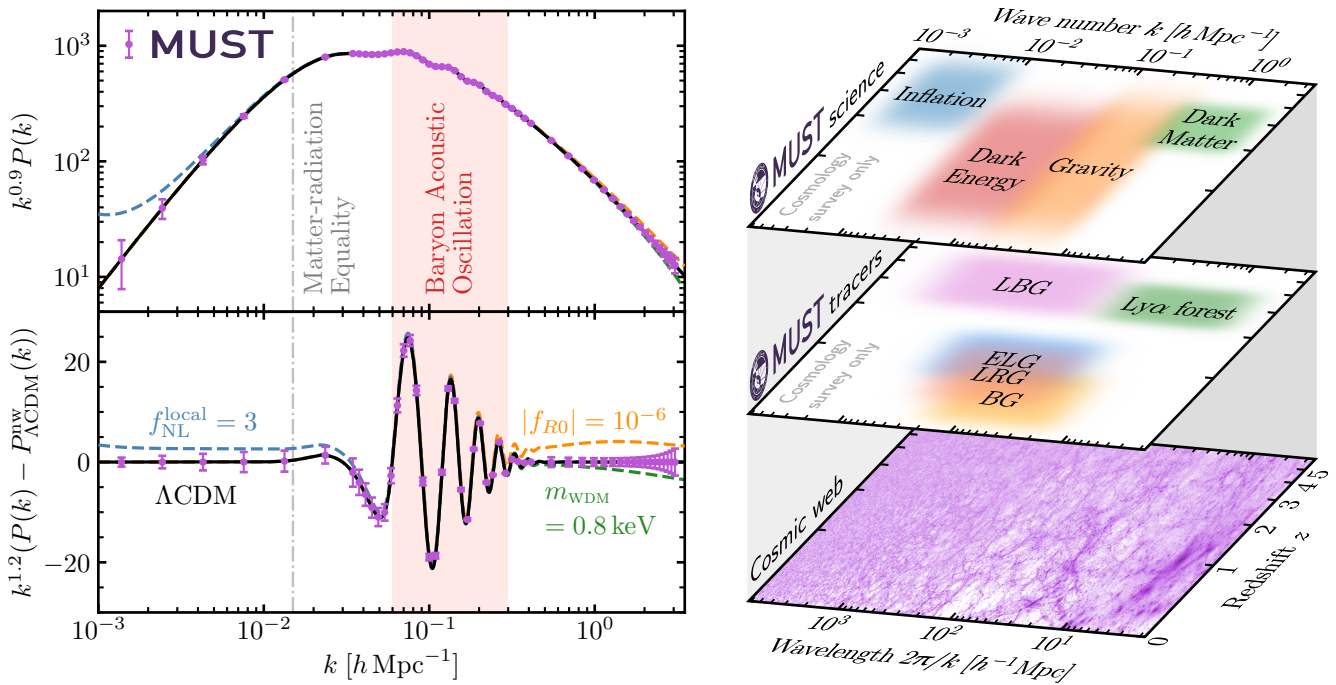


Figure 3 *Left panel:* linear galaxy power spectra for various cosmological models, with forecasted error bars based on the current survey design of MUST. The error bars are centered on the Planck 2018 Λ CDM cosmology [65], and the models include additional components that reflect the key science cases of MUST: local-type primordial non-Gaussianity with $f_{\text{NL}}^{\text{local}} = 3$, $f(R)$ gravity with $|f_{R0}| = 10^{-6}$, and warm dark matter with a particle mass of $m_{\text{WDM}} = 0.8$ keV. Error bars for $k < 0.4 h \text{ Mpc}^{-1}$ are estimated using Eq. (18), with the expected bias and number density of Lyman-break galaxies. For $k > 0.4 h \text{ Mpc}^{-1}$, errors are from forecasts of the Ly α 3D power spectrum, accounting for spectroscopic systematics and the quasar luminosity function. All power spectra and error bars are rescaled to match the amplitude of the matter power spectrum in the fiducial Λ CDM model for visual clarity. *Right panel:* illustration of the key science cases (top), primary LSS tracers (middle), and the underlying dark matter density field (bottom) across different scales and redshifts targeted by MUST.

leads to a time-evolving EoS parameter typically expressed as the so-called Chevallier-Polarski-Linder (CPL) parametrization [71, 72]:

$$w(a) = w_0 + w_a(1 - a), \quad (1)$$

where w_0 is the current value of w and w_a quantifies its time evolution. For instance, the quintessence model, which describes a dynamical scalar field minimally coupled to gravity, typically yields $w \gtrsim -1$, whereas the phantom energy, a

scalar field with negative kinetic energy, predicts $w < -1$. Observational constraints on w_0 and w_a provide a pathway to distinguishing these models.

The constraints on EoS parameters rely primarily on geometrical probes, including “standard(-isable) candles” such as Cepheids and type Ia supernovae (e.g., [7]), and “standard rulers” such as Baryon Acoustic Oscillations (BAO; [73]) and the matter-radiation equality scale (e.g., [74]). BAO arises from acoustic density waves in the primordial Universe and produces an excess of matter correlation amplitude at a characteristic comoving scale of $\sim 100 h^{-1}$ Mpc. By extracting the BAO signal from the clustering of matter tracers, such as galaxies and QSOs, we can probe the expansion rate of our Universe and thus constrain dark energy models. Recently, the tomographic Alcock–Paczynski (AP) test, which performs geometrical measurements based on the response of the apparent shape of galaxy clustering to the adopted cosmological model for redshift-to-distance conversion, has also been shown as a complementary probe of dark energy [75].

Observational programs for measuring the dark energy EoS have been strategically planned to proceed through successive stages of cosmic surveys, as outlined in the Dark Energy Task Force report [15]. Since the first detections of the BAO signal from galaxies at $z < 0.47$ [12, 76], subsequent spectroscopic surveys have extended BAO measurements to galaxies across a wide redshift range (up to $z < 1.5$), as well as QSOs and Lyman- α tracers at even higher redshifts [10]. These efforts have substantially improved the precision of w measurements. Recently, DESI, a Stage-IV dark energy survey, reported a w consistent with Λ CDM with an uncertainty of $\sim 2.5\%$ [77]. However, when the EoS is allowed to vary over time, current spectroscopic data hint at the potential dynamical behavior of dark energy [77, 78]. With its unprecedented survey efficiency, MUST is expected to deliver even more precise BAO measurements, covering a redshift range from the nearby Universe to $z \sim 5.5$. Thus, MUST meets the requirements of a Stage-V dark energy survey suggested by the Snowmass Cosmic Frontier report [79] and may offer deeper insights into the potential evolution of dark energy (see Section 5.2). Additionally, we will investigate the possibility of improving dark energy constraints using alternative probes, such as the tomographic AP test and the matter-radiation equality scale.

3.2 Growth of Structure & Nature of Gravity

Within the framework of hot Big Bang cosmology, gravity amplifies primordial density perturbations of the order of 10^{-5} , seeded by inflation, in an expanding cosmic background, leading to the formation and growth of large-scale structure (LSS). As a result, the growth of structures is a sen-

sitive probe of both gravity theories and dark energy. Notably, in modified gravity theories that deviate from General Relativity (GR), the intrinsic relationship between structure growth and geometrical quantities is generally altered or even disrupted. Thus, monitoring the structure growth over time provides stringent tests of gravity theories [80].

The growth of cosmic structures largely shapes the spatial correlations and the amplitude of peculiar velocities of galaxies. One prominent effect is redshift-space distortions (RSD; e.g., [81]), where the observed redshift maps of galaxies are distorted by their peculiar velocities along the line of sight. This distortion leads to the anisotropic clustering of galaxies, which allows for measurements of the autocorrelation of galaxy velocity divergence $P_{\theta\theta}$ and its cross-correlation with galaxy densities $P_{g\theta}$. In this context, the effect of structure growth can be parameterized through the combination of the linear growth rate and the amplitude of matter fluctuations $f\sigma_8$, as the power spectra scale as $P_{\theta\theta} \propto (f\sigma_8)^2$ and $P_{g\theta} \propto f\sigma_8$ (e.g., [82]).

Another common approach to testing gravity theories is to compare the two gravitational potentials Ψ and Φ by parameterizing them with phenomenological functions μ and Σ that linearly perturb GR (e.g., [10, 83, 84]). Many modified gravity theories of cosmological interest can be represented using the following equations, which allow the two potentials to differ:

$$k^2\Psi = -4\pi G a^2(1 + \mu(a, k))\rho\delta, \quad (2)$$

$$k^2(\Psi + \Phi) = -8\pi G a^2(1 + \Sigma(a, k))\rho\delta. \quad (3)$$

Here, ρ indicates the background matter density and δ is the comoving density perturbation. The functions μ and Σ effectively describe the variations of the matter density field and changes of the lensing effect on massless particles, respectively. Comparing measurements of μ and Σ to their fiducial values of zero thus constitutes a test of deviations from GR.

Galaxy spectroscopic surveys enable measurements of structure growth through both correlations of galaxy velocities and comparisons of the spatial clustering of galaxies across different redshifts. Testing gravity is, therefore, a primary scientific motivation of recent spectroscopic surveys, such as SDSS and DESI [11, 85]. Currently, measurements of structure growth at $z \lesssim 1$ have achieved precision at the $\lesssim 10\%$ level (e.g., [10], see also Section 5.3). While results from spectroscopic surveys are generally consistent with predictions of the GR- Λ CDM model, the structure growth history at high redshifts remains largely unexplored. Probing this regime is essential for differentiating between various gravity theories. As a Stage-V cosmological survey, MUST is expected to fill in this gap and provide substantial improvements in our understanding of gravity theory, as well as deeper insights into the tension between cosmic shear and matter perturbations from CMB measurements (e.g., [8]).

MUST also has the potential to measure relativistic effects, such as the gravitational redshifts, that are sensitive to gravity theories but have been too subtle to be detected with current data [86]. These effects can introduce additional distortions to galaxy clustering beyond RSD, primarily generating odd Legendre multipoles in the cross-correlation of different galaxy populations that can be measured from galaxy spectroscopic data.

3.3 Inflation & Primordial Physics

Large-scale structures (LSS) of the Universe not only trace the evolution of the Universe but also encode rich information about its initial conditions generated during a primordial era. The most prominent scenario for the primordial universe is cosmic inflation, which refers to a nearly exponential expansion of the universe by roughly 60 e -folds in a blink. To probe the microscopic quantum fluctuations of spacetime and matter/fields during inflation, which led to the formation of the LSS [87, 88], is a primary motivation for MUST.

Through setting the initial conditions of the LSS, inflationary cosmology provides a wealth of observables that reveal the dynamics of the primordial universe and, more interestingly, the fundamental physics at the inflation scale. Current theory and observations suggest that the inflation scale could be up to $O(10^{13} \text{ GeV})$ [89], which is much higher than the energy scale of any imaginable terrestrial experiments. Therefore, primordial fluctuations provide a unique window into high-energy fundamental physics, complementing other high-energy experiments.

The inflation predictions for the primordial scalar power spectrum have been delicately measured at the CMB scale through the overall amplitude, A_s , and the spectral index, n_s , [89]. These parameters are also expected to be measured by MUST by extracting the primordial scalar power spectrum from the LSS data. However, due to the near-scale invariance of the scalar fluctuation at large scales, the information extractable from the power spectrum is limited, although there have been ongoing efforts in searching and understanding tiny scale-dependent (and very often oscillatory) features in the power spectrum [90, 91]. On the other hand, a vast amount of information can be revealed by going to higher n -point ($n \geq 3$) correlations of scalar modes, which are traditionally known as primordial non-Gaussianity (PNG; [92, 93]). There is in principle fruitful information encoded in the PNG, though historically, many efforts have been made to the search of 3-point statistics, such as bispectra $B(k_1, k_2, k_3)$ on a few particular shapes (the bispectrum dependences on the ratios of k_i where $i = 1, 2, 3$), including the local, equilateral, and orthogonal shapes (e.g., [94-97]).

The overall amplitudes of these shapes are parameterized

by dimensionless parameters called f_{NL} , which are crucial cosmological parameters for the next generation LSS surveys. Within typical single-field slow-roll inflation models, it is worth noting that the minimal signal of equilateral bispectrum coming from the gravitational interaction of the scalar modes is $f_{\text{NL}} \sim O(10^{-2})$, which, if detected, would mark our detection of gravitational interaction [98]. However, other fundamental interactions, particles, and fields besides the inflaton field may carry stronger-than-gravity coupling to the scalar mode. Thus, it is possible that more significant signals can be detected, which will revolutionize our understanding of the primordial universe and fundamental physics. Typically, $f_{\text{NL}} \sim 1$ is a crucial threshold for the theories with and without the slow-roll condition [99, 100].

There have been active searches of f_{NL} , especially for the local shape ($f_{\text{NL}}^{\text{local}}$), but a firm detection has not been made yet. The state-of-the-art constraint comes from CMB measurements by Planck, with $f_{\text{NL}}^{\text{local}} = -0.9 \pm 5.1$ [101]. Meanwhile, galaxy spectroscopic surveys are becoming increasingly promising, as LSS clustering can be highly sensitive to the PNG through scale-dependent galaxy bias [87, 102, 103]. Current bound on the local shape PNG from spectroscopic surveys is $|f_{\text{NL}}^{\text{local}}| \sim O(10)$ [104]. MUST, as a Stage-V spectroscopic survey, is expected to improve the constraints on f_{NL} significantly with the benefit of the increasing survey volume and redshift range, surpassing current CMB constraints (see Section 5.4).

Besides the traditional PNG searches, recent years have witnessed the fast development of new directions, such as cosmological collider (CC) physics. For instance, oscillatory signals of n -point correlation functions can be generated by the resonance between heavy states spontaneously created during inflation and scalar (or tensor) modes and encode a wealth of information about the evolution history of spacetime and the dynamical information of the heavy particle, including the mass, spin, sound speed, chemical potential, interaction type, etc. [105, 106] Meanwhile, parity-odd patterns in galaxy clustering have gained considerable attention recently. If confirmed, they will be a clear signal of new physics. Active efforts are ongoing in search of these signals in current data and forecasts for detectability from future observations [103, 107-109]. To maximize the potential scientific outcome of MUST, we aim to explore the feasibility of achieving these goals with MUST in subsequent studies.

3.4 Neutrinos & Light Relics

The existence of neutrino mass, as revealed by atmospheric and solar neutrino experiments, provides strong evidence for new physics beyond the Standard Model. Neutrino oscillation experiments suggest two possible hierarchies in their

mass spectrum: the normal ($m_1 < m_2 < m_3$, $M_\nu \gtrsim 0.059$ eV) and the inverted ($m_3 < m_1 < m_2$, $M_\nu \gtrsim 0.099$ eV) hierarchies, where m_1 , m_2 , and m_3 indicate the 3 mass eigenstates, and M_ν denotes the total neutrino mass [110]. Determining the mass hierarchy is essential for understanding the nature of neutrinos (Dirac or Majorana) and formulating a generalized standard model. However, the most stringent constraint on M_ν from current particle physics experiments, set by the KATRIN experiment [111], is only $M_\nu \lesssim 1.4$ eV at the 90 % credible level (CL). This limit is insufficient to distinguish between the mass hierarchies.

Neutrinos act as radiation in the early Universe and subsequently contribute matter-energy budget at the late Universe with $\Omega_\nu = M_\nu/(93.14 h^2 \text{ eV})$, which alters the expansion rate and shifts the redshift of matter-radiation equality. Besides, due to their significant velocity dispersion, massive neutrinos slow down the growth of structures, resulting in a suppression of the matter power spectrum below the neutrino free-streaming scale [112, 113]. As a result, LSS probes are sensitive to the total neutrino mass, providing complementary constraints to particle physics experiments.

In addition to neutrino mass, the clustering of galaxies also permits constraints on the effective number of neutrino species N_{eff} , which can be used to probe non-standard neutrino interactions [114, 115] or extra light thermal relics from the primordial Universe, such as light sterile neutrinos [116] and axions [117-119]. This is because N_{eff} can be inferred from the phase shift of the BAO spectrum. Any deviation from the value $N_{\text{eff}} = 3.044$, as predicted by the standard cosmological model with 3 massive neutrino species, notably if exceeding 1%, would indicate new physics beyond the Standard Models of particle physics and cosmology.

It is worth noting that the constraints on M_ν and N_{eff} from CMB alone exhibit a geometrical degeneracy with H_0 (or Ω_m). BAO measurements can help break this degeneracy due to their ability to constrain Ω_m [4, 78]. Combining CMB and LSS data has already led to more stringent constraints on M_ν than those from terrestrial experiments, approaching the lower bound in the inverted hierarchical scenario [120-122]. Recently, DESI reported an upper bound of $M_\nu < 0.072$ eV (95% CL) with a prior of $M_\nu > 0$ eV, and updated the constraint $N_{\text{eff}} = 3.10 \pm 0.17$, which is in remarkable agreement with the Standard Model expectation. With its significantly larger survey volume and increased tracer number density, MUST is expected to substantially tighten constraints on both parameters and investigate the possibility of distinguishing between the two mass hierarchies in combination with data from next-generation CMB experiments (e.g., CMB-S4 [123]).

3.5 Dark Matter

Although dark matter (DM) – which constitutes $\sim 25\%$ of the energy density of the Universe – was first postulated almost 90 years ago [124], its fundamental nature remains unknown. Observational efforts have focused mainly on the cold dark matter (CDM) paradigm, yet its constituents remain elusive, prompting interest in alternative DM models. These alternative models aim to address specific challenges to the CDM model, such as the missing satellite, cusp-core (e.g., [125, 126]), and too-big-to-fail problems [127] (see [128] for a review).

Popular alternatives to the CDM model include warm dark matter (WDM; see e.g., [129, 130]), fuzzy dark matter (FDM; [131, 132]), self-interacting dark matter (SIDM; [133, 134]), and primordial black holes (PBH; see e.g., [135, 136]). These models gain traction for their potential to mitigate the challenges of CMB or for their natural origin, such as PBHs, which do not require new physics beyond the standard model. MUST can offer unique insight into discovering the nature of dark matter primarily through two avenues: Milky Way (MW) and Local Group (LG) observations, as well as the Ly α forest.

In the current *Gaia* [137] era, the measurement of the dark matter distribution around our Milky Way based on stellar kinematics still has significant uncertainties (e.g., [138]). One dominant reason is the lack of stellar tracers with full phase-space information in the outer Milky Way halo ($\gtrsim 100$ kpc). MUST can measure the line-of-sight velocities (LOSv) of a plethora of MW halo stars, which, in combination with a deep proper motion survey (e.g., the Roman space telescope high-latitude survey [139]), will allow for the mapping of the local distribution of dark matter (e.g., [140]) around our MW, enabling constraints on the radial mass profile and 3D shape of the MW dark halo, which will significantly benefit direct dark matter detection programs (e.g., [141]).

In particular, the ongoing Stage-IV DESI Milky Way survey (MWS; [142]) reaches $\sim 20 - 30\%$ completeness for MW targets in the flux range of $16 < r < 19$. MUST can potentially reach fainter magnitudes than DESI and thus can provide more distant MW halo star LOSVs, increasing completeness at similar magnitudes to DESI and providing better constraints on the dark matter distribution in the outer halo. In addition to halo stars, dwarf galaxies and stellar streams around our MW and in the LG carry valuable information on the nature of dark matter (e.g., [134, 143-148]), and MUST can potentially measure the LOSVs for member stars in distant dwarf galaxies or streams to better infer their mass content or past interactions with dark matter clumps.

The Ly α forest consists of absorption features in the spec-

tra of distant quasars caused by Lyman- α transitions of neutral hydrogen in the foreground intergalactic medium (IGM). Thus, the Ly α forest is a biased tracer of the neutral hydrogen distribution, and hence, it probes the underlying dark matter density field. As a dark matter probe covering higher redshifts than traditional galaxy surveys, the forest has been used to measure the BAO feature; nonetheless, its relatively high redshift $2 \lesssim z \lesssim 5$ and sensitivity to small-scale clustering (\gtrsim Mpc) make it an ideal probe of dark matter models⁹⁾. For instance, constraints from the 1D Ly α flux power spectrum, obtained from medium and high-resolution spectra, set a firm lower limit on the WDM particle mass of $m_\chi \geq 5.3 - 5.7$ keV [151, 152].

Although MW astrophysics and the Ly α forest can provide robust dark matter constraints, the accuracy of these constraints depends on careful modeling of baryonic physics and nonlinearities (e.g., [149]). In particular, Ly α forest constraints require precise modeling of IGM astrophysics [153-156] due to the degeneracies between the response of IGM to cosmic reionization and the impact of non-cold dark matter on the thermal state of the IGM. With a conservative flux limit of $r \leq 23.5$ (larger than that of DESI, which is $r < 23$) and an estimated quasar number density surpassing 80 deg^{-2} at $z > 2.1$, MUST is expected to refine our ability to constrain dark matter models using the Ly α forest (see Section 5.6 and Figure 13).

3.6 Synergy with Other Probes

3.6.1 Imaging surveys

Next-generation space-based wide-field imaging surveys, such as the China Space Station Telescope (CSST; [17]), Euclid [157], and Roman [158], will measure galaxy shears with unprecedented precision, providing tighter constraints on dark energy through weak lensing. The ground-based Legacy Survey of Space and Time (LSST; [20]) will observe the whole southern sky every few nights, building the most extensive catalog of transient phenomena of cosmological interest, such as type Ia supernovae or variable AGN. Other imaging surveys worth noting are the Hyper Suprime-Cam Subaru Strategic Program (HSC-SSP; [159, 160]) and the Mozi Wide Field Survey Telescope (WFST; [161]), which will provide deeper broadband sky coverage than currently available data, as well as the Javalambre Physics of the Accelerating Universe Survey (J-PAS; [162]), a narrow-band imaging survey with higher-precision photometric redshifts.

Apart from using imaging data from these surveys for MUST target selection, we aim to maximize the scientific

outcome through joint analyses of the data for cosmological measurements or even dedicated coordinated observations. For instance, the spectroscopic and photometric samples can be cross-correlated to break degeneracies associated with intrinsic alignments and galaxy bias, thus improving the precision of cosmological measurements (e.g., [163, 164]). Additionally, spare fibers from MUST can be used to complete the spectroscopic data of galaxies in color space, thereby expanding the training set for calibrating photometric or slitless spectroscopic redshift measurements (e.g., [31, 165]). The high efficiency and large survey volume of MUST offers opportunities to identify or confirm strong lensing systems, e.g., low- z bright galaxies with anomalously high- z emission lines [166]. Moreover, the cross-correlation between imaging data and Ly α forests from MUST may enable tracing LSS using Ly α intensity mapping [167].

3.6.2 CMB S4

The next generation of CMB experiments, such as AliCPT [168], Simons Observatory [169], CMB-S4 [170], LiteBIRD [171], and PICO [172], holds significant promise for detecting primordial gravitational waves from the early-universe inflationary epoch. Precisely measuring primordial gravitational waves faces two significant obstacles: foreground contamination and gravitational lensing distortions. Consequently, accurate reconstruction of the CMB lensing potential is critical for isolating the primordial signal. Multi-tracer delensing methods, which leverage galaxy survey data, are expected to significantly enhance the capability of CMB experiments to detect the elusive primordial gravitational waves [173].

In addition to enhancing our understanding of inflationary physics, MUST will facilitate synergistic investigations of large-scale structures. This includes the measurement of the kinetic Sunyaev-Zel'dovich (kSZ) effect, which provides insights into the dynamics of baryonic matter (e.g., [174]). Furthermore, cross-correlations with CMB lensing will improve our understanding of structure formation (e.g., [30]). With these complementary approaches, MUST, in combination with next-generation CMB experiments, promises to enrich our understanding of cosmic evolution.

3.6.3 Radio surveys

The Square Kilometre Array (SKA; [48]) will conduct an IM program using the 21 cm hyperfine transition of neutral Hydrogen. Due to the significant disparity in strength between foreground emissions and the cosmological 21 cm

⁹⁾ However, the Ly α forest is unlikely to detect subtle differences between dark matter models [149], such as the oscillations predicted by FDM at very small scales [150].

signal — differing by several orders of magnitude — confirming the cosmic origin of the signal, particularly at high redshifts ($z \gtrsim 1$), will likely require cross-correlations with other cosmological tracers. Current studies typically focus on cross-correlations with high-redshift galaxies [175, 176], LBG [177], and the Ly α forest [178, 179]. These complementary approaches, coupling 21 cm measurements with spectroscopic surveys, enhance our ability to discern the cosmological signal from foreground contamination, thus improving the robustness of IM measurements.

MUST will significantly enhance cross-correlation efforts involving 21 cm observations with high-redshift galaxies and the Lyman- α forest, enabling measurements with high signal-to-noise. Such cross-correlations will be instrumental in advancing our understanding of various cosmological phenomena, such as dark energy constraints [180], modified gravity [181], dark matter [182], and hydrogen reionization [179].

3.6.4 Gravitational waves and Fast Radio Bursts

Very high-energy, transient phenomena such as gravitational waves and Fast Radio Bursts (FRBs) may also provide valuable cosmological constraints. Ever since the first detection of a gravitational wave event by LIGO [183], several large observatories are projected, e.g., LISA [184], Taiji [185], TianQin [185] and the Einstein Telescope [186]. In addition to the detection of singular events, the gravitational wave background has also been recently detected by Pulsar Timing Array collaborations (e.g., NANOGrav, [187], CPTA [188], EPTA, [189]). Regarding FRBs, current radio observatories regularly detect these events, compiling ever-growing catalogs with hundreds of events (e.g., CHIME [190], ASKAP [191], MeerKAT [192], and FAST [193]).

The most direct synergy MUST will have is the measurement of redshifts and peculiar velocities for both gravitational waves and FRBs electromagnetic (EM) counterparts. Gravitational waves from binary inspirals act as standard sirens since their luminosity distance can be inferred from their observation [194]. Hence, a redshift measurement of its EM counterpart (either a transient event or a host galaxy) can provide an independent measurement of the Hubble constant [195], and a large spectroscopic catalog of gravitational wave EM counterparts may yield independent H_0 measurements with a precision of few percent [196]. In addition to the direct observation of gravitational wave EM counterparts, cross-correlation of gravitational wave events with spectroscopic galaxy catalogs may also yield improved joint constraints on H_0 [197, 198].

Similarly, the distance to FRBs may also be determined by their dispersion measure [199]. However, this method presents degeneracies with the baryon distribution in the FRB

sightline, which in turn allows FRBs to constrain the baryon content of the Universe [200, 201]. Regardless of these degeneracies, measurements of H_0 using FRBs and spectroscopic redshifts of their host galaxies are possible [202, 203]. Therefore, MUST will undoubtedly help with these measurements of H_0 by providing unprecedentedly large spectroscopic redshift catalogs of potential gravitational wave and FRB hosts.

4 Target Selection

We must pay special attention to selecting targets from imaging surveys to achieve the scientific goals outlined in the previous section. There are two main requirements for cosmological target selection: 1) There should be easily identifiable spectral features, such as strong emission lines, absorption features, or continuum breaks, to enable redshift determination with a minimal exposure time; 2) The target density must be optimized to balance the cosmic variance and shot noise to maximize the precision of cosmological measurements. This section explores target selection criteria suitable for MUST and addresses these concerns.

4.1 Challenges of Target Selection for Stage-V Spectroscopic Surveys

Unlike spectroscopic surveys using a prism (e.g., PRIMUS, [204, 205]), grism (e.g., 3D-HST, [206]; Euclid [18]), or IFS (e.g., HETDEX [207]), modern surveys using multi-slit instruments or robotic fiber positioners require careful and sophisticated target selection based on multi-band imaging data. Starting from the Main Galaxy Sample (MGS) in SDSS, a primarily flux-limited sample, the following surveys have gradually expanded the number of different samples. As a Stage-IV survey, the main survey of DESI has already included low-redshift bright galaxies (BGS; [208]), luminous red galaxies (LRG; [209]), emission-line galaxies (ELG; [210]), and quasi-stellar objects (QSO; [211]). Selecting these samples now involves more complex selection criteria, including multiple color cuts, cross-matching with multi-wavelength datasets, and the application of machine learning-based methods (e.g., [212, 213]).

These changes reflect the increasingly demanding scientific and operational requirements of modern surveys. A survey must design flexible programs for bright & dark nights and different observing conditions while maximizing the fiber efficiency and the scientific output of the project. More importantly, for LSS redshift surveys, target selection design needs to ensure the volume densities, redshift distributions, and average halo biases of different LSS tracers meet the re-

| Project | Survey Name | Survey Area (deg ²) | Imaging Depth (AB Mag) | | | | | | | | | Reference |
|---------------|--------------------------------|------------------------------------|------------------------|----------|----------|---------------|----------|----------|-------|-------|-------|--|
| | | | NUV | <i>u</i> | <i>g</i> | <i>r</i> | <i>i</i> | <i>z</i> | Y | J | H | |
| CSST | Optical Survey Wide | ~ 17,500 | 25.40 | 25.40 | 26.30 | 26.00 | 25.90 | 25.20 | 24.40 | | | Zhan et al. 2010; Cao et al. 2018; Zhan et al. 2021 |
| | Optical Survey Deep | ~ 400 | 26.70 | 26.70 | 27.50 | 27.20 | 27.00 | 26.50 | 25.70 | | | |
| Euclid | Wide Survey | ~ 14,500 | | | | $I_E = 26.20$ | | | 24.50 | 24.50 | 24.50 | Scarmamella et al. 2022 |
| LSST | Wide Fast Deep (WFD) | ~ 14,500 | | 25.30 | 26.84 | 27.04 | 26.35 | 25.22 | 24.47 | | | DESC et al. 2018 |
| | North Ecliptic Spur (NES) | ~ 4,160 | | | 25.64 | 25.84 | 25.15 | 24.02 | | | | Assuming 1/3 visits of WFD |
| UNIONS | UNIONS/CFIS | ~ 4,861 | | 24.30 | 25.20 | 24.90 | 24.30 | 24.10 | | | | Ibata et al. 2017 |
| | Extended UNIONS <i>u</i> -band | ~ 8,988 | | 24.30 | | | | | | | | |
| Legacy Survey | DECaLS | ~ 9,000 | | | 24.65 | 23.61 | 22.84 | | | | | Dey et al. 2019 |
| | BASS + MzLS | ~ 5,000 | | | 24.30 | 23.70 | 23.04 | | | | | |
| Mozi | Wide Field Survey | ~ 8,000 | | 24.82 | 25.85 | 25.36 | 24.83 | 23.90 | | | | Wang et al. 2023 |
| HSC SSP | SSP Wide | ~ 1,400 | | | 26.50 | 26.50 | 26.20 | 25.20 | 24.40 | | | Aihara et al. 2022 |
| | SSP Deep+UltraDeep | ~ 37 | | | 27.40 | 27.10 | 26.90 | 26.30 | 25.30 | | | |

Table 2 Summary of available, ongoing, and planned imaging surveys that overlap with the potential footprint of MUST and can contribute to the target selection for LSS tracers of MUST. Please see the reference for details. The imaging depths represent the 5σ point source detection limits. However, we ignore the minor differences in aperture choices and filter differences between surveys. Please see Figure 2 to visualize their footprints.

quirements for constraining the cosmological model. At the same time, the target selection should intentionally minimize the systematics inherited from the imaging surveys, such as target density fluctuations induced by variations in imaging depth, observing conditions, Galactic extinction, and data reduction issues. As the number of redshifts rapidly increases, the Stage-IV spectroscopic surveys have officially entered the low shot-noise regime, where systematic issues from target selection are becoming critical for the cosmological potential of the survey. Looking forward to the Stage-V era for MUST, we anticipate not only the continued development of these trends but also new challenges.

In particular, the LSS survey of MUST faces two outstanding challenges. First, the high-redshift ($2 < z < 5$) surveys of Stage V require new LSS tracers that differ from those adopted by Stage III and Stage IV projects, such as the ELG and LRG. The best candidates are Lyman Break Galaxies (LBG) selected using the Lyman-break “dropout” technique and the Lyman- α Emitters (LAEs) traditionally identified in narrow-band imaging surveys. These types of high- z populations, representing galaxies with a wide range of stellar mass, star-formation rate, and halo properties (e.g., halo bias), should be able to continuously cover the redshift range observable by the spectrograph of MUST ($2 < z < 5$) with sufficient tracer densities (e.g., [214]). However, while the high- z galaxy community has been studying these populations extensively for two decades now (e.g., Hu & McMahon 1996 [215]; Cowie & Hu 1998 [216]), we still have not acquired the demanding broad- and narrow-band imaging capabilities to select them for a Stage-V survey and also have not fully understood their cosmological potential as existing deep field studies are still limited by cosmic variance among other systematics. As the LSS survey community has begun

to pay attention and organize pilot programs (e.g., [21, 217]), we expect to gain a better understanding of these new LSS tracers before the first light of MUST. The proposed DESI-II project is exciting as it could start the first LSS survey using LBG and LAEs in ~2029, gaining valuable insights before the operation of MUST.

Secondly, given the site selection of MUST in the northern hemisphere, we do not enjoy the deep & uniform multi-band imaging coverage of the Legacy Survey of Space and Time (LSST) of the Vera C. Rubin Observatory in the south. Based on the current landscape of imaging surveys in the north, no similar survey is expected to be available before the 2030s. The *left* panel of Figure 2 visualizes the footprints of major imaging surveys that overlap with the potential footprint of MUST and can contribute to the target selection of MUST. We also summarize their survey areas and imaging depths in Table 2. Assuming MUST will observe targets with air-mass better than 1.5, at the Lenghu site, MUST can cover the $\delta \geq 10^\circ$ footprint. Within this area, no imaging survey can cover the high Galactic latitude region suitable for an LSS survey. In the ideal scenario, the Chinese Space Station Telescope’s optical survey (CSST-OS) will provide the best multi-band support from the NUV to the Y-band. The NUV and *u*-band observations are particularly important for selecting $z > 2$ LBG. Meanwhile, the *Euclid* mission will provide valuable near-infrared (NIR) coverage and deep observations in the broad I_E optical band. While the exact strategy has yet to be investigated, the synergy between optical and NIR images from space is expected to provide unique advantages and new perspectives for target selection. However, based on the current survey plan, both CSST and *Euclid* will avoid the region near the Ecliptic plane. For this region, the LSST survey should provide partial coverage, but most of it was covered by

10) <https://survey-strategy.lsst.io/baseline/minis.html>

the Northern Ecliptic Spur (NES) mini-survey¹⁰⁾ of ([218]), which will only observe in g , r , i , & z -filters with $\sim 1/3$ of the visits of the main Wide-Fast-Deep (WFD) survey. While the coadding depth is still competitive, the lack of u -band is unfortunate for the LBG selection. The ongoing Ultraviolet Near Infrared Optical Northern Survey (UNIONS) campaign using the 3.6 m CFHT, 2×1.8 m Pan-STARRS, and 8.2 m Subaru telescopes is another major candidate for multi-band target selection. In an ideal situation, the southern extension of UNIONS in the u -band to the northern limit ($\delta = +12^\circ$) of the main LSST survey will be especially valuable.

In addition to these ongoing or planned imaging surveys, we expect the available multi-band data from the Legacy Survey (in g , r , and z -bands; [219]) and the Hyper Suprime-Cam Subaru Strategic Program (HSC-SSP; [159]) will be essential for the development of target selection strategy for MUST: Legacy Survey satisfies the survey footprint requirements for a northern Stage-V project, while HSC-SSP, along with the UNIONS u -band data should meet or surpass the imaging depth requirements for MUST. Additionally, the 2.5 m Mozi wide-field survey telescope at Peak C of the Lenghu site has commenced operation. As a dedicated time-domain survey telescope that will continue its operation into the 2030s, its accumulated imaging depths will also be helpful to MUST. Moreover, the potential of imaging the northern sky using customized narrow- or medium-band filters to facilitate the selection of LAEs is an intriguing opportunity to be explored. We should also mention that CFHT, Subaru, and the 4.0 m Blanco telescope still have wide-field imaging capability that could support imaging campaigns to provide targeting selection support for any Stage-V spectroscopic surveys. In particular, the narrow- and medium-band surveys using the Dark Energy Camera (DECam; [220]), such as the One-hundred-deg² DECam Imaging in Narrowbands (ODIN; [221]), the Merian survey (e.g., [222]), and J-PAS (e.g., [162]) could demonstrate an interesting new approach for target selection for the Stage-V survey.

Put all together, we can see that MUST is facing the highly challenging task of developing a consistent target selection strategy that meets the strict requirements for a Stage-V survey. As this work focuses on the theoretical prediction of the potential of LSS cosmology, we will not dive deep into the details of target selection, as many of the imaging datasets mentioned above have yet to be available. Instead, in the following subsections, we will briefly introduce the concepts and assumptions of target selection for the LSS survey of MUST.

For the cosmological prediction, we will assume two scenarios for the survey footprints: the ideal scenario for the gray (dark) time survey will have a 13,000 deg² (11,000 deg²) footprint and a more conservative 11,000 deg² (8,000 deg²)

footprint.

4.2 Low-Redshift Tracers

Similar to the ongoing DESI survey, MUST can measure the redshift of $z < 1.57$ galaxies using the [O II] doublet emission lines at 3727 & 3729 Å, along with the other significant emission and absorption features in galaxies' spectra. While this "low-redshift" component is not the most critical one for the cosmological goals of MUST, it will be a valuable dataset that enables many other complementary cosmological probes, such as the multi-tracer clustering to explore the non-linear regime (e.g., [223, 224]), the cross-correlations with weak lensing surveys like CSST & *Euclid* and other multi-wavelength datasets (e.g., [9, 225, 226]), and the spectroscopic survey of galaxy clusters (e.g., [227, 228]).

For now, we assume that MUST will follow the recipes of DESI to select BGS [208], LRG [209], and ELG [210] samples as $z < 1.6$ LSS tracers. Conceptually, we plan to observe BGS and LRG samples as the bright night targets while observing ELG during the gray and dark nights.

By 2030, DESI and its extension should have finished collecting more than 40 million redshifts in this range. Therefore, we will only focus on targets fainter than those of DESI. Although the methods are similar, the BGS, LRG, and ELG samples for MUST were selected using photometric data from Legacy Survey DR10.1, rather than DR9. As Legacy Survey DR11 is scheduled for release in 2025, it would be interesting to check if the samples can be improved with this new release.

4.2.1 Bright Galaxy Sample (BGS)

For the high-density BGS sample, as DESI will have already observed BGS to $r < 20.175$ mag (including the FAINT sub-sample), MUST will observe fainter samples. Assuming that MUST can assign 2,000 fibers per deg² to observe BGS during a bright night, based on the target selection results of DESI, MUST will focus on the magnitude range of $20.175 < r < 21$ mag in the Legacy Survey data after making similar quality cleaning cuts in [208]. Firstly, we exclude stellar objects following [208] using the *Gaia* catalog to perform an additional magnitude cut:

$$G_{\text{Gaia}} - r_{\text{raw}} > 0.6. \quad (4)$$

Then, we use the spatial mask bits provided by the Legacy Survey to avoid targets polluted by bright stars in the vicinity. Those are defined as BITMASK 1, 12, and 13. Finally, to clean the sample from spurious objects and to ensure that the selection is based on high-quality observations, we perform

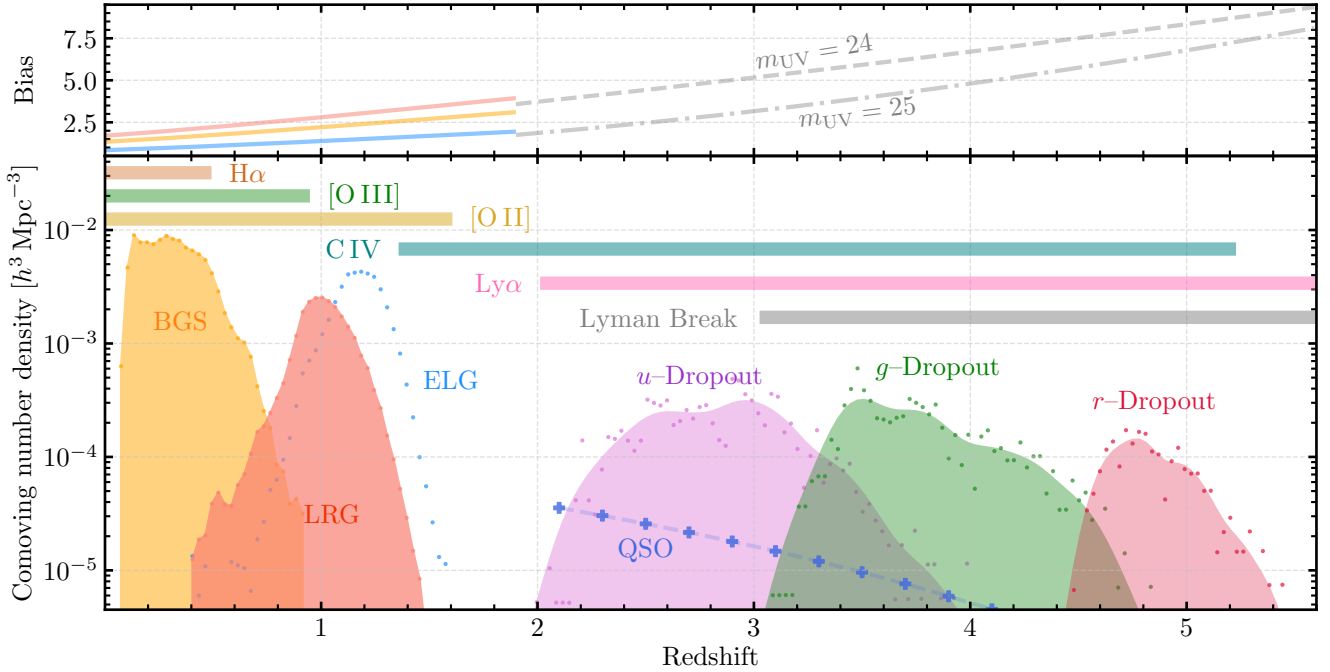


Figure 4 Preliminary target selection strategy for the LSS spectroscopic surveys of MUST. *Bottom* panel: redshift distributions and comoving number densities of the primary LSS tracers targeted by MUST at low-intermediate redshift ($z \lesssim 1.6$) and in the high-redshift Universe. At $z \lesssim 1.5$, MUST will densely sample the LSS using the low-redshift bright galaxy sample (BGS), luminous red galaxies (LRGs), and emission line galaxies (ELGs), with their [O II] doublets, other prominent optical emission lines ([O III], H_β , H_α , etc.), and significant absorption features. Horizontal colored bars indicate the wavelength coverage of the MUST spectrograph for different emission lines. At $z \gtrsim 2$, MUST will use the dropout technique to select Lyman-break galaxies (LBGs) over a large comoving volume to map the high- z LSS with unprecedented detail. Based on expected imaging data, we show initial target selection results for u -, g -, and r -dropout galaxies. For these LBGs, redshifts will be measured using the Lyman break feature, the Lyman- α emission line, and strong interstellar absorption lines such as C IV. MUST will also observe quasi-stellar objects (QSOs) at $z \gtrsim 2$ as complementary high-redshift LSS tracers. *Top* panel: redshift evolution models for the biases of BGS, LRGs, and ELGs at $z \gtrsim 2$, along with a bias model for LBGs with different UV magnitude limits. These models serve as the basis for the cosmological forecast presented in this work.

the following final cut:

$$\begin{aligned} -1 < (g - r) < 4, \\ -1 < (r - z) < 4, \end{aligned} \quad (5)$$

and we impose that the object has been observed at least once in the g , r and z bands. We have not made any cuts based on fiber magnitude as MUST will adopt a larger fiber size than DESI (1.3 v.s. 1.5 arcsec). We only require the target density and redshift distribution estimate for the cosmological forecast. For BGS, the detailed fiber magnitude or color cut should make little difference at this stage. We will apply them later for more accurate specifications.

In Figure 4, we show that the redshift distribution of the BGS sample ranges between $0.1 < z < 0.8$ with a broad peak between $z = 0.2$ to 0.4 . For the halo bias assumption for the BGS, as this work intends to compare with the forecast of DESI, we adopt the same bias evolution model used in the scientific requirement document of DESI [229]:

$$b_{\text{BGS}}(z) = 1.34/D(z), \quad (6)$$

where $D(z)$ is the linear growth factor that depends on the adopted cosmology [230].

In addition, by reaching $r < 21.5$ mag, MUST can increase the target density for BGS by $\sim 2,500 \text{ deg}^{-2}$. Even considering the fiber assignment efficiency and the redshift success rate, which should be higher than 95% given the fiducial exposure time, MUST can easily provide a dense sample of low- z galaxies for various cosmological probes.

4.2.2 Luminous Red Galaxies (LRG)

As their name suggests, LRG represents the massive and (mostly) quiescent galaxies at low redshift ($z \lesssim 0.8$). LRG typically resides in relatively massive dark matter halos with high LSS bias, making them a promising candidate to trace the matter distribution and provide high-quality BAO measurements (e.g., [12, 231]). As done for the BGS sample, we follow the LRG target selection recipe of DESI, but we avoid observing the same targets as the latter by setting a fainter magnitude limit. DESI adopted the z -band fiber magnitude $z_{\text{fiber}} < 21.6$ cut as the primary flux-limit cut for LRG. Although MUST will use fiber with a different core size, we use the same Legacy Survey z -band fiber magnitude definition to estimate the sample density and compare it with DESI.

Similar to the BGS, we assume a $2,000 \text{ deg}^{-2}$ fiber density for LRG as a bright or gray night target. After applying additional quality cleaning cuts, as in DESI, we can reach the desired target density using a sample with $21.6 < z_{\text{fiber}} < 22.8$. Firstly, we exclude stars on the $(r - z)$ v.s. $(z - W1)$ plane:

$$(z - W1) > 0.8 \times (r - z) - 0.6. \quad (7)$$

Then, to obtain targets at $z > 0.4$, we apply a $(g - r)$ v.s. $(r - W1)$ color cut:

$$(g - W1) > 2.97 \text{ OR } (r - W1) > 1.8. \quad (8)$$

Lastly, we make a color cut on the $(r - W1)$ v.s. $(W1)$ plane to isolate the most luminous galaxies (in $W1$ band) while keeping the same redshift distribution:

$$\begin{aligned} (r - W1) &> 1.83 \times (W1 - 17.13), \\ (r - W1) &> W1 - 16.31 \text{ OR } (r - W1) > 3.4. \end{aligned} \quad (9)$$

In all the above cuts, $W1$ is the $3.4 \mu\text{m}$ infrared band from the NEOWISE (e.g., [232]) data. Additional cuts to fine-tune the star-galaxy separation are performed by removing non-null proper motion or parallax having a signal-to-noise (SNR) ratio higher than 3 in the *Gaia* EDR3 catalogs [64]. Most *Gaia* detected objects have a magnitude higher than 18 mag, making them irrelevant to the LRG selection of MUST. Finally, as for the BGS, we applied the spatial masking BITMASK 1, 12, and 13 and required the object to have a minimum of one valid observation in g , r , z , and $W1$ band.

Figure 4 visualizes the target density and redshift distribution of our LRG selection, which ranges between $0.4 < z < 1.4$ and peaks at $z \sim 1.0$. For the bias evolution model of the LRG, we adopt the DESI one [229]:

$$b_{\text{LRG}}(z) = 1.7/D(z). \quad (10)$$

For LRG, our current z -band fiber magnitude limit approaches the detection limits of the Legacy Survey. But, at $z_{\text{fiber}} < 23.0$, MUST can already select a few hundred more LRG per deg^2 to compensate for the fiber assignment and redshift measurement loss to ensure the delivery of a $2,000 \text{ deg}^{-2}$ density LRG sample for cosmology. As we reach to fainter magnitude limit, the redshift distribution of the LRG sample for MUST shifts significantly toward a higher average redshift than DESI. As the current selection is still using LegacySurvey data, it is unclear whether this would be the best option for MUST, which should benefit from deeper imaging data from CSST, LSST, and Euclid. We will explore new approaches to select LRG using imaging data that are better suited to MUST in the upcoming work.

4.2.3 Emission Line Galaxies (ELG)

Emission-line galaxies represent the abundant, active star-forming galaxies at the peak of the cosmic star formation history ($1 \lesssim z \lesssim 2$). Their high comoving density and the relative ease of redshift confirmation via the doublet signature of the [O II] emission lines at rest-frame 3727 and 3729 Å make them appealing $z \gtrsim 1$ LSS tracers in the Stage-III and IV surveys (e.g., [210, 233]). Within the same redshift range, ELG represents the galaxy population that is less massive than the LRG. Therefore, the average halo mass and bias of ELGs are systematically lower than those of LRGs. There are also questions about their galaxy-halo connection model (e.g., [234, 235]), which could become a systematic for LSS analysis.

Stage-V surveys, such as MUST, can reach a significantly fainter magnitude limit, allowing for the observation of an even larger population of ELGs and exploration of their cosmological potential. Similar to the BGS and LRG samples, we will again follow the ELG selection method of DESI as described in [210] for our forecast. We assume that ELG are gray-time targets with an optimistic target density of $3,600 \text{ per deg}^2$ and a conservative density of $2,500 \text{ deg}^{-2}$. Compared to the ELG.LOP sample of DESI with a $\sim 1,940 \text{ deg}^{-2}$ density at g -band fiber magnitude brighter than 24.1 mag, we can achieve the desired target density by selecting ELG within the $24.1 < g_{\text{fiber}} < 24.6 \text{ mag}$ range and applying the same color and quality cuts used in DESI. Again, we ignore the difference in fiber core size between MUST and DESI.

Firstly, DESI designed two $(g - r)$ vs. $(r - z)$ color cuts to select ELG within the $0.6 < z < 1.6$ redshift range. These cuts also ensure the exclusion of stars while favoring the selection of strong [O II] emitters:

$$\begin{aligned} (g - r) &< 0.5 \times (r - z) + 0.1, \\ (g - r) &< -1.2 \times (r - z) + 1.3. \end{aligned} \quad (11)$$

At the same time, a $(r - z) > 0.15$ color cut is used to exclude $z > 1.6$ galaxies when their [O II] lines redshift out of the wavelength coverage of the spectrograph of DESI, which is very similar to that of MUST.

Similarly, we require the targets to have clean photometry in the g , r , and z bands and to be located far from bright stars or galaxies, using the spatial masking BITMASK 1, 12, and 13.

We show the redshift distribution of ELG and volume density in Figure 4. Since we copied the ELG selection recipe from DESI, it is unsurprising that this sample occupies the identical $0.6 < z < 1.6$ redshift range and peaks at $z \sim 1.2$. We adopt the same bias model as DESI [229]

$$b_{\text{ELG}}(z) = 0.84/D(z). \quad (12)$$

It is worth noting that while the density of ELG is significantly higher than that of DESI, our current target selection is still based on the relatively shallow Legacy Survey data, which was designed for Stage-IV surveys. Such selection is not optimized to isolate the targets at higher redshift, which should be the main focus of MUST. Deeper imaging data will help. Also, given the anticipated decrease of spectrograph throughput at $\lambda < 9000 \text{ \AA}$, the redshift success rate for faint ELG at the higher end of their redshift distribution strongly depends on the EW of the [O II] emission lines. We will search for improved color selections to isolate the strong-[O II] emitters at $z \gtrsim 1$.

4.3 High-Redshift Tracers

Starting from $z = 2.1$, the Lyman- α emission line at rest-frame 1216 \AA redshifts into the wavelength coverage at $\sim 370 \text{ nm}$ for the spectrograph of MUST and enables our high-redshift target selection for the Stage-V cosmological survey. Along with the Lyman break feature at rest-frame 912 \AA and a series of interstellar absorption lines, such as C II 1335 \AA , C IV 1548 \AA , O I 1302 \AA , Si II 1304 \AA , and more (e.g., [21, 236]), support the redshift measurements at $2.1 < z < 5.0$ of MUST. High- z LSS tracers are the bread and butter of a Stage-V cosmological survey, such as MUST. Until the Stage-IV surveys such as DESI, high- z QSOs are the primary LSS tracers at $z > 2$ (e.g., [237-240]). While these accreting super-massive black holes (SMBHs) present us the unique opportunity to explore the intergalactic medium (IGM) to constrain the nature of dark matter (e.g., [153, 241, 242]), their volume density is typically too low to become the principal LSS tracer in the Stage-V era.

Currently, the most promising candidates for $z > 2$ LSS tracers are the LBGs and LAEs (e.g., [21, 214, 217, 243]). Compared to LAEs, selecting LBG based on the broadband color criteria makes it easier to populate the $2 < z < 5$ redshift space continuously with sufficient density. Given the available data and previous works, we focus on the LBG populations as the primary LSS tracers for our cosmological forecast in this work. While not included in the Fisher forecast, we briefly discuss the potential for LAEs and QSOs.

We should note that LBG and LAEs are defined photometrically, not physically, with overlaps between these two populations. In fact, the success rate of redshift measurement for LBGs strongly depends on the presence of a prominent Lyman- α emission line, which often makes them LAEs.

4.3.1 Lyman-Break Galaxies (LBG)

LBG are galaxies with significant flux decrement, or a “break”, at the rest-frame wavelength shorter than the Lyman

limit (911.3 \AA) due to strong internal absorption by neutral Hydrogen. They represent the “normal”, young, star-forming high-redshift galaxies (e.g., [244-247]) with a large enough density to support LSS surveys. In observation, this break often translates into the non-detection in filters bluer than the observed frame of the Lyman limit (or a “dropout”) or a high color value using filters that place the break between them. Starting from [244], this method and its further development have helped select millions of LBG as candidates of high- z galaxies in $2 < z < 7$ (e.g., ~ 4.1 million from the Great Optically Luminous Dropout Research Using Subaru HSC, or GOLDRUSH project [248]). This mature approach is the foundation of high- z LSS tracer selection using deep broadband imaging surveys for Stage-IV and Stage-V surveys.

Motivated by the target selection for the proposed DESI-II, [21] validated the LBG selections based on a series of dropout criteria from the HSC SSP and the CLAUDS data using dedicated DESI campaigns and confirmed a $\sim 620 \text{ deg}^{-2}$ $r < 24.2 \text{ mag}$ LBG density at $2.3 < z < 3.5$ or a $\sim 470 \text{ deg}^{-2}$ $r < 24.5 \text{ mag}$ LBG density at $2.8 < z < 3.5$. Also aimed at the fixed $1,100 \text{ deg}^{-2}$ target density for DESI-II, [22] applies a Random Forest selection to the HSC+CLAUDS data and spectroscopically confirms a 493 deg^{-2} $z > 2.5$ under the imaging depth afforded by a UNIONS-like survey.

In [243], the authors considered the BX color selection in [249] centered at $z \sim 2.20$, the u -dropout selection based on the CFHTLS-Archive-Research-Survey (CARS; [250, 251]) centered at $z \sim 2.96$, and the g - & r -dropout selections based on GOLDRUSH centered at $z \sim 3.8$ & 4.9 . Based on imaging depths of LSST-Y10, the authors concluded that it is practical to spectroscopically confirm $2,000 R < 24.0 \text{ mag}$ BX galaxies, $500 i < 24.0 \text{ mag}$ u -dropouts, $330 i < 25.5 \text{ mag}$ g -dropouts, and $100 z < 25.5 \text{ mag}$ r -dropouts per square degree. Altogether, this supports a $\sim 3,000 \text{ deg}^{-2}$ confirmed high- z tracers that match the multiplex capability of MUST nicely. Interestingly, the authors note that the u -band imaging depth limits the photometric selection of u -dropouts. This assumes that one needs an actual detection in the u -band (or the band on the bluer side of the observed frame Lyman limit) to estimate the $u - g$ color to identify the break reliably, which is different from the dropout selections used to study the LBG populations (e.g., their luminosity function). It is worth investigating whether this is required to select LSS tracers with straightforward systematics. This is particularly important for MUST as heterogeneous imaging datasets will contribute to our target selection. In this work, we still assume that detection is optional in the band X to select the X -dropout populations.

In the WST Science White Paper [42], the authors estimated the relations between the surface densities of u -, g -, and r -dropouts down to different magnitude limits (see Fig-

ure 65): at $r_{\text{lim}} < 24.5$ mag, the available *photometric* density of u -dropout should be within 1,500 to 2,000 deg^{-2} for MUST. And, at $i_{\text{lim}} < 24.6$, there are $\sim 1,000 \text{ deg}^{-2}$ g -dropout for MUST to target. For r -dropout, the expected candidate density is ~ 300 (600) deg^{-2} for a $z_{\text{lim}} < 24.5$ (25.0) mag sample. These values represent the most optimistic estimations for MUST. In reality, the photometric selection will include contamination from galaxies outside of the desired redshift range. MUST will not be able to measure the redshifts of all candidates as the success rate should strongly depend on the presence and the strength of the $\text{Ly}\alpha$ emission line.

For the cosmological forecast in this work, we will not delve into the details of target selection, as we do not yet have the multi-band images and spectroscopic validation data required for a definitive Stage-V selection strategy. Instead, based on previous work, we provide optimistic and conservative estimates of number density for each population. For u -dropout in $2.1 < z < 3.5$, we assume that a $r < 24.5$ selection could result in a 1,200 deg^{-2} sample in an optimistic and a 600 deg^{-2} sample in a conservative situation. For g -dropout in $3.3 < z < 4.5$, we expect a 800 deg^{-2} and 300 deg^{-2} sample for the optimistic and conservative scenarios, respectively. As for the r -dropout in $4.5 < z < 5.5$, we assume the optimistic sample has a density of 200 deg^{-2} , while the conservative sample halves this value. We summarize these assumptions in Table 2. We do not include the BX selection sample in our forecast as it was defined using a different series of broadband filters than the Sloan *ugriz* ones [252]. Hence, the BX criteria require filter conversions to work on the imaging data for MUST, or need to be updated. Moreover, the BX-selected sample often centers at $z \sim 2$, leading to a significant fraction that falls outside the redshift range covered by MUST. Still, the current estimate suggests that the potential LSS tracer density at $z < 2.5$ can be much higher when better selection criteria are implemented.

To provide the initial estimates of the redshift distributions for each population, we adopt a simple method based on the COSMOS2020¹¹⁾ photometric and photo- z catalog [253]. Following the previous dropout-selection recipes, we designed the color cuts for the magnitude-limited samples for MUST to roughly reach the desired target density while ensuring a photometric redshift distribution consistent with the design. We apply the bright object masks from the COSMOS field of the HSC-SSP Ultra-Deep survey. It results in a 1.5 deg^2 effective footprint to estimate the target density. We confirm that the choice of photometric measurements and the photo- z estimations do not affect the derived redshift distribution.

For the u -dropouts, we recover a $\sim 1,500 \text{ deg}^{-2}$ sample

within $22.4 < r < 24.5$ mag using the following criteria:

$$\begin{aligned} (u - g) &> 0.95, \\ -0.5 &< (g - r) < 1.1, \\ (u - g) &> 1.17 \times (g - r) + 0.71. \end{aligned} \quad (13)$$

About 88% of the target has photo- z within $2.2 < z < 3.5$ and shows a clear peak at $z = 3$. We confirm that, while using different choices of *ugr* or *ugi* color cuts can change the target density from ~ 800 to $> 2,000 \text{ deg}^{-2}$, the redshift distribution does not vary significantly.

For the g -dropouts, we design the following *grz* color cuts to select a $\sim 870 \text{ deg}^{-2}$ sample peaked at $z \sim 3.4$. $\sim 84\%$ of the sample falls into $3.2 < z < 4.5$ based on photo- z , resulting in a $\sim 760 \text{ deg}^{-2}$ sample within $23.0 < i < 24.6$ mag:

$$\begin{aligned} (g - r) &> 1.0, \\ (g - r) &> 1.2 \times (r - z) + 0.65. \end{aligned} \quad (14)$$

As for the r -dropouts, we can define a $23.0 < z < 25.0$ mag sample within $4.0 < z < 5.5$, centered at $z \sim 4.5$ using these *riz* color cuts:

$$\begin{aligned} (r - i) &> 0.65, \\ -0.5 &< (i - z) < 0.9, \\ (r - i) &> 1.5 \times (i - z) + 0.65. \end{aligned} \quad (15)$$

Using photo- z , this sample has a $\sim 390 \text{ deg}^{-2}$ density within the desired redshift range. Like the u -dropouts, tweaking these preliminary color cuts can significantly change the target density but will not affect the redshift distributions.

We want to emphasize that these color cuts are *not* designed for actual target selection, but only to support our *assumptions* for a more optimistic high- z LSS tracer selection in the 2030s. For the clustering forecasts, we adopt the bias model of *ugr*-dropout LBGs in [243]:

$$b_{\text{LBG}}(z, m) = A(m)(1 + z) + B(m)(1 + z)^2, \quad (16)$$

where $A(m) = -0.98(m - 25) + 0.11$ and $B(m) = 0.12(m - 25) + 0.17$, with m being the rest-frame UV magnitude.

LBG will be the highest priority target for the dark time program of MUST. However, based on the empirical estimation of the required exposure time (e.g., [42, 243]) for LBG and the results from recent DESI campaigns (e.g., [21, 22]), successfully recover redshifts down to $r \sim 24.5$ mag or deeper is still a challenging task for a 6.5 m telescope. Not only does this challenge require a careful review of scientific requirements to guide the design of the scientific instruments, but it also motivates us to investigate an improved selection strategy that focuses on LBG with a clear $\text{Ly}\alpha$ emission line. As the throughput of the telescope, fiber, and detector all drop significantly toward the blue end at $\lambda < 4500 \text{ \AA}$, we expect the redshift success rate for u -dropout to also reflect this at

11) <https://astroweaver.github.io/project/cosmos2020-galaxy-catalog/>

$z < 2.5$. Given that we have not yet included the BX selection with a high target density, in principle, MUST should be able to guarantee the 3D tracer density for cosmology at $z < 2.5$. More importantly, despite the uncertainties around the fiber assignment and redshift efficiencies for LBG, the contrast between our optimistic and conservative target density estimation should make our cosmological forecast more realistic for MUST.

4.3.2 Lyman- α Emitters (LAE)

LAEs are high- z galaxies with strong ($EW \geq 20 \text{ \AA}$) Lyman- α emission lines (e.g., [254]), which are typically young, star-forming galaxies with low stellar and dust mass. As LAEs live in dark matter halos with a lower average halo mass than LBG, their potential density should be significant enough to make them competitive high-redshift LSS tracers. In [217], the authors spectroscopically confirm 822 (1,099) $z = 2.40 \pm 0.03$ (3.10 ± 0.03) LAEs in the 8.90 (9.34) deg^2 ODIN fields using the N419 (N501) narrow-band filters down to 25.5 (25.7) 5σ detection limit. These samples correspond to a $\sim 10^{-3} h^{-1} \text{Mpc}^{-3}$ 3D density in two narrow redshift windows, higher than the optimistic prediction of LBG 3D density across the whole redshift range. If such performance can be extrapolated to a broader redshift range, LAEs can become an extremely interesting LSS tracer: not only do they dramatically improve the density of high- z LSS tracers, but their halo bias should also be significantly lower than the dropout-selected LBG (e.g., $b \sim 1.7$ and 2.0 for the two ODIN samples), making a multi-tracer probe potentially possible at high- z .

However, due to their faint continuum emission and the limited number of spectral features (often just the Ly α line), the selection of LAEs requires deep narrow-band imaging (e.g., [221]) or IFS (e.g., [255]) observations. Most ongoing LAE surveys either cover much smaller areas than the MUST footprint (e.g., ODIN; [221]) or are not deep enough for MUST (e.g., JPAS; [256, 257]). Furthermore, the bias of LAEs has only been measured on relatively small fields ($\lesssim 100 \text{deg}^2$, e.g., [217, 258]). We do not include LAEs in our current cosmological forecast for these reasons. At the same time, this implies that the cosmological constraining power of MUST could be further enhanced when a wide & deep LAE sample becomes available in the future. We should note that the DECam on the 4 m Blanco telescope (e.g., [220]) and the HSC on the 8.2 m Subaru (e.g., [159, 160]) can carry out deep narrow- or medium-band surveys in the following years. It is worth noting that DESI has conducted pilot spectroscopic observations of LAEs, demonstrating their promise

as LSS tracers of the high-redshift Universe.

4.3.3 Quasi-Stellar Objects (QSO)

Quasi-stellar objects (QSOs) or quasars¹²⁾ are both direct tracers of the dark matter field and sources for Lyman- α forest detections. The transition in their usage — from tracers to sources — typically occurs around $z \sim 2$, depending on their comoving densities. QSOs have been an essential ingredient in major spectroscopic surveys, serving as primary targets for probing the $z \gtrsim 2$ Universe. The Stage-III and IV spectroscopic surveys, such as BOSS [259], eBOSS [260], DESI [211, 261], and WEAVE [262, 263] define the modern standard of QSO target selection using multi-band deep imaging data and broad-band color cuts to isolate quasar candidates from stars and other galaxies (e.g., [264–272]). At the same time, these surveys have explored QSO selection based on flux variability (e.g., [273]) and the use of machine learning algorithms (e.g., [211, 274, 275]).

While QSOs will certainly enable a wide range of interesting scientific topics in the age of Stage-V surveys, their low 3D density and color degeneracy with abundant Milky Way stars at $z > 2$ (e.g., see Figure 4) make them less appealing LSS tracers. Therefore, we do not include QSO in the Fisher forecast to constrain cosmological parameters. In Figure 4, we adopt the pure luminosity function evolution model in [273] to estimate the 3D density of QSOs at $r < 23.5$. Assuming 80% of the QSOs will be observed, MUST will reach a QSO density of ~ 310 per deg^{-2} with $\sim 90 \text{deg}^{-2}$ at $z > 2.1$, including the QSOs already observed by BOSS/eBOSS and DESI ($\sim 60 \text{deg}^{-2}$ at $z > 2.1$).

It is worth noting that, while not being the most promising high- z LSS tracers, at $z > 2.1$, QSOs provide a vital capability for studying the IGM using the Ly α forest, which contains intriguing cosmological potential such as constraining the nature of dark matter. We will forecast the potential of Ly α -QSO and provide a more thorough discussion in the following work of this series.

4.4 Summary of the Target Selection

In Table 3, we summarize the preliminary target selection discussed above and provide an initial estimate of the survey cost, measured in total fiber-hours. All but the QSO samples are considered in the cosmological forecast.

The effective collecting area of MUST will be $\sim 3.2\times$ that of DESI¹³⁾. Considering the additional throughput loss caused by the secondary mirror, WFC, fiber route, and spectrograph, we assume that for the same target, MUST can

12) We use the term QSO and quasar interchangeably in this work.

13) We assume the DESI primary mirror has a diameter of 3.8 m with a central obscuration of 1.8 m. For MUST, we adopt a central obscuration of 2.5 m.

| Sample Name | Magnitude Limit (AB mag) | Redshift Distribution | Angular Density (deg ⁻²) | Number of Redshift Bins | 3D Density (10 ⁻³ h ³ Mpc ⁻³) | Bias Value | Survey Area (deg ²) | T _{Exp} (Hour) | Total Number of Redshift (10 ⁶) | Total Fiber Hours (10 ⁶) |
|-------------------|---------------------------------------|-----------------------|--------------------------------------|-------------------------|---|------------|---------------------------------|-------------------------|---|--------------------------------------|
| BGS | 20.18 < <i>r</i> < 21.0 | 0.1 < <i>z</i> < 0.7 | 2,000 | 2 | 5.7 | 1.6 | ~13,000 | 0.12 | 26.0 | 3.12 |
| LRG | 21.6 < <i>z</i> _{fib} < 22.8 | 0.8 < <i>z</i> < 1.3 | 2,000 | 2 | 1.0 | 2.8 | ~13,000 | 1.00 | 26.0 | 26.0 |
| ELG | 24.1 < <i>g</i> _{fib} < 24.6 | 0.8 < <i>z</i> < 1.4 | Opt:3,600 | 2 | 1.49 | 1.5 | ~13,000 | 0.30 | 46.8 | 14.0 |
| | | | Con:2,500 | 2 | 1.03 | 1.5 | ~11,000 | 0.30 | 27.5 | 8.25 |
| <i>u</i> -Dropout | 22.4 < <i>r</i> < 24.5 | 2.2 < <i>z</i> < 3.5 | Opt:1,200 | 3 | 0.21 | 4.5 | ~11,000 | 2.50 | 15.6 | 39.0 |
| | | | Con:600 | 3 | 0.11 | | ~8,000 | 2.50 | 6.0 | 15.0 |
| <i>g</i> -Dropout | 23.0 < <i>i</i> < 24.6 | 3.2 < <i>z</i> < 4.5 | Opt:800 | 2 | 0.16 | 5.3 | ~11,000 | 6.00 | 10.4 | 62.4 |
| | | | Con:300 | 2 | 0.06 | | ~8,000 | 6.00 | 3.0 | 18.0 |
| <i>r</i> -Dropout | 23.0 < <i>z</i> < 25.0 | 4.0 < <i>z</i> < 5.5 | Opt:200 | 1 | 0.06 | 6.4 | ~11,000 | 8.00 | 2.6 | 20.8 |
| | | | Con:100 | 1 | 0.03 | | ~8,000 | 8.00 | 1.0 | 8.0 |
| QSO | <i>r</i> < 23.5 | 2.0 < <i>z</i> < 5.0 | 90 | | | | ~13,000 | 0.12 | 1.2 | 0.14 |

Table 3 Summary of the low- and high-redshift samples selected in this work. All but the QSO samples are considered in the cosmological forecast. For the ELG, *u*-, *g*-, and *r*-dropout galaxies, we estimate an optimistic (“Opt”) and conservative (“Con”) surface density to design the survey.

reach the same S/N 2.5 times faster than DESI. This ignores the differences caused by seeing (the Lenghu site is likely to have better median seeing than Kitt Peak) and fiber core diameter (1.5 arcsec for DESI vs. 1.3 arcsec for MUST). For the same target type, MUST will observe fainter targets than DESI. We assume the exposure time will increase $10^{2\delta m/2.5}$ times for the fainter sample, where δm is the magnitude difference. We assume DESI can achieve the designed redshift success rate using 200 seconds of exposure time for BGS and 1,000 seconds of exposure time for LRG, ELG, and QSO. Hence, we estimate that MUST can achieve the same 95% to 99% redshift success rate using 440, 3600, 729, and 440 seconds of exposure time for BGS, LRG, ELG, and QSO.

Estimating the exposure time for the LBG is more difficult. Based on the recent LBG observation campaign by DESI [21], for a $r < 24.2$ mag *u*-dropout sample, DESI can already achieve a $\sim 70\%$ redshift efficiency in 2.5 hours of exposure time. However, the efficiency seems to plateau after 2.5 hours as a 5-hour exposure still cannot improve it to $> 80\%$. It is worth noting that there is certainly room to improve the LBG redshift estimation in the near future with the arrival of more accurate spectral models or templates. Therefore, for the *u*-dropout sample, we apply the simple empirical scaling relation and assume that MUST can achieve the same success rate for our $r < 24.5$ mag sample with a 2.5-hour exposure. For the *g*- and *r*-dropouts, it is less straightforward to estimate the required exposure time as there is no statistically meaningful DESI sample to compare with. In [243], the authors estimated that an 80-minute exposure would be enough for a $z = 24$ mag galaxy using a 6.5 m telescope. Scaling this up to a $z < 24.50$ mag sample would require a 3.4-hour exposure time.

4.5 Conceptual Survey Design

This section briefly describes the conceptual survey designs for the bright-gray and dark-time programs of MUST based on the previous description of the telescope & instrument design and the target selection under several oversimplified assumptions. In the upcoming work of this series, we will present a more proper survey design backed by detailed instrument specifications, an exposure time calculator (ETC) for MUST, and an improved target selection strategy.

4.5.1 Dark Time Survey

We assume that the CSST photometry will support the selection of dark-time targets for MUST, which will mainly include the LBG at $2.2 < z < 5.0$. The right panel of Figure 5 shows a preliminary observing pattern, where each pointing corresponds to the 5 deg² effective FoV of MUST. Given the latitude of the Lenghu site, MUST cannot access the full CSST footprint. Assuming a maximum airmass of 1.5 ($\sim 40^\circ$ above the horizon) for observation, we restrict the footprint to declinations above -10° . Surveying 11,000 deg², or 3,000 pointings with a minimal overlap for a continuous coverage, and adopting an average exposure time of 2.5 hours per target, this requires a total of 750 effective dark nights, with an average of 10 observing hours per night. Assuming a 70% clear-night fraction and 35% dark-time availability per year that accounts for an 80% survey efficiency, this corresponds to an 8.5-year observing program. In total, this dark-time survey is expected to produce 30 million redshift measurements, assuming an overall 70% redshift measurement efficiency.

4.5.2 Gray Time Survey

As the gray-time program will primarily focus on BGS, LRG, and ELG, we use the Legacy Survey footprint to simulate the pointings needed for MUST, as shown in the left panel of Figure 5. With the declination limited to $> -10^\circ$, MUST can access a total of $\sim 13,000$ deg² of the Legacy Survey foot-

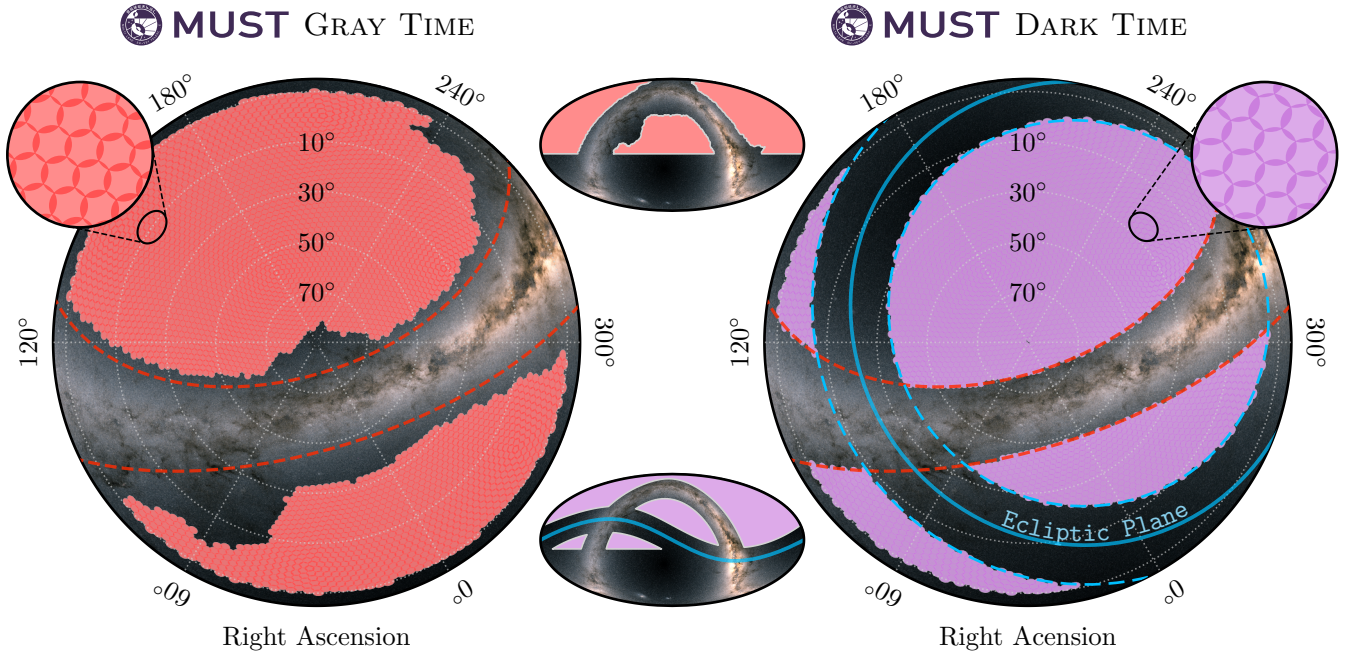


Figure 5 Footprint and an example tiling for MUST gray-time (*left*) and dark-time (*right*) observations. Each filled circle represents the sky projection of the MUST focal plane (5 deg^2). The gray-time footprint is based on the DECaLS imaging sample, while the dark-time footprint follows the expected CSST sky coverage. Both footprints are restricted to declinations above -10° , reflecting the latitude constraint of the Lenghu site. Background color maps indicate the *Gaia* EDR3 stellar density [64]. The gray-time and dark-time tilings yield around 3,500 and 3,000 pointings, covering $\sim 13,000$ and $11,000 \text{ deg}^2$, respectively.

print, corresponding to $\sim 3,500$ contiguous MUST pointings. With an average exposure time of 1 hour per target and a target density of approximately twice the fiber density of MUST ($\sim 4,000 \text{ deg}^{-2}$), which may include, for example, $2,000 \text{ deg}^{-2}$ BGS, $2,000 \text{ deg}^{-2}$ LRG, $3,600 \text{ deg}^{-2}$ ELG, and 400 deg^{-2} of other targets, the program would require a total of 700 effective gray nights with 10 observing hours per night. Assuming 40% of gray time per year, that accounts for an overall 80% survey efficiency and a 70% clear-night fraction, the gray-time survey would span ~ 7 years. In total, this program is expected to accumulate ~ 88 million redshift measurements, assuming an overall 85% redshift measurement efficiency.

Among the gray-time targets, LRG requires significantly longer exposure time (e.g., ~ 1 hour for a target with $z_{\text{fiber}} = 22.8 \text{ mag}$) compared to the others. With a carefully optimized survey strategy, the average exposure time per gray-time target could be shortened to speed up the current program, leaving space for a further increase in target density. For example, within the current detection limits of the Legacy Survey, we could select BGS down to $r < 21.5 \text{ mag}$ with a density of $\sim 4,000 \text{ deg}^{-2}$ and LRG down to $z_{\text{fiber}} = 23.0 \text{ mag}$ with a density of $\sim 3,000 \text{ deg}^{-2}$. Combining them with the current ELG sample will result in a total target density ~ 2.7 times the fiber density. Assuming a 1-hour *average* exposure time, this enhanced program will require ~ 9.5 years of gray time to finish and yield a ~ 114 million redshifts at $z < 1.6$ with an

80% average redshift efficiency. Safely assuming a fraction of these gray-time targets can be observed during bright time, it is possible to complete this program alongside the 8.5-year dark-time survey.

Putting the gray and dark programs together, MUST has the capability of collecting ~ 120 million redshifts at $0.1 < z < 5.0$ before 2040 (see Figure 2, with a comparison with historical and upcoming spectroscopic surveys).

5 Cosmological Forecasts

To quantitatively evaluate the scientific potential of MUST in addressing the fundamental cosmological questions outlined in Section 3, we forecast statistical errors for several key science cases based on the expected target densities and biases detailed in Section 4, with a Planck 2018 ΛCDM fiducial cosmology.¹⁴⁾ We perform two sets of forecasts — optimistic and conservative — based on different estimations of available imaging data to ensure a comprehensive evaluation of the scientific potential of MUST. To illustrate the potential improvements achievable by MUST, we compare our forecasts with those for DESI, the current state-of-the-art Stage-IV survey, using its target specifications from [229]. Specifically, we focus on the DESI galaxy samples, i.e., BGS, LRG, and ELG.

¹⁴⁾ Marginalized means of parameters from the Planck likelihood, see Table 1 of [4].

To fully assess the constraining power of next-generation cosmological data, we incorporate external CMB priors from Planck [276] and Simons Observatory (SO; [45]) into our Fisher forecasts, following the methodology in [16]. Additionally, we perform Bayesian cosmological parameter inferences using Markov-Chain Monte-Carlo (MCMC) methods without these CMB priors, and directly compare our forecasts to constraints derived from the existing Planck and Atacama Cosmology Telescope (ACT; [277]) CMB data, as well as the Pantheon+ [5] Type Ia SN compilation.

5.1 Methodology

5.1.1 Fisher forecast

The Fisher forecast method is widely used to estimate the statistical uncertainty of cosmological parameters inferred from expected clustering measurements in observations. This method is based on the Cramér-Rao inequality [278, 279], which establishes that no unbiased estimator can achieve a covariance matrix smaller than the inverse of the Fisher information matrix \mathbf{F} . Consequently, the standard deviation of the i -th measured parameter, θ_i , is bounded from below by $\sigma(\theta_i) \geq \sqrt{(F^{-1})_{ii}}$. Following the formulation in [280], the Fisher information matrix for a redshift survey can be approximated as

$$F_{ij} \sim \frac{\partial \mathbf{P}^T}{\partial \theta_i} \mathbf{C}^{-1} \frac{\partial \mathbf{P}}{\partial \theta_j}, \quad (17)$$

where \mathbf{P} is the data vector with $P_i = P(k_i, \mu_i)$ representing the power spectrum of the i -th bin in \mathbf{k} -space, and \mathbf{C} is the corresponding covariance matrix of the power spectrum. With the usual assumption that the overdensity field is approximately a Gaussian random field, the covariance matrix \mathbf{C} is given by

$$C_{ij} \sim \delta_{ij} \frac{2P_i^2}{V_i V_{\text{eff}}}, \quad (18)$$

where V_i is the volume of the i -th bin in \mathbf{k} -space, and V_{eff} is the effective survey volume.

Throughout this work, we perform Fisher forecasts using the tracer power spectrum $P(\mathbf{k})$ with

$$k_{\text{max}} = 0.4 h \text{ Mpc}^{-1}, \quad (19)$$

which corresponds to the smallest scale where a state-of-the-art perturbation theory achieves sub-percent accuracy (e.g. [281]). In our forecasts, the tracer power spectrum is computed using either full-shape models or a template-based approach. For the full-shape model, we use the forecast tool

FishLSS¹⁵⁾ described in [16]. FishLSS computes the non-linear tracer power spectrum using Lagrangian perturbation theory with a linear tracer bias model, refined by a single-parameter counter-term for small-scale corrections [282] that is calibrated to the HaloFit prescription [283]. Shot noise and the finger-of-god effect are incorporated based on the density of the tracers. The template-based approach is used only for the $f\sigma_8$ forecasts (Section 5.3). In this case, we use a code¹⁶⁾ developed for a recent spectroscopic survey forecast [284], which refers to the RSD template from [285].

5.1.2 Cosmological inference

To convert the cosmological distances from BAO and structure growth parameters from RSD into cosmological parameters, we use the cosmological inference code COBAYA [286] with our forecast results, along with the Planck 2018 PR3 likelihoods¹⁷⁾ [65], their combination with the ACT DR6 results with CMB lensing¹⁸⁾ [277], and the Pantheon+ SN data [5]. For most cases, we use the Boltzmann code CAMB [287] to evaluate the theoretical power spectra, while for modified gravity, we employ ISiTGR [288]. Bayesian inference is performed using the MCMC Metropolis sampler [289] in COBAYA, and the resulting chains are visualized as parameter posteriors with the GETDIST package [290].

For the warm dark matter mass (m_X) forecast, we implement the m_X -dependent Ly α power spectrum and its covariance matrix, as described in Section 5.6, and use the EMCEE [291] toolkit for MCMC sampling.

5.2 Cosmic Expansion History & Dark Energy

As a cosmic “standard ruler” (see Section 3.1), the BAO feature provides geometric measurements at various redshifts, revealing the cosmic expansion history and constraining the density and evolution of cosmic components, particularly dark energy. The characteristic BAO scale corresponds to the sound horizon at the drag epoch, r_d , and relates directly to the angular ($\Delta\theta$) and redshift (Δz) separations of tracer pairs that exhibit excess correlations in the transverse and line-of-sight directions, respectively. In a flat Universe, these relationships are given by

$$r_d = (1+z)D_A(z)\Delta\theta = \Delta\theta \int_0^\infty \frac{c dz'}{H(z')}, \quad (20)$$

$$r_d \approx \frac{c\Delta z}{H(z)}, \quad (21)$$

15) <https://github.com/NoahSailer/FishLSS>

16) https://github.com/wdougmerg/Forecast_highz_spectroscopic_survey

17) We use likelihoods from the temperature (TT), polarization (EE), and their cross-correlation (TE) power spectra, with both low- ℓ and high- ℓ results.

18) We use the official ‘actplanck.baseline’ likelihood when including ACT results, see https://github.com/ACTCollaboration/act_dr6_lenslike.

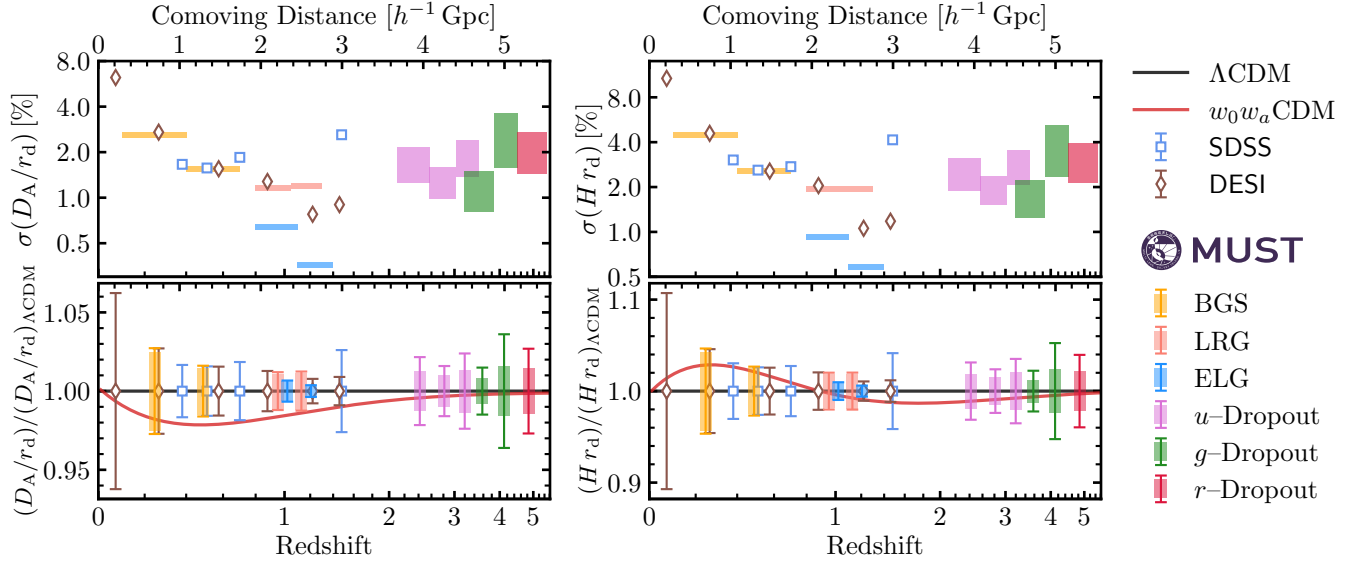


Figure 6 Top panels: expected uncertainties in $D_A(z)/r_d$ (left) and $H(z)r_d$ (right) from DESI and MUST galaxy samples, compared with existing SDSS measurements [10]. Shaded regions indicate the range between optimistic and conservative MUST forecasts. Bottom panels: forecasted distance measurements assuming the fiducial ΛCDM cosmology, compared with predictions from the best-fit $w_0w_a\text{CDM}$ model obtained in the DESI Y1 analysis [78]. For MUST, error bars indicate conservative forecasts, while boxes denote optimistic results.

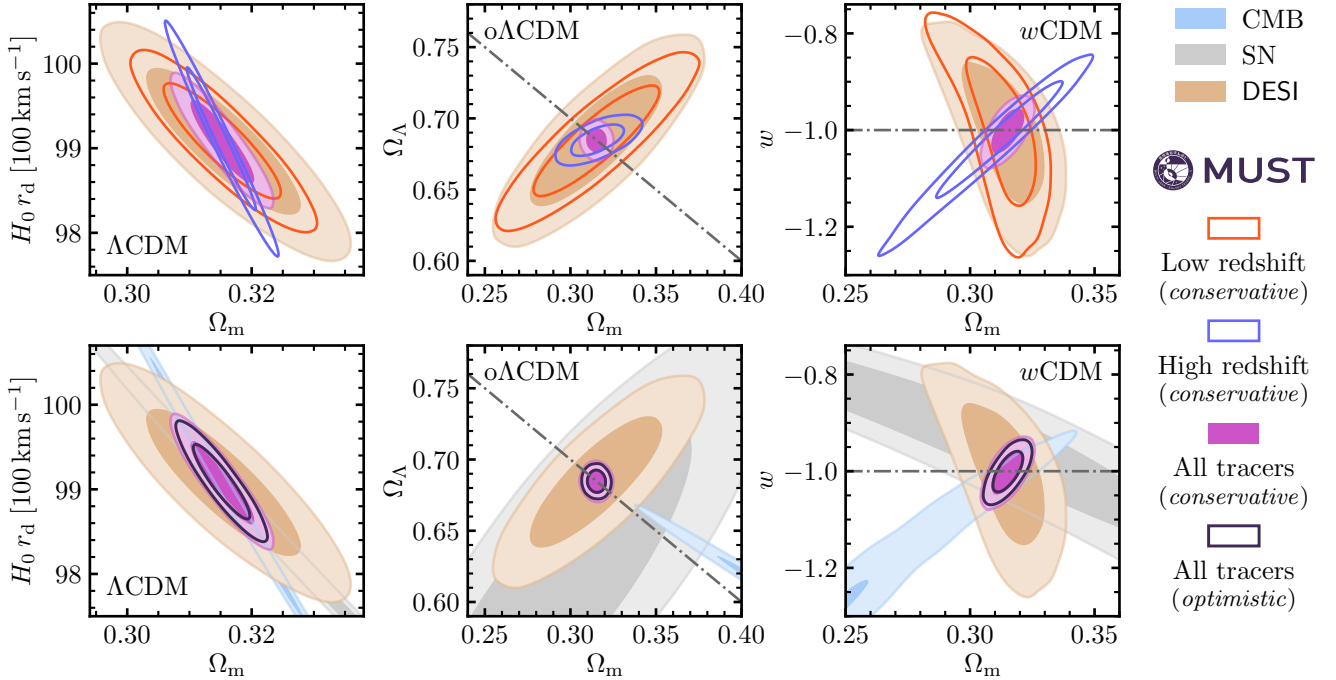


Figure 7 Cosmological parameter constraints from our DESI and MUST distance forecasts. All distance forecasts assume the fiducial ΛCDM cosmology, while parameter inferences are performed in three models: ΛCDM (left), $o\Lambda\text{CDM}$ (center), and $w\text{CDM}$ (right). Top panels: constraints from MUST low-redshift ($z \leq 1.5$) and high-redshift ($z \geq 2$) galaxy samples are shown separately to highlight the contribution of the novel high-redshift tracers. Bottom panels: comparisons of our forecasts with current constraints from Planck 2018 PR3 [65] and Pantheon+ [5] data. Gray dash-dotted lines indicate the ΛCDM parameter space.

where $D_A(z)$ is the angular diameter distance and $H(z)$ is the Hubble parameter. Thus, BAO measurements constrain the combinations $D_A(z)/r_d$ and $H(z)r_d$ as functions of redshift.

Figure 6 presents the forecasted uncertainties in $D_A(z)/r_d$

and $H(z)r_d$ for different MUST and DESI tracers, compared with existing SDSS measurements [10]. In the nearby Universe ($z \lesssim 0.7$), the precision from MUST is comparable to that of current surveys, primarily due to limitations imposed

by cosmic variance. At intermediate redshifts ($0.7 \lesssim z \lesssim 1.5$), the high-density ELG samples from MUST are expected to provide a twofold improvement in distance measurement precision. Importantly, MUST will deliver unprecedented, percent-level measurements of the cosmic expansion history over $2 \lesssim z \lesssim 5.5$, offering crucial geometric constraints spanning from cosmic noon to the post-reionization era. Notably, it is at high redshift where the difference between our optimistic and conservative forecasts becomes most significant – nearly a factor of two. This reflects the challenges and uncertainties associated with imaging surveys of high-redshift galaxies and quasars.

The impact of these distance measurements on cosmological parameter constraints is shown in Figure 7, for the Λ CDM cosmology and its two one-parameter extensions: $\text{o}\Lambda$ CDM and w CDM, which include Ω_k and w as additional parameters, respectively. In all cases, significant improvements over DESI forecasts are observed. These gains are primarily driven by the inclusion of high-redshift samples, which alter the degeneracy directions due to the redshift dependence of parameter constraints. As a result, the statistical errors of Ω_k and w are reduced by approximately 88% and 70%, respectively, when comparing MUST to DESI. The optimistic and conservative forecasts for MUST yield nearly identical results. However, these improvements become marginal when BAO measurements are combined with existing CMB and SN constraints. For the Λ CDM model, this is mainly due to the different degeneracy directions of the CMB and SN results in the $H_0 r_d - \Omega_m$ plane. In contrast, the combined results for $\text{o}\Lambda$ CDM and w CDM should be interpreted with caution, as the statistical precision of the MUST forecasts leads to significant tension between our fiducial cosmology and current CMB constraints. If future MUST measurements are more consistent with other probes, substantial improvements are still expected. Conversely, if such discrepancies are confirmed, they could point to unaccounted systematics or even new physics.

To evaluate the potential contribution of MUST to the recent indications of evolving dark energy reported by DESI [77, 78], we perform cosmological inferences in the flat- $w_0 w_a$ CDM cosmology under two scenarios. In the first, we use our fiducial Λ CDM cosmology for the distance forecasts; whereas in the second, we assume the best-fit $w_0 w_a$ CDM cosmology from [78]. The results, shown in Figure 8, are compared with DESI forecasts and current constraints from CMB and SN data. In both cases, the statistical precision of w_0 and w_a is significantly improved relative to DESI. If the DESI best-fit $w_0 w_a$ CDM model reflects the true cosmology, MUST alone would achieve a 3.1σ deviation from Λ CDM in the optimistic case, and 2.7σ in the conservative case. In summary, MUST will provide the most stringent constraints on

evolving dark energy from purely geometrical measurements, significantly outperforming current CMB and SN results. It is worth noting, however, that the commonly used CPL parameterization in Eq. (1) may bias measurements of the high-redshift behavior of the dark energy equation of state [292]. Meanwhile, the time-evolving term w_a enters as a factor of $(1-a)$, which evolves slowly at high redshift, thereby limiting sensitivity to late-time changes (see the bottom panel of Figure 6). Since the primary advantage of MUST lies in its high-redshift ($z \gtrsim 2$) coverage, it is important to explore alternative parameterizations of $w(z)$ that better capture its high-redshift evolution. We leave such investigations to future work.

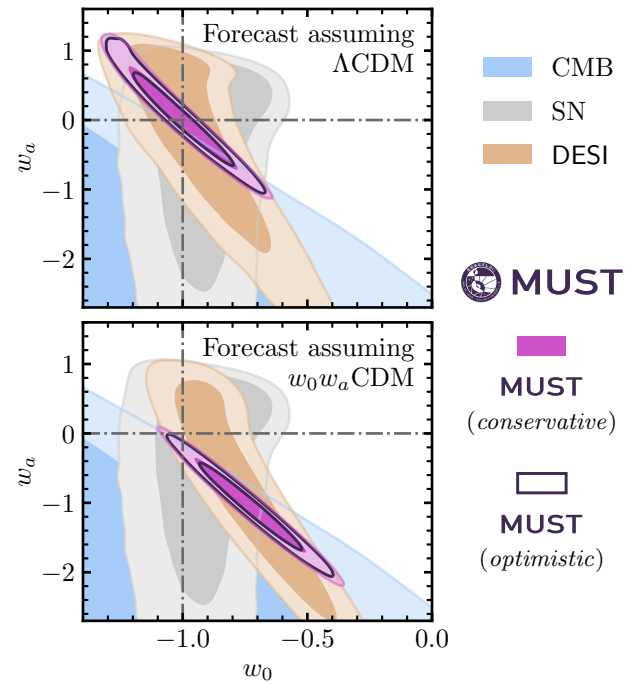


Figure 8 Constraints on w_0 and w_a from parameter inferences in the $w_0 w_a$ CDM model, based on our DESI and MUST distance forecasts, compared with existing Planck 2018 PR3 [65] and Pantheon+ [5] results. Forecasts are performed assuming either the fiducial Λ CDM cosmology (*top*) or the best-fit $w_0 w_a$ CDM model from DESI Y1 data [78] (*bottom*). Gray dashed lines indicate the Λ CDM parameter values.

5.3 Structure Growth & Modified Gravity

The distinction between GR and alternative gravity models can be probed through measurements of structure growth inferred from anisotropic galaxy clustering, commonly parameterized by $f\sigma_8$ (see Section 3.2). Figure 9 shows Fisher forecasts for the statistical uncertainties in $f(z)\sigma_8(z)$ from different MUST and DESI galaxy samples, based on RSD measurements with template power spectra. The results are compared with existing constraints from previous surveys and with predictions from several modified gravity models

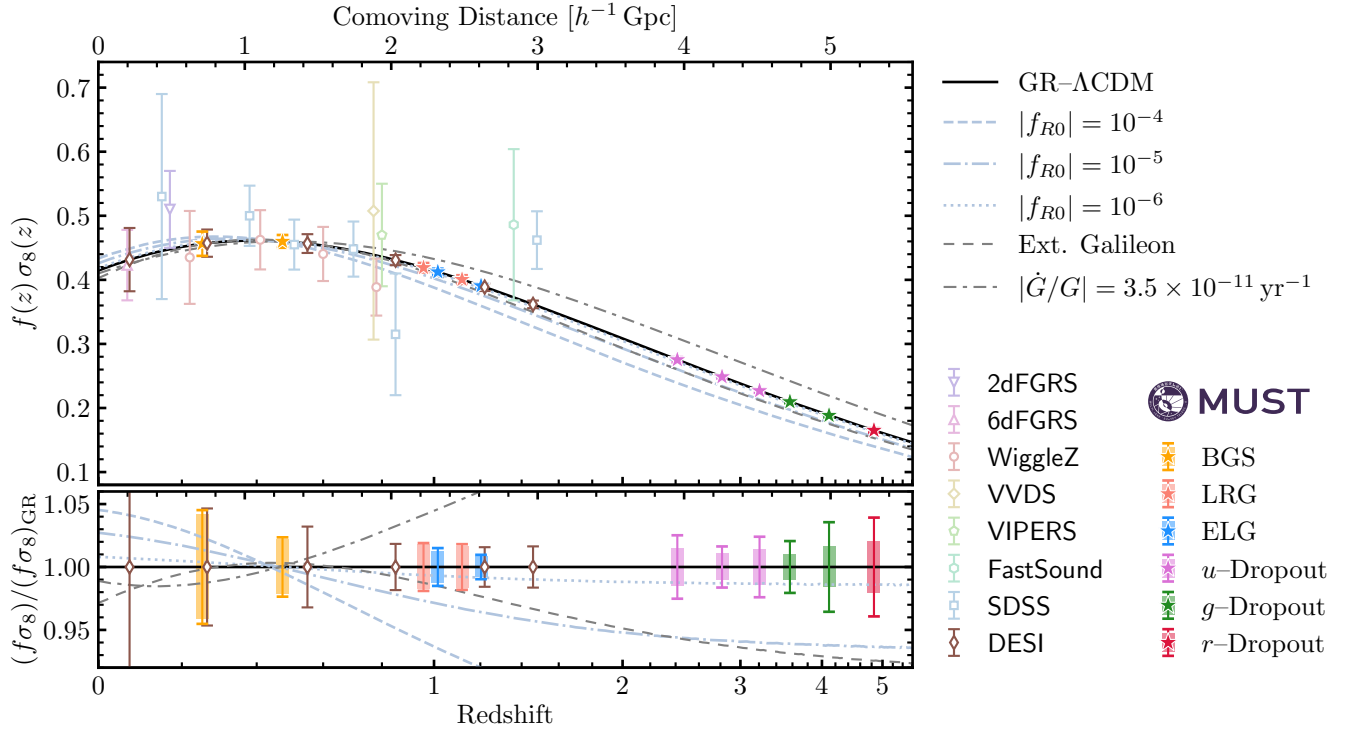


Figure 9 Fisher forecasts for $f(z)\sigma_8(z)$ measurements from MUST and DESI galaxy samples. *Top panel:* comparison with existing measurements from SDSS [10, 293, 294], 2dFGRS [82, 295], VVDS [296], VIPERS [297], WiggleZ [298], 6dFGRS [299], and FastSound [300]. *Bottom panel:* forecasted relative errors on $f(z)\sigma_8(z)$ compared to the fiducial GR- Λ CDM cosmology. Error bars and shaded boxes represent conservative and optimistic forecasts, respectively. Also shown are predictions from various modified gravity models that remain consistent with current observations, including the covariant Galileon model [301], extended Galileon gravity [302], a varying gravitational constant model with $|\dot{G}/G| = 3.5 \times 10^{-11} \text{ yr}^{-1}$ [303], and $f(R)$ gravity [304] with $|f_{R0}| = 10^{-4}$, 10^{-5} , and 10^{-6} .

that remain viable under current datasets. We observe trends similar to those seen in the distance forecasts discussed in Section 5.2. Specifically, the performance of MUST is comparable to that of DESI at $z \lesssim 0.7$. There are modest improvements at $0.7 \lesssim z \lesssim 1.5$, which could be further enhanced through future multi-tracer analyses combining different galaxy populations from both MUST and DESI. The most significant contribution from MUST lies in its ability to achieve percent-level structure growth measurements at high redshift ($z \gtrsim 2$), a regime that remains largely unexplored. As with the distance forecasts, uncertainties in the availability of high-redshift imaging data lead to substantial differences between optimistic and conservative error estimates. Nonetheless, these additional high-redshift measurements will be essential for distinguishing among modified gravity models that remain consistent with current observations.

We translate the forecasts of cosmological distances from BAO and of structure growth parameters from RSD into constraints on modified gravity using the $\mu(a, k)$ and $\Sigma(a, k)$ parameterization defined in Eqs. (2) and (3). For simplicity, we assume that the distance and structure growth measurements are independent, and focus on a scale-independent form of μ

and Σ , with the time dependence modeled as (e.g., [305]):

$$\mu(a) = \mu_0 \frac{\Omega_\Lambda(a)}{\Omega_\Lambda}, \quad (22)$$

$$\Sigma(a) = \Sigma_0 \frac{\Omega_\Lambda(a)}{\Omega_\Lambda}. \quad (23)$$

Constraints on μ_0 and Σ_0 derived from our $f\sigma_8$ forecasts are shown in Figure 10, along with existing CMB constraints from Planck 2018 DR3 [65] and ACT DR6 [277]. As expected, galaxy clustering data constrain only the μ_0 parameter. Compared to DESI, the expected uncertainty in μ_0 is reduced by 41% and 55% under the conservative and optimistic MUST forecasts, respectively. When combined with CMB data, the improvements become 20% and 30%. These results highlight the strong potential of MUST for precision tests of General Relativity.

It is worth noting that, under the μ_0 and Σ_0 parameterization adopted here, deviations from GR may appear less significant if the actual time evolution differs from the form assumed in Eqs. (22) and (23) [305]. To fully exploit the high-redshift structure growth measurements enabled by MUST, it will be important to explore alternative phenomenological parameterizations and physically motivated models of modified gravity in future work. For instance, as shown in Figure 9,

MUST is expected to constrain the strength of $f(R)$ gravity, $|f_{R0}|$, down to the 10^{-6} level.

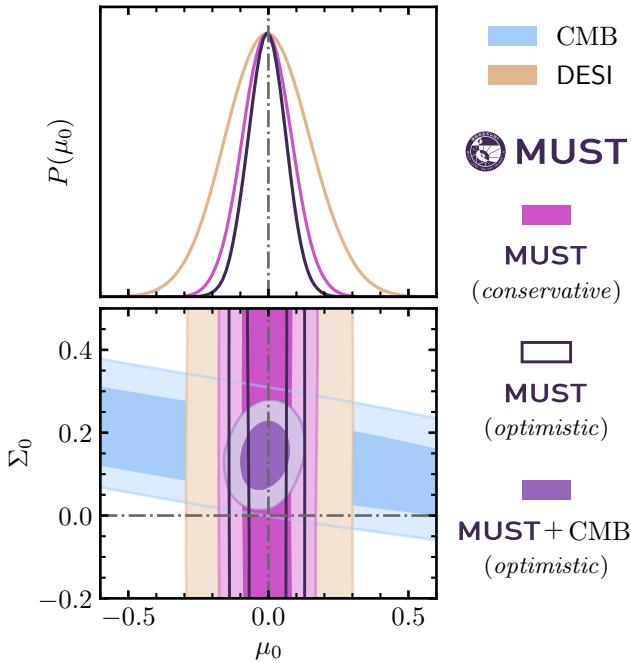


Figure 10 Constraints on Σ_0 and μ_0 derived from BAO and RSD forecasts for MUST and DESI, assuming the fiducial Λ CDM cosmology. Results are compared with current CMB constraints from Planck PR3 [65] and ACT DR6 [277]. The joint constraint from optimistic MUST forecasts combined with CMB data is also shown. Gray dash-dotted lines indicate the Λ CDM parameter values.

5.4 Primordial Non-Gaussianity

The presence of local-type PNG (see Section 3.3) introduces a dependence on the initial gravitational potential field, ϕ , into the galaxy bias model [306]. At leading order, this results in a so-called “scale-dependent bias” term in the galaxy power spectrum:

$$P_{\text{gg}}(k, z) = \left(b_1 + f_{\text{NL}}^{\text{local}} b_\phi \frac{3H_0^2 \Omega_m}{2k^2 T(k) D(z)} \right)^2 P_{\text{mm}}(k, z) + P_{\text{shot}}(z), \quad (24)$$

where $b_1(z)$ denotes the linear galaxy bias, $b_\phi(z)$ quantifies the response of galaxy bias to ϕ , $T(k)$ is the matter transfer function and $D(z)$ is the linear growth factor normalized to redshift z during the matter-dominated epoch. The transfer function $T(k)$ is normalized to unity on large scales, where the PNG signal is most prominent, hence the scale-dependent bias typically follows a k^{-2} dependence. This effect can be readily probed through 2-point galaxy clustering statistics. For this reason, our forecasts focus exclusively on the local-shape PNG amplitude $f_{\text{NL}}^{\text{local}}$. For the scale-dependent bias term, we adopt the commonly used universality relation

$b_\phi = 2\delta_c(b_1 - 1)$, where δ_c is the critical overdensity for spherical collapse. It is worth noting that recent studies suggest this relation may vary depending on the specific galaxy sample [307, 308]. We leave a detailed investigation of such effects for future work.

Our forecast results for MUST and DESI based on the galaxy power spectra are shown in Figure 11, alongside existing constraints from SDSS [309] and Planck [101]. To assess the full potential of future PNG constraints, we further perform Fisher forecasts incorporating priors from Planck and Simons Observatory (SO; [45]) CMB observations, enabling joint constraints from galaxy spectroscopic and CMB data. We find that the expected 1σ uncertainty on $f_{\text{NL}}^{\text{local}}$ from MUST alone ranges from ~ 1.8 (optimistic) to ~ 2.5 (conservative), depending on the assumed availability of imaging survey data. These values represent an approximate five-fold improvement over DESI and surpass the current CMB constraint of $\sigma(f_{\text{NL}}^{\text{local}}) = 5.1$ [101]. When combined with CMB data, the constraint is expected to tighten further to $\sigma(f_{\text{NL}}^{\text{local}}) \sim 1.4$ to 1.8 . Additional methods not included in this forecast, such as the multi-tracer technique [310] and bispectrum analyses [311], are expected to further enhance the constraining power of MUST. These approaches may allow $\sigma(f_{\text{NL}}^{\text{local}})$ to reach below unity, a critical threshold from a theoretical perspective, as a non-detection at this level would exclude many scenarios involving the curvaton mechanism [99, 312].

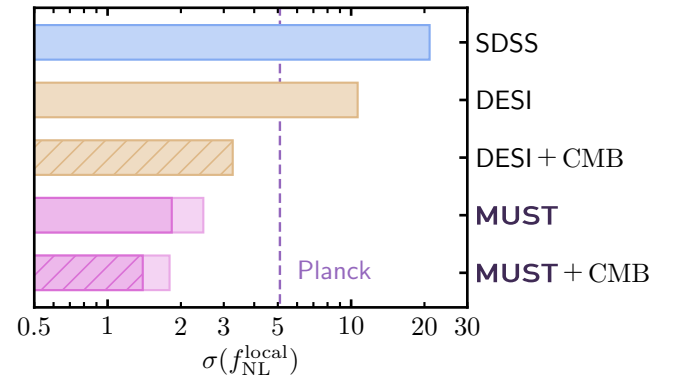


Figure 11 Forecasted 1σ constraints on $f_{\text{NL}}^{\text{local}}$ from MUST and DESI using galaxy power spectra, along with their combinations with CMB constraints from Planck low- ℓ [276] and Simons Observatory (SO; [45]) high- ℓ measurements. Current constraints from SDSS [309] and Planck CMB data [101] are also shown for comparison.

5.5 Neutrinos

The influence of neutrinos on both the expansion history of the Universe and the growth of cosmic structures enables constraints on the total neutrino mass, M_ν , through galaxy clustering measurements. The most prominent signature is the

suppression of the matter power spectrum on scales below the neutrino free-streaming length, which is a cumulative effect arising from the integrated expansion history (see Section 3.4). As a Stage-V spectroscopic survey with high tracer number density and large survey volume, MUST is expected to enable precise clustering measurements and place stringent constraints on M_ν , particularly when combined with CMB observations.

Since the total neutrino mass is small, near-future galaxy clustering data alone cannot yield a $> 1\sigma$ detection of a non-zero M_ν . In such cases, the Gaussian assumption underlying Fisher forecasts breaks down when a physical (positive) prior on M_ν is imposed. For this reason, we present only forecasts for the uncertainty on M_ν derived from the combination of galaxy clustering and current CMB observations from Planck and ACT. Specifically, we perform cosmological inferences using Planck PR3 [65] and ACT DR6 [277] data, and incorporate the resulting covariances into the Fisher matrix derived from our full-shape galaxy clustering forecasts to obtain joint constraints. We consider both MUST and DESI samples and adopt a fiducial value of $M_\nu = 0.06$ eV, which is approximately the lower bound allowed by the normal hierarchy within the Λ CDM cosmology. The forecast results are shown in Figure 12. With $k_{\text{max}} = 0.4 h \text{ Mpc}^{-1}$, we find that the combination of DESI and CMB data can constrain M_ν with a precision corresponding to a $\sim 1.1\sigma$ sensitivity to the mass hierarchy. MUST, when combined with CMB data, further reduces the statistical uncertainty by approximately 25%, yielding $\sigma(M_\nu) \simeq 0.026$ eV under both optimistic and conservative assumptions about the available targets.

It is important to note that our forecasts are not directly comparable to current constraints from observational data (e.g., [313]). Under the Λ CDM framework, existing datasets tend to prefer an effective negative neutrino mass, leading to much tighter M_ν constraints than would be expected from Fisher forecasts [314]. This preference arises because the measured amplitude of matter clustering is higher than predicted by Λ CDM and can be partially compensated by the inverse suppression effect of an (unphysical) negative neutrino mass. This tension can be significantly alleviated by allowing for a time-evolving dark energy, as discussed in [313]. For this reason, we further perform forecasts assuming the best-fit $w_0 w_a$ CDM cosmology from [78], as shown in Figure 12. In this case, the uncertainties on M_ν are generally larger due to the increased model freedom. Nonetheless, the joint DESI and CMB constraint is still expected to yield a $\sim 1\sigma$ detection of a non-zero total neutrino mass, while the combination of MUST and CMB achieves a $\sim 15\%$ reduction in the M_ν uncertainty. In summary, MUST will provide valuable insights into the apparent “negative neutrino mass” problem and may offer further cosmological clues about the neutrino mass hi-

erarchy.

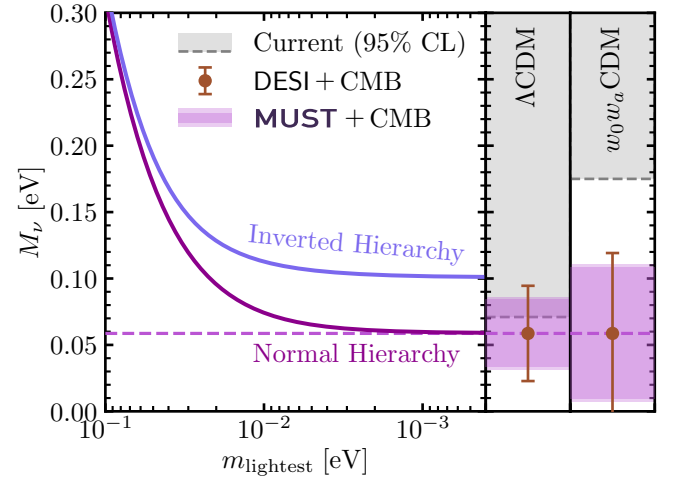


Figure 12 Fisher forecasts for the total neutrino mass, M_ν , based on the MUST and DESI galaxy power spectrum with $k_{\text{max}} = 0.4 h \text{ Mpc}^{-1}$, combined with existing CMB constraints from Planck PR3 [65] and ACT DR6 [277] data. *Left*: M_ν as a function of the mass of the lightest neutrino species, for both the normal and inverted mass hierarchies. *Center*: forecasted 1σ M_ν uncertainties assuming the fiducial Λ CDM model. *Right*: forecasts assuming the best-fit $w_0 w_a$ CDM cosmology from [78]. The gray shaded region shows the 95% CL upper bound from the combination of BAO and Planck CMB data [315].

5.6 Warm Dark Matter

The Ly α forest is a powerful probe of small-scale structures, offering constraints on dark matter models that suppress small-scale clustering power. When accounting for the effects of inhomogeneous H I reionization [155], the Ly α forest power spectrum can distinguish between different dark matter scenarios even on relatively large scales ($k \lesssim 0.6 h \text{ Mpc}^{-1}$) (Zhang et al. in prep.). In this work, we focus on warm dark matter models, whose characteristic suppression of small-scale clustering is representative of a broader class of models with similar cutoff behavior. We forecast the ability of MUST to place competitive constraints on the WDM particle mass by leveraging the reionization imprints on the Ly α forest power spectrum.

Following [155], the three-dimensional flux power spectrum is given by

$$P_F^{3D}(\mathbf{k}, z, m_X) = b_F^2(1 + \beta_F \mu^2) P_m + 2b_F b_T(1 + \beta_F \mu^2) P_{m,\psi}, \quad (25)$$

where b_F and β_F are the flux bias and RSD parameter, respectively. b_T is the radiation bias [316], $\mu \equiv k_{\parallel}/k$ is the cosine of the angle between the wavevector and the line of sight, and $P_{m,\psi}$ is the cross-power spectrum between matter and the IGM transparency, which captures the response of the IGM to reionization. The second term in Eq. (25) links the small-scale suppression caused by warm dark matter during

reionization to a distinct large-scale signature in the Ly α forest, i.e., the impact of inhomogeneous reionization. These reionization imprints are associated with the scale of ionized bubbles, which typically range from a few to several tens of Mpc. On such large scales, the need of nonlinear modeling and the dependence of the bias terms on m_X can be reasonably neglected.

To forecast constraints on the WDM mass m_X from MUST, we include both m_X and σ_8 as free parameters to account for potential degeneracies. The analysis considers 12 redshift bins from 2.0 to 3.8 and 45 k bins spanning 0.09 to $0.67 h \text{ Mpc}^{-1}$. We adopt an estimated quasar luminosity function for MUST with $r < 23.5$ and evaluate the results with three survey areas: 5,000, 10,000, and 14,000 deg^2 . The covariance matrices are computed following [317, 318], including an aliasing term that accounts for the sparse sampling of quasars. Figure 13 shows the m_X constraints from MUST for different survey areas, along with a comparison to current limits from existing observational data. We adopt a fiducial model corresponding to the CDM limit ($m_X \rightarrow \infty$). In this case, we constrain the lower bound of the WDM particle mass. An optimistic survey covering 14,000 deg^2 would yield the most stringent lower bound on m_X to date, with a 95% CL limit of 10.5 keV. Even a conservative 10,000 deg^2 survey would achieve $m_X > 7.6 \text{ keV}$, exceeding the current strongest Ly α forest-only constraint of $m_X > 5.7 \text{ keV}$ [152].

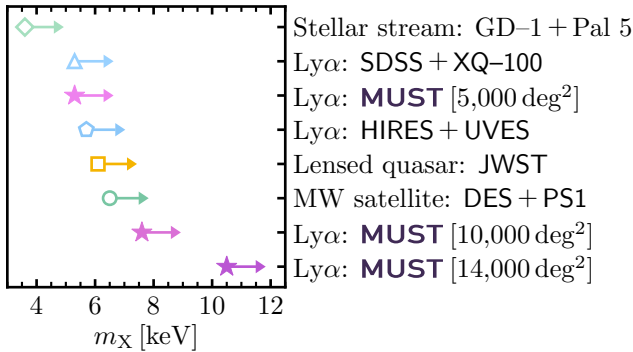


Figure 13 Warm dark matter constraints. Arrows indicate the allowed parameter space (lower bounds) at the 95% confidence level (CL), which extend towards infinity, corresponding to the CDM limit—the fiducial model for the forecasts. For comparison, we include representative constraints from MW stellar streams [319], MW satellite counts [320, 321], Lyman- α forest measured from eBOSS + XQ-100 [151] and HIRES + UVES [152], as well as strongly lensed quasars from JWST [322].

6 Conclusions

The MULTiplexed Survey Telescope (MUST) is a 6.5-meter telescope dedicated to multi-object spectroscopic observa-

tions. It features a modularized focal plane with 336 triangular modules that accommodate over 20,000 fibers at the Cassegrain focus. The spectrographs are designed with three channels to cover a wavelength range of $\sim 3700\text{--}9600 \text{ \AA}$ at a resolution of $R \sim 2000\text{--}4000$. Initial monitoring of observing conditions indicates that the MUST candidate site, Peak A of the Saishiteng Mountain near Lenghu Town, could provide over 2,400 observing hours annually, making MUST at least 10 times more efficient than currently operating spectroscopic surveys. As a result, MUST is expected to collect over 100 million spectra that are significantly fainter than those in existing spectroscopic databases in the 2030s.

While designed as a flexible spectroscopic platform, the primary mission of MUST is to conduct the first Stage-V galaxy spectroscopic survey¹⁹⁾ to address fundamental questions in cosmology and physics. With its unprecedented photon collecting capability as a spectroscopic telescope, MUST will produce the first 3D map of galaxies spanning from the nearby Universe out to $z \sim 5.5$, which corresponds to ~ 1 billion years after the Big Bang. This large survey volume enables in-depth studies of the dynamic evolution of the dark Universe and signatures of fundamental physics from the primordial era. Thus, the primary scientific objectives of MUST include, but are not limited to, investigating the nature and evolution of dark energy, testing gravity theories, probing inflation physics through primordial non-Gaussianity, and exploring the properties of neutrinos and dark matter.

Different types of targets are required to cover the extensive redshift range with sufficient density to achieve these ambitious scientific goals. For the low-redshift Universe ($z \lesssim 1.6$), MUST will utilize the same galaxy targets and similar selection criteria as DESI, but will focus on fainter samples to avoid redundant observations. Beyond $z \sim 2$, MUST will mainly rely on LBGs and LAEs to map large-scale structures. Although the actual target selection and redshift measurement efficiencies are not yet fully verified, current multi-band imaging and spectroscopic validation data in limited areas suggest that these tracers will be abundant enough for precise cosmological inferences. Meanwhile, QSOs will play a vital complementary role in probing the IGM, which is crucial for studying specific physical effects, such as the mass of dark matter particles.

We have performed forecasts for several key science cases of MUST. The increased galaxy density at low redshift ($z \lesssim 1.5$) and the introduction of new tracers at high redshift ($z \gtrsim 2$) enable percent-level measurements of cosmological distances and structure growth across the entire redshift range of $0 < z \lesssim 5.5$. As a result, constraints on density parameters (including Ω_m and Ω_k), the dark energy equa-

¹⁹⁾ proposed by the Snowmass Cosmic Frontier report [79] as a continuation of the stages defined by the Dark Energy Task Force [15]

tion of state (w_0 , w_a), and the phenomenological modified gravity parameter μ_0 will be substantially tighter than those forecasted for DESI, the current state-of-the-art Stage-IV survey. This demonstrates the potential of MUST not only to distinguish among different dark energy and gravity models, but also to provide stringent cross-checks of observational systematics when compared with other cosmological probes such as CMB. With MUST data, constraints on the amplitude of local-type primordial non-Gaussianity (f_{NL}^{local}), when combined with current CMB results, are expected to reach the ~ 1 level. Even stronger constraints may be achievable with more advanced summary statistics and data analysis methods, offering a powerful test of inflation models. The combination of MUST and CMB data is further expected to yield a statistical uncertainty of ~ 0.03 eV on the total neutrino mass within the Λ CDM framework, enabling valuable insights into the absolute neutrino mass and the mass hierarchy. Additionally, using Lyman- α forest data, MUST can place a lower limit of ~ 10.5 keV on the warm dark matter particle mass for a 14,000 deg² survey area, surpassing the current best constraints by nearly a factor of two. Together, these forecasts demonstrate that the MUST spectroscopic survey will make a substantial contribution to addressing some of the long-standing fundamental questions in cosmology and particle physics.

The MUST project is supported by the Ministry of Science and Technology, China (Grant No. 2023YFA1605600) and the Ministry of Education, China.

We want to express our sincere gratitude to Mr. Tian-Pei Chen for his generous donation and unwavering trust, which have significantly supported the MUST project. We also thank Mr. Dong-Hua Dong for his donation.

The authors thanks Noah Sailer, Anand Raichoor, Christophe Yèche, Teppei Okumura, Ji Yao for useful discussions.

Song Huang acknowledges the support from the National Natural Science Foundation of China (NSFC) Grant No. 12273015 & No. 12433003 and the China Crewed Space Program through its Space Application System.

JPK, AR, DF, JY, AV, RG, and SH acknowledge the support from the SNF 200020_175751 and 200020_207379 “Cosmology with 3D Maps of the Universe” research grant.

Si-Wei Zou acknowledges the support from the National Science Foundation of China (No. 12303011).

Yu Liu acknowledges the support from the National Science Foundation of China (No. 12303005) and the Shuimu Tsinghua Scholar Program (No. 2022SM173).

Pablo Renard acknowledges the support by the Tsinghua Shui Mu Scholarship, funding of the National Key R&D Program of China (grant no. 2023YFA1605600), and the science research grants from the China Manned Space Project with No. CMS-CSST2021-A05, the Tsinghua University Initiative Scientific Research Program (No. 20223080023), and the National Science Foundation of China (No. 12350410365).

Conflict of interest The authors declare that they have no conflict of interest.

- 1 J. Huchra, M. Davis, D. Latham, and J. Tonry, *ApJS***52**, 89 (1983).
- 2 V. de Lapparent, M. J. Geller, and J. P. Huchra, *ApJ***302**, L1 (1986).
- 3 C. L. Bennett, D. Larson, J. L. Weiland et al., *ApJS***208**, 20 (2013), arXiv: [1212.5225](#).
- 4 Planck Collaboration, N. Aghanim, Y. Akrami et al., *A&A***641**, A6 (2020), arXiv: [1807.06209](#).
- 5 D. Scolnic, D. Brout, A. Carr et al., *ApJ***938**, 113 (2022), arXiv: [2112.03863](#).
- 6 M. Betoule, R. Kessler, J. Guy et al., *A&A***568**, A22 (2014), arXiv: [1401.4064](#).
- 7 DES Collaboration, T. M. C. Abbott, M. Acevedo et al., arXiv e-prints **973**, arXiv:2401.02929 (2024), arXiv: [2401.02929](#).
- 8 T. M. C. Abbott, M. Aguena, A. Alarcon et al., *Phys. Rev. D***105**, 023520 (2022), arXiv: [2105.13549](#).
- 9 C. Heymans, T. Tröster, M. Asgari et al., *A&A***646**, A140 (2021), arXiv: [2007.15632](#).
- 10 S. Alam, M. Aubert, S. Avila et al., *Phys. Rev. D***103**, 083533 (2021), arXiv: [2007.08991](#).
- 11 DESI Collaboration, B. Abareshi, J. Aguilar et al., *AJ***164**, 207 (2022), arXiv: [2205.10939](#).
- 12 D. J. Eisenstein, I. Zehavi, D. W. Hogg et al., *ApJ***633**, 560 (2005), arXiv: [astro-ph/0501171](#).
- 13 N. Kaiser, *MNRAS***227**, 1 (1987).
- 14 DESI Collaboration, A. G. Adame, J. Aguilar et al., arXiv e-prints arXiv:2404.03000 (2024), arXiv: [2404.03000](#).
- 15 A. Albrecht, G. Bernstein, R. Cahn et al., arXiv e-prints astro-ph/0609591 (2006), arXiv: [astro-ph/0609591](#).
- 16 N. Sailer, E. Castorina, S. Ferraro, and M. White, *J. Cosmology Astropart. Phys.***2021**, 049 (2021), arXiv: [2106.09713](#).
- 17 H. Zhan, *Chinese Sci. Bull.* **66**, 1290 (2021), URL <https://www.sciengine.com/10.1360/TB-2021-0016>.
- 18 Euclid Collaboration, Y. Mellier, Abdurro'uf et al., arXiv e-prints arXiv:2405.13491 (2024), arXiv: [2405.13491](#).
- 19 D. Spergel, N. Gehrels, J. Breckinridge et al., arXiv e-prints arXiv:1305.5422 (2013), arXiv: [1305.5422](#).
- 20 Ž. Ivezić, S. M. Kahn, J. A. Tyson et al., *ApJ***873**, 111 (2019), arXiv: [0805.2366](#).
- 21 V. Ruhlmann-Kleider, C. Yèche, C. Magneville et al., *J. Cosmology Astropart. Phys.***2024**, 059 (2024), arXiv: [2404.03569](#).
- 22 C. Payerne, W. d'Assignies Doumerg, C. Yèche et al., arXiv e-prints arXiv:2410.08062 (2024), arXiv: [2410.08062](#).
- 23 J. McCullough, D. Gruen, A. Amon et al., *MNRAS***531**, 2582 (2024), arXiv: [2309.13109](#).
- 24 S. Samuroff, R. Mandelbaum, J. Blazek et al., *MNRAS***524**, 2195 (2023), arXiv: [2212.11319](#).
- 25 C. Lamman, D. Eisenstein, J. N. Aguilar et al., *MNRAS***522**, 117 (2023), arXiv: [2209.03949](#).
- 26 R. C. Wolf, C. B. D'Andrea, R. R. Gupta et al., *ApJ***821**, 115 (2016), arXiv: [1602.02674](#).
- 27 M. T. Soumagnac, P. Nugent, R. A. Knop et al., arXiv e-prints arXiv:2405.03857 (2024), arXiv: [2405.03857](#).
- 28 J. Koda, C. Blake, T. Davis et al., *MNRAS***445**, 4267 (2014), arXiv: [1312.1022](#).
- 29 K. Said, C. Howlett, T. Davis et al., arXiv e-prints arXiv:2408.13842 (2024), arXiv: [2408.13842](#).
- 30 E. Kitanidis and M. White, *MNRAS***501**, 6181 (2021), arXiv: [2010.04698](#).
- 31 J. Myles, A. Alarcon, A. Amon et al., *MNRAS***505**, 4249 (2021), arXiv: [2012.08566](#), URL <https://dx.doi.org/10.1093/mnras/stab1515>.

- 32 S. Yuan, C. Blake, A. Krolewski et al., *MNRAS***533**, 589 (2024), arXiv: [2403.00915](#).
- 33 J. U. Lange, C. Blake, C. Saulder et al., *The Open Journal of Astrophysics* **7**, 57 (2024), arXiv: [2404.09397](#).
- 34 S. Chen, J. DeRose, R. Zhou et al., arXiv e-prints arXiv:2407.04795 (2024), arXiv: [2407.04795](#).
- 35 M. Amiri, K. Bandura, T. Chen et al., *ApJ***947**, 16 (2023), arXiv: [2202.01242](#).
- 36 C. L. Chang, L. Newburgh, D. Shoemaker et al., arXiv e-prints arXiv:2209.08265 (2022), arXiv: [2209.08265](#).
- 37 J. Annis, J. A. Newman, and A. Slosar, arXiv e-prints arXiv:2209.08049 (2022), arXiv: [2209.08049](#).
- 38 D. J. Schlegel, J. A. Kollmeier, G. Aldering et al., arXiv e-prints arXiv:2209.04322 (2022), arXiv: [2209.04322](#).
- 39 G. A. Blanc, J. H. Silber, S. Smee et al., in *Ground-based and Airborne Telescopes IX*, (edited by H. K. Marshall, J. Spyromilio, and T. Usuda), volume 12182 of *Society of Photo-Optical Instrumentation Engineers (SPIE) Conference Series*, 1218230 (2022).
- 40 S. Asai, A. Ballarino, T. Bose et al., arXiv e-prints arXiv:2407.19176 (2024), arXiv: [2407.19176](#).
- 41 A. Sheinis, S. C. Barden, and J. Sobek, *Astronomische Nachrichten* **344**, e20230108 (2023), arXiv: [2307.07667](#).
- 42 V. Mainieri, R. I. Anderson, J. Brinchmann et al., arXiv e-prints arXiv:2403.05398 (2024), arXiv: [2403.05398](#).
- 43 D.-q. Su, H. Bai, X. Yuan, and X. Cui, *Science China Physics, Mechanics, and Astronomy* **67**, 279511 (2024), arXiv: [2310.04697](#).
- 44 Y. Zhang, H. Jiang, S. Shectman et al., *Photonix* **4**, 16 (2023).
- 45 N. Galitzki, A. Ali, K. S. Arnold et al., in *Millimeter, Submillimeter, and Far-Infrared Detectors and Instrumentation for Astronomy IX*, (edited by J. Zmuidzinas and J.-R. Gao), volume 10708 of *Society of Photo-Optical Instrumentation Engineers (SPIE) Conference Series*, 1070804 (2018), arXiv: [1808.04493](#).
- 46 K. N. Abazajian, P. Adshead, Z. Ahmed et al., arXiv e-prints arXiv:1610.02743 (2016), arXiv: [1610.02743](#).
- 47 LiteBIRD Collaboration, E. Allys, K. Arnold et al., *Progress of Theoretical and Experimental Physics* **2023**, 042F01 (2023), arXiv: [2202.02773](#).
- 48 Square Kilometre Array Cosmology Science Working Group, D. J. Bacon, R. A. Battye et al., *PASA***37**, e007 (2020), arXiv: [1811.02743](#).
- 49 J. B. Oke and J. E. Gunn, *ApJ***266**, 713 (1983).
- 50 D. J. Schlegel, S. Ferraro, G. Aldering et al., arXiv e-prints arXiv:2209.03585 (2022), arXiv: [2209.03585](#).
- 51 G. Marchiori, S. De Lorenzi, L. Ghedin et al., in *Ground-based and Airborne Telescopes X*, (edited by H. K. Marshall, J. Spyromilio, and T. Usuda), volume 13094 of *Society of Photo-Optical Instrumentation Engineers (SPIE) Conference Series*, 1309439 (2024).
- 52 P. Li, Z. Wang, S. Huang et al., *Optics Express* **32**, 20931 (2024).
- 53 X. Xing, C. Zhai, H. Du, W. Li, H. Hu, R. Wang, and D. Shi, in *Advanced Technology Optical/IR Telescopes VI*, (edited by L. M. Stepp), volume 3352 of *Society of Photo-Optical Instrumentation Engineers (SPIE) Conference Series*, 839–849 (1998).
- 54 G. Smith, J. Brzeski, S. Miziarski, P. R. Gillingham, A. Moore, and A. McGrath, in *Astronomical Structures and Mechanisms Technology*, (edited by J. Antebi and D. Lemke), volume 5495 of *Society of Photo-Optical Instrumentation Engineers (SPIE) Conference Series*, 348–359 (2004).
- 55 M. Akiyama, S. Smedley, P. Gillingham et al., in *Advanced Optical and Mechanical Technologies in Telescopes and Instrumentation*, (edited by E. Atad-Ettingui and D. Lemke), volume 7018 of *Society of Photo-Optical Instrumentation Engineers (SPIE) Conference Series*, 70182V (2008).
- 56 N. F. Staszak, J. Lawrence, D. M. Brown et al., in *Advances in Optical and Mechanical Technologies for Telescopes and Instrumentation II*, (edited by R. Navarro and J. H. Burge), volume 9912 of *Society of Photo-Optical Instrumentation Engineers (SPIE) Conference Series*, 99121W (2016).
- 57 J. Brzeski, G. Baker, S. Baker et al., in *Ground-based and Airborne Instrumentation for Astronomy VII*, (edited by C. J. Evans, L. Simard, and H. Takami), volume 10702 of *Society of Photo-Optical Instrumentation Engineers (SPIE) Conference Series*, 1070279 (2018).
- 58 M. Schubnell, J. Ameel, R. W. Besuner et al., in *Ground-based and Airborne Instrumentation for Astronomy VI*, (edited by C. J. Evans, L. Simard, and H. Takami), volume 9908 of *Society of Photo-Optical Instrumentation Engineers (SPIE) Conference Series*, 990892 (2016).
- 59 M. Rombach, X. Xu, R. Araujo et al., in *Ground-based and Airborne Instrumentation for Astronomy X*, (edited by J. J. Bryant, K. Motohara, and J. R. D. Vernet), volume 13096 of *Society of Photo-Optical Instrumentation Engineers (SPIE) Conference Series*, 130969V (2024).
- 60 J. H. Silber, D. J. Schlegel, R. Araujo et al., arXiv e-prints arXiv:2212.07908 (2022), arXiv: [2212.07908](#).
- 61 R. Besuner, A. Dey, A. Drlica-Wagner et al., arXiv e-prints arXiv:2503.07923 (2025), arXiv: [2503.07923](#).
- 62 L. Deng, F. Yang, X. Chen et al., *Nature***596**, 353 (2021).
- 63 JUST Team, C. Liu, Y. Zu et al., *Astronomical Techniques and Instruments* **1**, 16 (2024), arXiv: [2402.14312](#).
- 64 Gaia Collaboration, A. G. A. Brown, A. Vallenari et al., *A&A***649**, A1 (2021), arXiv: [2012.01533](#).
- 65 Planck Collaboration, N. Aghanim, Y. Akrami et al., *A&A***641**, A5 (2020), arXiv: [1907.12875](#).
- 66 A. G. Riess, A. V. Filippenko, P. Challis et al., *AJ***116**, 1009 (1998), arXiv: [astro-ph/9805201](#).
- 67 S. Perlmutter, G. Aldering, G. Goldhaber et al., *ApJ***517**, 565 (1999), arXiv: [astro-ph/9812133](#).
- 68 S. M. Carroll, W. H. Press, and E. L. Turner, *ARA&A***30**, 499 (1992).
- 69 L. Perivolaropoulos and F. Skara, *New A Rev.***95**, 101659 (2022), arXiv: [2105.05208](#).
- 70 E. J. Copeland, M. Sami, and S. Tsujikawa, *International Journal of Modern Physics D* **15**, 1753 (2006), arXiv: [hep-th/0603057](#).
- 71 M. Chevallier and D. Polarski, *International Journal of Modern Physics D* **10**, 213 (2001), arXiv: [gr-qc/0009008](#).
- 72 E. V. Linder, *Phys. Rev. Lett.***90**, 091301 (2003), arXiv: [astro-ph/0208512](#).
- 73 D. J. Eisenstein and W. Hu, *ApJ***496**, 605 (1998), arXiv: [astro-ph/9709112](#).
- 74 O. H. E. Philcox, B. D. Sherwin, G. S. Farren, and E. J. Baxter, *Phys. Rev. D***103**, 023538 (2021), arXiv: [2008.08084](#).
- 75 F. Dong, C. Park, S. E. Hong, J. Kim, H. S. Hwang, H. Park, and S. Appleby, *ApJ***953**, 98 (2023), arXiv: [2305.00206](#).
- 76 S. Cole, W. J. Percival, J. A. Peacock et al., *MNRAS***362**, 505 (2005), arXiv: [astro-ph/0501174](#).
- 77 DESI Collaboration, M. Abdul-Karim, J. Aguilar et al., arXiv e-prints arXiv:2503.14738 (2025), arXiv: [2503.14738](#).
- 78 DESI Collaboration, A. G. Adame, J. Aguilar et al., arXiv e-prints arXiv:2404.03002 (2024), arXiv: [2404.03002](#).
- 79 A. S. Chou, M. Soares-Santos, T. M. P. Tait et al., arXiv e-prints arXiv:2211.09978 (2022), arXiv: [2211.09978](#).
- 80 D. Huterer, *A&A Rev.***31**, 2 (2023), arXiv: [2212.05003](#).
- 81 A. J. S. Hamilton, in *The Evolving Universe*, (edited by D. Hamilton), volume 231 of *Astrophysics and Space Science Library*, 185 (1998), arXiv: [astro-ph/9708102](#).
- 82 Y.-S. Song and W. J. Percival, *J. Cosmology Astropart. Phys.***2009**, 004 (2009), arXiv: [0807.0810](#).
- 83 G.-B. Zhao, T. Giannantonio, L. Pogosian et al., *Phys. Rev. D***81**, 103510 (2010), arXiv: [1003.0001](#).
- 84 T. M. C. Abbott et al. (DES), *Phys. Rev. D* **107**, 083504 (2023), arXiv: [2207.05766](#).
- 85 K. S. Dawson, J.-P. Kneib, W. J. Percival et al., *AJ***151**, 44 (2016), arXiv: [1508.04473](#).
- 86 P. McDonald, *J. Cosmology Astropart. Phys.***2009**, 026 (2009), arXiv:

- 0907.5220.
- 87 A. Achúcarro, M. Biagetti, M. Braglia et al., arXiv e-prints arXiv:2203.08128 (2022), arXiv: [2203.08128](#).
 - 88 J. Ellis and D. Wands, arXiv e-prints arXiv:2312.13238 (2023), arXiv: [2312.13238](#).
 - 89 Planck Collaboration, Y. Akrami, F. Arroja et al., A&A**641**, A10 (2020), arXiv: [1807.06211](#).
 - 90 R. Flauger, L. McAllister, E. Pajer, A. Westphal, and G. Xu, J. Cosmology Astropart. Phys.**2010**, 009 (2010), arXiv: [0907.2916](#).
 - 91 X. Chen and M. H. Namjoo, Physics Letters B **739**, 285 (2014), arXiv: [1404.1536](#).
 - 92 X. Chen, Advances in Astronomy **2010**, 638979 (2010), arXiv: [1002.1416](#).
 - 93 P. D. Meerburg, D. Green, R. Flauger et al., BAAS**51**, 107 (2019), arXiv: [1903.04409](#).
 - 94 D. Karagiannis, T. Shanks, and N. P. Ross, MNRAS**441**, 486 (2014), arXiv: [1310.6716](#).
 - 95 M. S. Cagliari, E. Castorina, M. Bonici, and D. Bianchi, Optimal constraints on Primordial non-Gaussianity with the eBOSS DR16 quasars in Fourier space (2024), arXiv: [2309.15814](#).
 - 96 R. Scoccimarro, L. Hui, M. Manera, and K. C. Chan, Phys. Rev. D**85**, 083002 (2012), arXiv: [1108.5512](#).
 - 97 W. R. Coulton, F. Villaescusa-Navarro, D. Jamieson et al., ApJ**943**, 178 (2023), arXiv: [2206.15450](#).
 - 98 J. Maldacena, Journal of High Energy Physics **2003**, 013 (2003), arXiv: [astro-ph/0210603](#).
 - 99 M. Kawasaki, T. Kobayashi, and F. Takahashi, Phys. Rev. D**84**, 123506 (2011), arXiv: [1107.6011](#).
 - 100 Y.-F. Cai, W. Xue, R. Brandenberger, and X. Zhang, J. Cosmology Astropart. Phys.**2009**, 011 (2009), arXiv: [0903.0631](#).
 - 101 Planck Collaboration, Y. Akrami, F. Arroja et al., A&A**641**, A9 (2020), arXiv: [1905.05697](#).
 - 102 N. Dalal, O. Doré, D. Huterer, and A. Shirokov, Phys. Rev. D**77**, 123514 (2008), arXiv: [0710.4560](#).
 - 103 D. Green, Y. Guo, J. Han, and B. Wallisch, J. Cosmology Astropart. Phys.**2024**, 090 (2024), arXiv: [2311.04882](#).
 - 104 E. Chaussidon, C. Yèche, A. de Mattia et al., arXiv e-prints arXiv:2411.17623 (2024), arXiv: [2411.17623](#).
 - 105 X. Chen and Y. Wang, Phys. Rev. D**81**, 063511 (2010), arXiv: [0909.0496](#).
 - 106 N. Arkani-Hamed and J. Maldacena, arXiv e-prints arXiv:1503.08043 (2015), arXiv: [1503.08043](#).
 - 107 P. D. Meerburg, M. Münchmeyer, J. B. Muñoz, and X. Chen, J. Cosmology Astropart. Phys.**2017**, 050 (2017), arXiv: [1610.06559](#).
 - 108 G. Cabass, O. H. E. Philcox, M. M. Ivanov, K. Akitsu, S.-F. Chen, M. Simonović, and M. Zaldarriaga, arXiv e-prints arXiv:2404.01894 (2024), arXiv: [2404.01894](#).
 - 109 W. Sohn, D.-G. Wang, J. R. Fergusson, and E. P. S. Shellard, arXiv e-prints arXiv:2404.07203 (2024), arXiv: [2404.07203](#).
 - 110 S. Navas, C. Amsler, T. Gutsche et al., Phys. Rev. D**110**, 030001 (2024).
 - 111 M. Aker, D. Batzler, A. Beglarian et al., arXiv e-prints arXiv:2406.13516 (2024), arXiv: [2406.13516](#).
 - 112 J. Lesgourgues and S. Pastor, Phys. Rep.**429**, 307 (2006), arXiv: [astro-ph/0603494](#).
 - 113 J. Lesgourgues and S. Pastor, arXiv e-prints arXiv:1212.6154 (2012), arXiv: [1212.6154](#).
 - 114 Y. Du and J.-H. Yu, Journal of High Energy Physics **2021**, 58 (2021), arXiv: [2101.10475](#).
 - 115 P. F. de Salas, S. Gariazzo, P. Martínez-Miravé, S. Pastor, and M. Tórtola, Physics Letters B **820**, 136508 (2021), arXiv: [2105.08168](#).
 - 116 K. N. Abazajian, M. A. Acero, S. K. Agarwalla et al., arXiv e-prints arXiv:1204.5379 (2012), arXiv: [1204.5379](#).
 - 117 R. D. Peccei and H. R. Quinn, Phys. Rev. Lett.**38**, 1440 (1977).
 - 118 S. Weinberg, Phys. Rev. Lett.**40**, 223 (1978).
 - 119 F. Wilczek, Phys. Rev. Lett.**40**, 279 (1978).
 - 120 S. Hannestad and T. Schwetz, J. Cosmology Astropart. Phys.**2016**, 035 (2016), arXiv: [1606.04691](#).
 - 121 S. Gariazzo, M. Archidiacono, P. F. de Salas, O. Mena, C. A. Ternes, and M. Tórtola, J. Cosmology Astropart. Phys.**2018**, 011 (2018), arXiv: [1801.04946](#).
 - 122 S. R. Choudhury and S. Hannestad, J. Cosmology Astropart. Phys.**2020**, 037 (2020), arXiv: [1907.12598](#).
 - 123 K. Abazajian, A. Abdughafour, G. E. Addison et al., arXiv e-prints arXiv:2203.08024 (2022), arXiv: [2203.08024](#).
 - 124 F. Zwicky, ApJ**86**, 217 (1937).
 - 125 R. A. Flores and J. R. Primack, ApJ**427**, L1 (1994), arXiv: [astro-ph/9402004](#).
 - 126 B. Moore, Nature**370**, 629 (1994).
 - 127 M. Boylan-Kolchin, J. S. Bullock, and M. Kaplinghat, MNRAS**415**, L40 (2011), arXiv: [1103.0007](#).
 - 128 M. R. Buckley and A. H. G. Peter, Phys. Rep.**761**, 1 (2018), arXiv: [1712.06615](#).
 - 129 R. Schaeffer and J. Silk, ApJ**332**, 1 (1988).
 - 130 E. O. Nadler, S. Birrer, D. Gilman et al., ApJ**917**, 7 (2021), arXiv: [2101.07810](#).
 - 131 W. Hu, R. Barkana, and A. Gruzinov, Phys. Rev. Lett.**85**, 1158 (2000), arXiv: [astro-ph/0003365](#).
 - 132 R. Hlozek, D. Grin, D. J. E. Marsh, and P. G. Ferreira, Phys. Rev. D**91**, 103512 (2015), arXiv: [1410.2896](#).
 - 133 D. N. Spergel and P. J. Steinhardt, Phys. Rev. Lett.**84**, 3760 (2000), arXiv: [astro-ph/9909386](#).
 - 134 Z. C. Zeng, A. H. G. Peter, X. Du et al., MNRAS**513**, 4845 (2022), arXiv: [2110.00259](#).
 - 135 S. Hawking, MNRAS**152**, 75 (1971).
 - 136 P. Montero-Camacho, X. Fang, G. Vasquez, M. Silva, and C. M. Hirata, J. Cosmology Astropart. Phys.**2019**, 031 (2019), arXiv: [1906.05950](#).
 - 137 Gaia Collaboration, T. Prusti, J. H. J. de Bruijne et al., A&A**595**, A1 (2016), arXiv: [1609.04153](#).
 - 138 W. Wang, J. Han, M. Cautun, Z. Li, and M. N. Ishigaki, Science China Physics, Mechanics, and Astronomy **63**, 109801 (2020), arXiv: [1912.02599](#).
 - 139 C.-H. Lin, R. Mandelbaum, M. A. Troxel, C. M. Hirata, and M. Jarvis, MNRAS**512**, 3312 (2022), arXiv: [2106.10273](#).
 - 140 R. E. Sanderson, A. Helmi, and D. W. Hogg, ApJ**801**, 98 (2015), arXiv: [1404.6534](#).
 - 141 P. Salucci, A&A Rev.**27**, 2 (2019), arXiv: [1811.08843](#).
 - 142 A. P. Cooper, S. E. Koposov, C. Allende Prieto et al., ApJ**947**, 37 (2023), arXiv: [2208.08514](#).
 - 143 M. R. Lovell, V. Eke, C. S. Frenk et al., MNRAS**420**, 2318 (2012), arXiv: [1104.2929](#).
 - 144 K. A. Oman, J. F. Navarro, A. Fattahi et al., MNRAS**452**, 3650 (2015), arXiv: [1504.01437](#).
 - 145 J. Bovy, D. Erkal, and J. L. Sanders, MNRAS**466**, 628 (2017), arXiv: [1606.03470](#).
 - 146 A. Bonaca, D. W. Hogg, A. M. Price-Whelan, and C. Conroy, ApJ**880**, 38 (2019), arXiv: [1811.03631](#).
 - 147 N. Banik, J. Bovy, G. Bertone, D. Erkal, and T. J. L. de Boer, MNRAS**502**, 2364 (2021), arXiv: [1911.02662](#).
 - 148 F. Jiang, A. Benson, P. F. Hopkins et al., MNRAS**521**, 4630 (2023), arXiv: [2206.12425](#).
 - 149 M. Valluri, S. Chabanier, V. Irsic et al., arXiv e-prints arXiv:2203.07491 (2022), arXiv: [2203.07491](#).
 - 150 A. Laguë, J. R. Bond, R. Hlozek, D. J. E. Marsh, and L. Söding, MNRAS**504**, 2391 (2021), arXiv: [2004.08482](#).
 - 151 N. Palanque-Delabrouille, C. Yèche, N. Schöneberg, J. Lesgourgues, M. Walthers, S. Chabanier, and E. Armengaud, J. Cosmology Astropart. Phys.**2020**, 038 (2020), arXiv: [1911.09073](#).

- 152 V. Iršič, M. Viel, M. G. Haehnelt et al., Phys. Rev. D**109**, 043511 (2024), arXiv: [2309.04533](#).
- 153 A. Garzilli, A. Magalich, O. Ruchayskiy, and A. Boyarsky, MNRAS**502**, 2356 (2021), arXiv: [1912.09397](#).
- 154 E. Puchwein, J. S. Bolton, L. C. Keating et al., MNRAS**519**, 6162 (2023), arXiv: [2207.13098](#).
- 155 P. Montero-Camacho, C. M. Hirata, P. Martini, and K. Honscheid, MNRAS**487**, 1047 (2019), arXiv: [1902.02892](#).
- 156 P. Montero-Camacho, Y. Zhang, and Y. Mao, MNRAS**529**, 3666 (2024), arXiv: [2307.10598](#).
- 157 Euclid Collaboration, R. Scaramella, J. Amiaux et al., A&A**662**, A112 (2022), arXiv: [2108.01201](#).
- 158 R. Akeson, L. Armus, E. Bachelet et al., arXiv e-prints arXiv:1902.05569 (2019), arXiv: [1902.05569](#).
- 159 H. Aihara, N. Arimoto, R. Armstrong et al., PASJ**70**, S4 (2018), arXiv: [1704.05858](#).
- 160 H. Aihara, Y. Aisayyad, M. Ando et al., PASJ**74**, 247 (2022), arXiv: [2108.13045](#).
- 161 T. Wang, G. Liu, Z. Cai et al., Science China Physics, Mechanics, and Astronomy **66**, 109512 (2023), arXiv: [2306.07590](#).
- 162 N. Benitez, R. Dupke, M. Moles et al., arXiv e-prints arXiv:1403.5237 (2014), arXiv: [1403.5237](#).
- 163 B. Joachimi, R. Mandelbaum, F. B. Abdalla, and S. L. Bridle, A&A**527**, A26 (2011), arXiv: [1008.3491](#).
- 164 I. Tutusaus, M. Martinelli, V. F. Cardone et al., A&A**643**, A70 (2020), arXiv: [2005.00055](#).
- 165 J. L. van den Busch, A. H. Wright, H. Hildebrandt et al., A&A**664**, A170 (2022), arXiv: [2204.02396](#).
- 166 T. Treu, ARA&A**48**, 87 (2010), arXiv: [1003.5567](#).
- 167 P. Renard, D. Spinoso, P. Montero-Camacho, Z. Sun, H. Zou, and Z. Cai, MNRAS**535**, 826 (2024), arXiv: [2406.18775](#).
- 168 H. Li, S.-Y. Li, Y. Liu et al., arXiv e-prints arXiv:1710.03047 (2017), arXiv: [1710.03047](#).
- 169 P. Ade, J. Aguirre, Z. Ahmed et al., J. Cosmology Astropart. Phys.**2019**, 056 (2019), arXiv: [1808.07445](#).
- 170 K. Abazajian, G. Addison, P. Adshead et al., arXiv e-prints arXiv:1907.04473 (2019), arXiv: [1907.04473](#).
- 171 T. Ghigna, A. Adler, K. Aizawa et al., arXiv e-prints arXiv:2406.02724 (2024), arXiv: [2406.02724](#).
- 172 B. M. Sutin, M. Alvarez, N. Battaglia et al., in *Space Telescopes and Instrumentation 2018: Optical, Infrared, and Millimeter Wave*, (edited by M. Lystrup, H. A. MacEwen, G. G. Fazio, N. Batalha, N. Siegler, and E. C. Tong), volume 10698 of *Society of Photo-Optical Instrumentation Engineers (SPIE) Conference Series*, 106984F (2018), arXiv: [1808.01368](#).
- 173 T. Namikawa, A. I. Lonappan, C. Baccigalupi et al., J. Cosmology Astropart. Phys.**2024**, 010 (2024), arXiv: [2312.05194](#).
- 174 Y.-C. Li, Y.-Z. Ma, M. Remazeilles, and K. Moodley, Phys. Rev. D**97**, 023514 (2018), arXiv: [1710.10876](#).
- 175 S. R. Furlanetto and A. Lidz, ApJ**660**, 1030 (2007), arXiv: [astro-ph/0611274](#).
- 176 P. La Plante, J. Mirocha, A. Gorce, A. Lidz, and A. Parsons, ApJ**944**, 59 (2023), arXiv: [2205.09770](#).
- 177 F. Villaescusa-Navarro, M. Viel, D. Alonso, K. K. Datta, P. Bull, and M. G. Santos, J. Cosmology Astropart. Phys.**2015**, 034 (2015), arXiv: [1410.7393](#).
- 178 I. P. Carucci, F. Villaescusa-Navarro, and M. Viel, J. Cosmology Astropart. Phys.**2017**, 001 (2017), arXiv: [1611.07527](#).
- 179 P. Montero-Camacho, C. Morales-Gutiérrez, Y. Zhang, H. Long, and Y. Mao, MNRAS**536**, 1645 (2025), arXiv: [2409.11613](#).
- 180 C. B. V. Dash and T. Guha Sarkar, J. Cosmology Astropart. Phys.**2021**, 016 (2021), arXiv: [2010.05816](#).
- 181 C. B. V. Dash, T. G. Sarkar, and A. K. Sarkar, Journal of Astrophysics and Astronomy **44**, 5 (2023).
- 182 A. K. Sarkar, A. K. Pal, and T. Guha Sarkar, J. Cosmology Astropart. Phys.**2019**, 058 (2019), arXiv: [1907.10309](#).
- 183 LIGO Scientific Collaboration, J. Aasi, B. P. Abbott et al., Classical and Quantum Gravity **32**, 074001 (2015), arXiv: [1411.4547](#).
- 184 P. Amaro-Seoane, H. Audley, S. Babak et al., arXiv e-prints arXiv:1702.00786 (2017), arXiv: [1702.00786](#).
- 185 Z. Luo, Y. Wang, Y. Wu, W. Hu, and G. Jin, Prog. Theor. Exp. Phys.**2021** (2021), URL <https://dx.doi.org/10.1093/ptep/ptaa083>.
- 186 M. Punturo, M. Abernathy, F. Acernese et al., Classical and Quantum Gravity **27**, 194002 (2010).
- 187 G. Agazie, A. Anumalapudi, A. M. Archibald et al., ApJ**951**, L8 (2023), arXiv: [2306.16213](#).
- 188 H. Xu, S. Chen, Y. Guo et al., Research in Astronomy and Astrophysics **23**, 075024 (2023), arXiv: [2306.16216](#).
- 189 EPTA Collaboration, InPTA Collaboration, J. Antoniadis et al., A&A**678**, A50 (2023), arXiv: [2306.16214](#).
- 190 CHIME/FRB Collaboration, M. Amiri, B. C. Andersen et al., ApJS**257**, 59 (2021), arXiv: [2106.04352](#).
- 191 W. Lu and A. L. Piro, ApJ**883**, 40 (2019), arXiv: [1903.00014](#).
- 192 K. M. Rajwade, M. C. Bezuidenhout, M. Caleb et al., MNRAS**514**, 1961 (2022), arXiv: [2205.14600](#).
- 193 C.-H. Niu, D. Li, R. Luo et al., ApJ**909**, L8 (2021), arXiv: [2102.10546](#).
- 194 D. E. Holz and S. A. Hughes, ApJ**629**, 15 (2005), arXiv: [astro-ph/0504616](#).
- 195 B. P. Abbott, R. Abbott, T. D. Abbott et al., Nature**551**, 85 (2017), arXiv: [1710.05835](#).
- 196 A. Palmese, O. Graur, J. T. Annis et al., BAAS**51**, 310 (2019), arXiv: [1903.04730](#).
- 197 C. Cigarrán Díaz and S. Mukherjee, MNRAS**511**, 2782 (2022), arXiv: [2107.12787](#).
- 198 N. Borghi, M. Mancarella, M. Moresco, M. Tagliazucchi, F. Iacovelli, A. Cimatti, and M. Maggiore, ApJ**964**, 191 (2024), arXiv: [2312.05302](#).
- 199 X. P. You, G. Hobbs, W. A. Coles et al., MNRAS**378**, 493 (2007), arXiv: [astro-ph/0702366](#).
- 200 M. McQuinn, ApJ**780**, L33 (2014), arXiv: [1309.4451](#).
- 201 Y. Huang, K.-G. Lee, N. I. Libeskind, S. Simha, A. Valade, and J. X. Prochaska, arXiv e-prints arXiv:2410.22098 (2024), arXiv: [2410.22098](#).
- 202 C. W. James, E. M. Ghosh, J. X. Prochaska et al., MNRAS**516**, 4862 (2022), arXiv: [2208.00819](#).
- 203 S. Hagstotz, R. Reischke, and R. Lilow, MNRAS**511**, 662 (2022), arXiv: [2104.04538](#).
- 204 A. L. Coil, M. R. Blanton, S. M. Burles et al., ApJ**741**, 8 (2011), arXiv: [1011.4307](#).
- 205 R. J. Cool, J. Moustakas, M. R. Blanton et al., ApJ**767**, 118 (2013), arXiv: [1303.2672](#).
- 206 G. B. Brammer, P. G. van Dokkum, M. Franx et al., ApJS**200**, 13 (2012), arXiv: [1204.2829](#).
- 207 K. Gebhardt, E. Mentuch Cooper, R. Ciardullo et al., ApJ**923**, 217 (2021), arXiv: [2110.04298](#).
- 208 C. Hahn, M. J. Wilson, O. Ruiz-Macias et al., AJ**165**, 253 (2023), arXiv: [2208.08512](#).
- 209 R. Zhou, B. Dey, J. A. Newman et al., AJ**165**, 58 (2023), arXiv: [2208.08515](#).
- 210 A. Raichoor, J. Moustakas, J. A. Newman et al., AJ**165**, 126 (2023), arXiv: [2208.08513](#).
- 211 E. Chaussidon, C. Yèche, N. Palanque-Delabrouille et al., ApJ**944**, 107 (2023), arXiv: [2208.08511](#).
- 212 B. Hoyle, K. Paech, M. M. Rau, S. Seitz, and J. Weller, MNRAS**458**, 4498 (2016), arXiv: [1508.06280](#).
- 213 E. Darragh-Ford, J. F. Wu, Y.-Y. Mao et al., ApJ**954**, 149 (2023), arXiv: [2212.07433](#).
- 214 S. H. Im, H. S. Hwang, J. Park et al., ApJ**972**, 196 (2024), arXiv: [2407.18602](#).

- 215 E. M. Hu and R. G. McMahon, *Nature***382**, 231 (1996), arXiv: [astro-ph/9606135](#).
- 216 L. L. Cowie and E. M. Hu, *AJ***115**, 1319 (1998), arXiv: [astro-ph/9801003](#).
- 217 M. White, A. Raichoor, A. Dey et al., *J. Cosmology Astropart. Phys.***2024**, 020 (2024), arXiv: [2406.01803](#).
- 218 M. E. Schwamb, K. Volk, H. Wen et al., arXiv e-prints arXiv:1812.01149 (2018), arXiv: [1812.01149](#).
- 219 A. Dey, D. J. Schlegel, D. Lang et al., *AJ***157**, 168 (2019), arXiv: [1804.08657](#).
- 220 B. Flaugher, H. T. Diehl, K. Honscheid et al., *AJ***150**, 150 (2015), arXiv: [1504.02900](#).
- 221 K.-S. Lee, E. Gawiser, C. Park et al., *ApJ***962**, 36 (2024), arXiv: [2309.10191](#).
- 222 Y. Luo, A. Leauthaud, J. Greene et al., *MNRAS***530**, 4988 (2024), arXiv: [2305.19310](#).
- 223 P. Bull, *MNRAS***471**, 12 (2017), arXiv: [1610.08948](#).
- 224 G. Favole, D. Sapone, and J. Silva Lafaurie, arXiv e-prints arXiv:1912.06155 (2019), arXiv: [1912.06155](#).
- 225 B. Joachimi, C. A. Lin, M. Asgari et al., *A&A***646**, A129 (2021), arXiv: [2007.01844](#).
- 226 J. U. Lange, A. P. Hearin, A. Leauthaud et al., *MNRAS***520**, 5373 (2023), arXiv: [2301.08692](#).
- 227 J. Sohn, M. J. Geller, H. S. Hwang, A. Diaferio, K. J. Rines, and Y. Utsumi, *ApJ***923**, 143 (2021), arXiv: [2106.11429](#).
- 228 J. Sohn, M. J. Geller, H. S. Hwang, D. G. Fabricant, Y. Utsumi, and I. Damjanov, *ApJ***945**, 94 (2023), arXiv: [2210.16499](#).
- 229 DESI Collaboration, A. Aghamousa, J. Aguilar et al., arXiv e-prints arXiv:1611.00036 (2016), arXiv: [1611.00036](#).
- 230 D. J. Heath, *MNRAS***179**, 351 (1977).
- 231 S. Alam, M. Ata, S. Bailey et al., *MNRAS***470**, 2617 (2017), arXiv: [1607.03155](#).
- 232 A. Mainzer, J. Bauer, T. Grav et al., *ApJ***731**, 53 (2011), arXiv: [1102.1996](#).
- 233 A. Raichoor, J. Comparat, T. Delubac et al., *MNRAS***471**, 3955 (2017), arXiv: [1704.00338](#).
- 234 S. Yuan, R. H. Wechsler, Y. Wang et al., arXiv e-prints arXiv:2310.09329 (2023), arXiv: [2310.09329](#).
- 235 H. Gao, Y. P. Jing, K. Xu et al., *ApJ***961**, 74 (2024), arXiv: [2309.03802](#).
- 236 A. E. Shapley, C. C. Steidel, M. Pettini, and K. L. Adelberger, *ApJ***588**, 65 (2003), arXiv: [astro-ph/0301230](#).
- 237 J. M. Le Goff, C. Magneville, E. Rollinde et al., *A&A***534**, A135 (2011), arXiv: [1107.4233](#).
- 238 H. du Mas des Bourboux, J.-M. Le Goff, M. Blomqvist et al., *A&A***608**, A130 (2017), arXiv: [1708.02225](#).
- 239 C. Ravoux, E. Armengaud, M. Walther et al., *J. Cosmology Astropart. Phys.***2020**, 010 (2020), arXiv: [2004.01448](#).
- 240 H. du Mas des Bourboux, J. Rich, A. Font-Ribera et al., *ApJ***901**, 153 (2020), arXiv: [2007.08995](#).
- 241 B. Villaseñor, B. Robertson, P. Madau, and E. Schneider, *Phys. Rev. D***108**, 023502 (2023), arXiv: [2209.14220](#).
- 242 L. Fuß and M. Garny, *J. Cosmology Astropart. Phys.***2023**, 020 (2023), arXiv: [2210.06117](#).
- 243 M. J. Wilson and M. White, *J. Cosmology Astropart. Phys.***2019**, 015 (2019), arXiv: [1904.13378](#).
- 244 C. C. Steidel, M. Giavalisco, M. Pettini, M. Dickinson, and K. L. Adelberger, *ApJ***462**, L17 (1996), arXiv: [astro-ph/9602024](#).
- 245 C. C. Steidel, K. L. Adelberger, M. Giavalisco, M. Dickinson, and M. Pettini, *ApJ***519**, 1 (1999), arXiv: [astro-ph/9811399](#).
- 246 N. A. Reddy and C. C. Steidel, *ApJ***692**, 778 (2009), arXiv: [0810.2788](#).
- 247 M. Giavalisco, *ARA&A***40**, 579 (2002).
- 248 Y. Ono, M. Ouchi, Y. Harikane et al., *PASJ***70**, S10 (2018), arXiv: [1704.06004](#).
- 249 N. A. Reddy, C. C. Steidel, M. Pettini, K. L. Adelberger, A. E. Shapley, D. K. Erb, and M. Dickinson, *ApJS***175**, 48 (2008), arXiv: [0706.4091](#).
- 250 H. Hildebrandt, J. Pielorz, T. Erben, L. van Waerbeke, P. Simon, and P. Capak, *A&A***498**, 725 (2009), arXiv: [0903.3951](#).
- 251 J. Cooke, Y. Omori, and E. V. Ryan-Weber, *MNRAS***433**, 2122 (2013), arXiv: [1305.0562](#).
- 252 J. E. Gunn, M. Carr, C. Rockosi et al., *AJ***116**, 3040 (1998), arXiv: [astro-ph/9809085](#).
- 253 J. R. Weaver, O. B. Kauffmann, O. Ilbert et al., *ApJS***258**, 11 (2022), arXiv: [2110.13923](#).
- 254 M. Ouchi, Y. Ono, and T. Shibuya, *ARA&A***58**, 617 (2020), arXiv: [2012.07960](#).
- 255 R. Bacon, J. Brinchmann, S. Conseil et al., *A&A***670**, A4 (2023), arXiv: [2211.08493](#).
- 256 A. Torralba-Torregrosa, S. Gurung-López, P. Arnalte-Mur et al., *A&A***680**, A14 (2023), arXiv: [2307.10215](#).
- 257 A. Torralba-Torregrosa, P. Renard, D. Spinoso et al., *A&A***690**, A388 (2024), arXiv: [2407.19020](#).
- 258 M. Ouchi, Y. Harikane, T. Shibuya et al., *PASJ***70**, S13 (2018), arXiv: [1704.07455](#).
- 259 N. P. Ross, A. D. Myers, E. S. Sheldon et al., *ApJS***199**, 3 (2012), arXiv: [1105.0606](#).
- 260 A. D. Myers, N. Palanque-Delabrouille, A. Prakash et al., *ApJS***221**, 27 (2015), arXiv: [1508.04472](#).
- 261 C. Yèche, N. Palanque-Delabrouille, C.-A. Claveau et al., *Research Notes of the American Astronomical Society* **4**, 179 (2020), arXiv: [2010.11280](#).
- 262 G. Dalton, S. C. Trager, D. C. Abrams et al., in *Ground-based and Airborne Instrumentation for Astronomy IV*, (edited by I. S. McLean, S. K. Ramsay, and H. Takami), volume 8446 of *Society of Photo-Optical Instrumentation Engineers (SPIE) Conference Series*, 84460P (2012).
- 263 M. M. Pieri, S. Bonoli, J. Chaves-Montero et al., in *SF2A-2016: Proceedings of the Annual meeting of the French Society of Astronomy and Astrophysics*, (edited by C. Reylé, J. Richard, L. Cambrésy, M. Deleuil, E. Pécontal, L. Tresse, and I. Vauglin), 259–266 (2016), arXiv: [1611.09388](#).
- 264 X. Fan, M. A. Strauss, G. T. Richards et al., *AJ***131**, 1203 (2006), arXiv: [astro-ph/0512080](#).
- 265 L. Jiang, X. Fan, J. Annis et al., *AJ***135**, 1057 (2008), arXiv: [0708.2578](#).
- 266 C. J. Willott, P. Delorme, C. Reylé et al., *AJ***139**, 906 (2010), arXiv: [0912.0281](#).
- 267 B. P. Venemans, J. R. Findlay, W. J. Sutherland et al., *ApJ***779**, 24 (2013), arXiv: [1311.3666](#).
- 268 S. L. Reed, R. G. McMahon, M. Banerji et al., *MNRAS***454**, 3952 (2015), arXiv: [1504.03264](#).
- 269 Y. Matsuoka, M. Onoue, N. Kashikawa et al., *ApJ***828**, 26 (2016), arXiv: [1603.02281](#).
- 270 E. Bañados, B. P. Venemans, R. Decarli et al., *ApJS***227**, 11 (2016), arXiv: [1608.03279](#).
- 271 F. Wang, X.-B. Wu, X. Fan et al., *ApJ***819**, 24 (2016), arXiv: [1602.04659](#).
- 272 J. Yang, X.-B. Wu, D. Liu et al., *AJ***155**, 110 (2018), arXiv: [1801.01245](#).
- 273 N. Palanque-Delabrouille, C. Magneville, C. Yèche et al., *A&A***587**, A41 (2016), arXiv: [1509.05607](#).
- 274 C. Yèche, P. Petitjean, J. Rich et al., *A&A***523**, A14 (2010).
- 275 X. Jin, Y. Zhang, J. Zhang, Y. Zhao, X.-b. Wu, and D. Fan, *MNRAS***485**, 4539 (2019), arXiv: [1903.03335](#).
- 276 Planck Collaboration, N. Aghanim, Y. Akrami et al., *A&A***641**, A1 (2020), arXiv: [1807.06205](#).
- 277 M. S. Madhavacheril, F. J. Qu, B. D. Sherwin et al., *ApJ***962**, 113 (2024), arXiv: [2304.05203](#).

- 278 C. Radhakrishna Rao, *Bulletin of the Calcutta Mathematical Society* **37**, 81 (1945).
- 279 H. Cramér, *Mathematical Methods of Statistics*, Princeton Landmarks in Mathematics and Physics, (Princeton University Press 1999).
- 280 M. Tegmark, *Phys. Rev. Lett.* **79**, 3806 (1997), arXiv: [astro-ph/9706198](#).
- 281 T. Konstandin, R. A. Porto, and H. Rubira, *J. Cosmology Astropart. Phys.* **2019**, 027 (2019), arXiv: [1906.00997](#).
- 282 S.-F. Chen, Z. Vlah, and M. White, *J. Cosmology Astropart. Phys.* **2020**, 062 (2020), arXiv: [2005.00523](#).
- 283 R. Takahashi, M. Sato, T. Nishimichi, A. Taruya, and M. Oguri, *ApJ* **761**, 152 (2012), arXiv: [1208.2701](#).
- 284 W. d'Assignies D, C. Zhao, J. Yu, and J.-P. Kneib, *MNRAS* **521**, 3648 (2023), arXiv: [2301.02289](#).
- 285 M. White, Y.-S. Song, and W. J. Percival, *MNRAS* **397**, 1348 (2009), arXiv: [0810.1518](#).
- 286 J. Torrado and A. Lewis, *J. Cosmology Astropart. Phys.* **2021**, 057 (2021), arXiv: [2005.05290](#).
- 287 A. Lewis, A. Challinor, and A. Lasenby, *ApJ* **538**, 473 (2000), arXiv: [astro-ph/9911177](#).
- 288 J. N. Dossett, M. Ishak, and J. Moldenhauer, *Phys. Rev. D* **84**, 123001 (2011), arXiv: [1109.4583](#).
- 289 A. Lewis, *Phys. Rev. D* **87**, 103529 (2013), arXiv: [1304.4473](#).
- 290 A. Lewis, arXiv e-prints arXiv:1910.13970 (2019), arXiv: [1910.13970](#).
- 291 D. Foreman-Mackey, D. W. Hogg, D. Lang, and J. Goodman, *PASP* **125**, 306 (2013), arXiv: [1202.3665](#).
- 292 S. Linden and J.-M. Virey, *Phys. Rev. D* **78**, 023526 (2008), arXiv: [0804.0389](#).
- 293 L. Samushia, W. J. Percival, and A. Raccanelli, *MNRAS* **420**, 2102 (2012), arXiv: [1102.1014](#).
- 294 B. A. Reid, L. Samushia, M. White et al., *MNRAS* **426**, 2719 (2012), arXiv: [1203.6641](#).
- 295 W. J. Percival, D. Burkey, A. Heavens et al., *MNRAS* **353**, 1201 (2004), arXiv: [astro-ph/0406513](#).
- 296 L. Guzzo, M. Pierleoni, B. Meneux et al., *Nature* **451**, 541 (2008), arXiv: [0802.1944](#).
- 297 S. de la Torre, L. Guzzo, J. A. Peacock et al., *A&A* **557**, A54 (2013), arXiv: [1303.2622](#).
- 298 C. Blake, S. Brough, M. Colless et al., *MNRAS* **415**, 2876 (2011), arXiv: [1104.2948](#).
- 299 F. Beutler, C. Blake, M. Colless et al., *MNRAS* **423**, 3430 (2012), arXiv: [1204.4725](#).
- 300 T. Okumura, C. Hikage, T. Totani et al., *PASJ* **68**, 38 (2016), arXiv: [1511.08083](#).
- 301 H. Okada, T. Totani, and S. Tsujikawa, *Phys. Rev. D* **87**, 103002 (2013), arXiv: [1208.4681](#).
- 302 A. De Felice and S. Tsujikawa, *J. Cosmology Astropart. Phys.* **2012**, 007 (2012), arXiv: [1110.3878](#).
- 303 T. Baker, P. Ferreira, and C. Skordis, *Phys. Rev. D* **89**, 024026 (2014), arXiv: [1310.1086](#).
- 304 W. Hu and I. Sawicki, *Phys. Rev. D* **76**, 064004 (2007), arXiv: [0705.1158](#).
- 305 F. Simpson, C. Heymans, D. Parkinson et al., *MNRAS* **429**, 2249 (2013), arXiv: [1212.3339](#).
- 306 V. Desjacques, D. Jeong, and F. Schmidt, *Physics Reports* **733**, 1 (2018).
- 307 T. Lazeyras, A. Barreira, F. Schmidt, and V. Desjacques, *J. Cosmology Astropart. Phys.* **2023**, 023 (2023), arXiv: [2209.07251](#).
- 308 A. Gutiérrez Adame, S. Avila, V. Gonzalez-Perez et al., PNG-UNITsims: Halo clustering response to primordial non-Gaussianities as a function of mass (2024), arXiv: [2312.12405](#).
- 309 E.-M. Mueller, M. Rezaie, W. J. Percival et al., *MNRAS* **514**, 3396 (2022).
- 310 J. M. Sullivan, T. Prijon, and U. Seljak, *J. Cosmology Astropart. Phys.* **2023**, 004 (2023), arXiv: [2303.08901](#).
- 311 S. Ferraro and M. J. Wilson, *BAAS* **51**, 72 (2019), arXiv: [1903.09208](#).
- 312 A. Ghoshal and A. Naskar, *European Physical Journal C* **84**, 999 (2024), arXiv: [2302.00668](#).
- 313 DESI Collaboration, A. G. Adame, J. Aguilar et al., arXiv e-prints arXiv:2411.12022 (2024), arXiv: [2411.12022](#).
- 314 D. Green and J. Meyers, *Phys. Rev. D* **111**, 083507 (2025), arXiv: [2407.07878](#).
- 315 M. Tristram, A. J. Banday, M. Douspis et al., *A&A* **682**, A37 (2024), arXiv: [2309.10034](#).
- 316 A. Arinyo-i-Prats, J. Miralda-Escudé, M. Viel, and R. Cen, *J. Cosmology Astropart. Phys.* **2015**, 017 (2015), arXiv: [1506.04519](#).
- 317 P. Montero-Camacho and Y. Mao, *MNRAS* **508**, 1262 (2021), arXiv: [2106.14492](#).
- 318 A. Font-Ribera, P. McDonald, N. Mostek, B. A. Reid, H.-J. Seo, and A. Slosar, *J. Cosmology Astropart. Phys.* **2014**, 023 (2014), arXiv: [1308.4164](#).
- 319 N. Banik, J. Bovy, G. Bertone, D. Erkal, and T. J. L. de Boer, *J. Cosmology Astropart. Phys.* **2021**, 043 (2021), arXiv: [1911.02663](#).
- 320 A. Dekker, S. Ando, C. A. Correa, and K. C. Y. Ng, *Phys. Rev. D* **106**, 123026 (2022), arXiv: [2111.13137](#).
- 321 E. O. Nadler, A. Drlica-Wagner, K. Bechtol et al., *Phys. Rev. Lett.* **126**, 091101 (2021), arXiv: [2008.00022](#).
- 322 R. E. Keeley, A. M. Nierenberg, D. Gilman et al., arXiv e-prints arXiv:2405.01620 (2024), arXiv: [2405.01620](#).